

NASA Technical Memorandum 104801

11-15
92583

Liquid Flyback Booster Pre-Phase A Study Assessment

Volume 1

W. Peterson, W. Ankney, J. Bell, M. Berning, L. Bryant, A. Bufkin, L. Cain,
J. Caram, E. Cockrell, D. Curry, T. Diegelman, R. Gomez, A. Hong, D. Jih,
S. Labbe, M. Le, M. Leblanc, B. Lunney, J. Masciarelli, J. Musler, R. Nuss,
J. Powell, J. Riccio, E. Robertson, P. Royall, B. Scheffer, C. Sham, E. Smith,
T. Stowe, A. Strahan, K. Templin, M. Tigges, M. Valentine, M. Vantino, K. Wong,
E. Zetka, H. Campbell, R. Toelle, T. Feaster, L. Schultz, R. Thornburg

SEPTEMBER 1994



NASA Technical Memorandum 104801

Liquid Flyback Booster Pre-Phase A Study Assessment

Volume 1

W. Peterson, W. Ankney, J. Bell, M. Beming, L. Bryant, A. Bufkin,
L. Cain, J. Caram, B. Cockrell, D. Curry, T. Diegelman, R. Gomez,
A. Hong, D. Jih, S. Labbe, M. Le, M. Leblanc, B. Lunney, J. Masciarelli,
J. Musler, R. Nuss, J. Powell, J. Riccio, E. Robertson, P. Royall, B. Scheffer,
C. Sham, E. Smith, T. Stowe, A. Strahan, K. Templin, M. Tigges, M. Valentine,
M. Vantino, K. Wong, E. Zetka
Johnson Space Center, Houston, Texas

H. Campbell, R. Toelle
Marshall Space Flight Center

T. Feaster, L. Schultz, R. Thornburg
Kennedy Space Center



National Aeronautics and
Space Administration

Contributors

This document has been prepared by members of a study team representing the NASA Johnson Space Center (JSC), Kennedy Space Center (KSC), and Marshall Space Flight Center (MSFC). The following personnel have made significant contributions in their respective technical disciplines:

Jay Greene	Study Manager
Eric McHenry	Assistant Study Manager
Wayne Peterson	Lead Engineer
W. Sam Ankney	Integrated Avionics Team Lead
Jerry Bell	Mission Operations Team Lead
Mike Berning	Ascent Performance, Growth Options
Lee Bryant	Entry Trajectory and Performance
Ann Bufkin	Mass Properties, Subsystem Database
Leroy Cain	Operations, GN&C
Hugh Campbell	Main Propulsion System Design
Joe Caram	Aerthermodynamic Analysis
Butch Cockrell	Operations Concept Team Lead
Don Curry	Thermal Protection/Insulation
Thomas Diegelman	Operations, Ground Systems
Tom Feaster	KSC Team Lead
Ray Gomez	Computational Fluid Dynamics
Andrew Hong	Thermal Analysis
David Jih	Data Management System
Steve Labbe	Aeroscience Team Lead
Michael Le	Power System
Marvin Leblanc	Operations, Control Center
Brian Lunney	Operations, Propulsion Systems
James Masciarelli	Vehicle Sizing, Configuration Layout, Growth Options
Jeff Musler	Operations, Training
Ray Nuss	Nav aids
Jefferson Powell	Operations, Reconfiguration
Joe Riccio	Reaction Control System
Edward Robertson	Config. Lead, Air-Breathing Propulsion
Paul Royall	Aerodynamics
Brent Scheffer	Schedule, Operations Concept, Requirements
Larry Schultz	KSC Facilities
Catherine Sham	Communications System
Emery Smith, Jr.	Operations, Flight Analysis
Terri Stowe	Operations, Booster Systems
Alan Strahan	Guidance, Navigation and Control
Kevin Templin	Ascent Performance Lead, Growth Options
Richard Thornburg	Processing Timelines, Transition Planning
Mike Tigges	Entry Trajectory and Performance
Ron Toelle	MSFC Team Lead
Richard Tuntland	Operations Concept, Landing Strategy
Mark Valentine	Safety, Reliability, and Risk Analyses
Mary Vantino	Ascent Performance
Ken Wong	Structures
Eugene Zetka	Test and Verification

Preface

The Concept

Provide a cost-effective solution to long-term access to space through a fully reusable liquid propellant booster

Which:

- Increases Shuttle safety by enhancing abort capability and failure tolerance during first stage
- Increases Shuttle performance capability to high inclinations and high orbit altitudes
- Significantly reduces Shuttle operations costs
- Provides a development path to mitigate critical Shuttle obsolescence (i.e., computers, integrated navigation systems, electromechanical actuators, etc. are designed to also replace obsolete Orbiter systems)

While:

- Providing a reusable first stage for unmanned launches
- Providing a growth path to a heavy-lift launch capability

All of the above can be accomplished with a single configuration and a single infrastructure including:

- One processing facility
- One vendor/logistics support activity
- One sustaining engineering activity
- Maximum synergism with Shuttle infrastructure

RESULT: COST-EFFECTIVE ACCESS TO SPACE

Contents

Section		Page
1	Introduction	1
1.1	Background	1
1.2	Study Purpose/Goals	1
1.3	Approach/Scope	2
1.4	Groundrules	2
1.5	Requirements.....	3
2	Booster Sizing and Performance	4
2.1	Sizing Methodology and Results	4
2.1.1	Sizing Model Description.....	4
2.1.2	Booster Sizing Constraints.....	4
2.1.3	Results and Selection of Reference Configuration	4
2.2	Ascent Performance	11
2.2.1	Ascent Constraints	11
2.2.2	Ascent Performance	12
2.2.3	Abort Performance	14
2.3	Post-Separation/Return Performance	16
2.3.1	LFBB Trajectory Design	16
2.3.2	Post-Separation Mode.....	18
2.3.3	Cruise Mode	23
2.3.4	Loiter Mode	24
2.3.5	Landing Mode	24
3	Configuration	26
3.1	Design Goals.....	26
3.2	Geometry Constraints	26
3.2.1	KSC Facilities Considerations (supplied by Roger Mathews/KSC).....	26
3.2.2	Aerodynamic, Aerothermal, and Performance Considerations	29
3.3	Options Considered	31
3.4	Description of Selected Configuration.....	34
4	Aerodynamics and Aerothermodynamics	41
4.1	Aerodynamic & Aerothermodynamic Assessments	41
4.2	Preliminary Aerodynamic Configuration Trade Study and Development	41
4.2.1	Design Philosophy of the Scissor Wing Concept.....	41
4.2.2	Design Study Baseline Configuration.....	41
4.2.3	Baseline Configuration - Optimization for Landing (Minimum Wing Area)	44
4.3	LFBB Entry Aerodynamic Characteristics	45
4.3.1	Baseline Configuration Aerodynamics	46
4.3.2	Baseline Configuration Aerodynamic Stability Assessment	46
4.3.3	Crosswind Landing Capability	47
4.3.4	Summary.....	47
4.4	LFBB Ascent Aerodynamic Impacts to Shuttle	47
4.4.1	LFBB-Induced Ascent Aerodynamic F&M Factors.....	48
4.4.2	CFD Analysis of a Preliminary Shuttle with LFBBs Ascent Configuration	51
4.4.3	Conclusions.....	52
4.5	Aerothermodynamic Analysis of the LFBB.....	53
4.5.1	Reference Heating to a 1-ft Sphere	53
4.5.2	ET Impacts Assessment	53

Contents (continued)

Section		Page
4.5.3	Aerodynamic Heating to LFBB	54
4.5.3.1	Ascent Heating Methodology	54
4.5.3.2	Entry Heating Methodology	54
4.5.3.3	Integrated Ascent and Entry Heating Results	55
4.5.3.4	30° Angle of Attack Entry Results	55
4.5.4	Conclusions.....	55
4.6	Preliminary LFBB Study Ascent Performance Inputs.....	59
5	Systems Definition	63
5.1	Structures	63
5.1.1	Structural Factors of Safety.....	63
5.1.2	Design Load Factors	63
5.1.3	Booster Sizing	63
5.1.4	Booster Stiffness	63
5.1.5	Structure-TPS Configuration Options.....	63
5.1.5.1	Configuration 1: Aluminum 2219 With TABI.....	64
5.1.5.2	Configuration 2: Aluminum 2219 Without TPS.....	64
5.1.5.3	Configuration 3: Titanium Ti-6-4 Without TPS	64
5.1.5.4	Recommendations and Conclusions.....	64
5.1.6	Material Selection.....	65
5.1.7	Landing Gear Trade Between Skids & Wheels.....	65
5.1.8	Ascent Aerodynamic Loads on Orbiter	65
5.1.9	LFBB / External Tank Attach Strut Loads	66
5.1.9.1	Buildup and Liftoff	66
5.1.9.2	Ascent	67
5.2	Thermal Protection System/Insulation	67
5.3	Ascent Propulsion	71
5.3.1	LFBB Main Propulsion System Description.....	71
5.3.2	Propellant Tank Pressurization Scenario Flyback Phase of Flight.....	83
5.4	RCS Propulsion.....	83
5.4.1	Introduction	83
5.4.2	Requirements.....	83
5.4.2.1	General	83
5.4.2.2	Thruster and Manifold	84
5.4.3	Propellant Selection	85
5.4.3.1	Combinations Considered.....	85
5.4.3.2	Combinations Not Selected.....	86
5.4.3.3	Propellant Combination Selected.....	86
5.4.4	Technology Development Identified	90
5.5	Separation Propulsion	90
5.6	Air-Breathing Propulsion	91
5.6.1	Air-Breathing Engine Mounting Options	91
5.6.2	Types of Air-Breathing Engines.....	92
5.6.3	Selection of the LFBB Air-Breathing Engine	92
5.6.4	Air-Breathing Engine Airstart	95
5.6.5	Air-Breathing Engine Accessory Power	95
5.6.6	Alternate Fuel Capability	95
5.7	Power System	96
5.7.1	Assumptions.....	96
5.7.2	System Description	96

Contents (continued)

Section	Page
5.8	Control Actuation 99
5.8.1	Assumptions..... 100
5.8.2	System Descriptions 100
5.8.2.1	Booster Engine Actuation 100
5.8.2.2	Aerosurface Actuation..... 100
5.8.2.3	Landing Gear Actuation 101
5.8.2.4	Wing and Canard Deployment Actuation 101
5.9	Integrated Avionics..... 102
5.9.1	General Issues 102
5.9.1.1	Assumptions..... 102
5.9.1.2	Summary Description..... 102
5.9.1.3	Avionics Issues 103
5.9.1.3.1	Active/Passive Thermal Control 103
5.9.1.3.2	GPC I/O Margins..... 103
5.9.1.3.3	Thrust Balancing for Engine Shutdown..... 104
5.9.1.3.4	Avionics Integrated Testing..... 104
5.9.1.3.5	Guidelines and Groundrules for Vehicle Health Management System (VHMS) 104
5.9.2	GN&C System..... 105
5.9.2.1	Assumptions..... 105
5.9.2.2	Summary Description..... 106
5.9.3	Data Management System..... 106
5.9.3.1	System Description 106
5.9.3.2	Major Hardware Components 109
5.9.4	Communication System 109
5.9.4.1	Assumptions..... 109
5.9.4.2	Summary Description..... 109
5.9.4.3	Major Hardware Components and Assemblies..... 112
5.9.5	Navajds System 110
5.9.5.1	System Description 110
5.9.5.2	Hardware..... 111
5.10	Thermal Control 111
5.10.1	Introduction 111
5.10.2	Assumptions..... 111
5.10.3	Analysis..... 112
5.10.4	Results and Conclusions..... 112
5.11	Mass Properties and Center of Gravity 113
5.11.1	Mass Property Statement 113
5.11.2	Time History of CG (Nominal Mission)..... 114
 Volume 2	
6	Operations Concept 117
6.1	Operations Concept 117
6.2	Integrated Flight 117
6.2.1	Philosophy and Assumptions 118
6.3	LFBB Post-Separation/Return Flight..... 119
6.3.1	Philosophy and Assumptions 121
6.3.2	Flight Modes..... 121
6.4	Operational Mission Timelines 123
6.5	Ground Operations Processing and Timelines 125
6.5.1	Landing Operations..... 126
6.5.2	LFBB Processing Facility Operations..... 127
6.5.3	VAB Operations 128

Contents (continued)

Section		Page
6.5.4	Pad and Flight Operations	128
6.5.5	LFBB Processing Timelines	129
6.5.6	LFBB Transition Planning	130
7	Facility Impacts	133
7.1	KSC Facilities	133
7.1.1	Launch Pad	134
7.1.2	Mobile Launcher Platform	134
7.1.3	Vehicle Assembly Building	135
7.1.4	Flyback Booster Processing Facility	136
7.1.5	Launch Control Center	136
7.1.6	Landing Site	137
7.1.7	Impact of a Hypergol Reaction Control System on KSC Facilities	137
7.2	JSC Facilities	137
7.2.1	General Philosophy and Assumptions	138
7.2.1.1	Flight Systems	138
7.2.1.1.1	Integrated Vehicle Flight System (integrated ascent)	138
7.2.1.1.2	LFBB Flight System (post-separation and -return)	138
7.2.1.2	Mission Control	139
7.2.1.3	Training	140
7.2.2	User Operations Concept and Support Requirements	140
7.2.2.1	Control Teams	140
7.2.2.1.1	MCC Booster Control Team Concept	140
7.2.2.1.2	LFBB Control Team Concept	141
7.2.2.2	Training	142
7.2.2.2.1	Integrated Ascent	142
7.2.2.2.2	LFBB Flyback	142
7.2.3	Flight Design and Dynamics	142
7.2.4	Reconfiguration	143
7.2.5	Mission Control Center	144
7.2.6	Shuttle Mission Training Facility Cost and Design Study for the LFBB	144
7.2.6.1	Methodology	145
7.2.6.2	Scope	145
7.2.6.3	Derived Programmatic Implementation Guidelines and Recommendations	145
7.2.6.4	Trainer Requirements	146
7.2.6.5	General Operational Assumptions	146
7.2.6.6	SMTF Simulation Requirements, Assumptions and Implications (ascent phase only)	146
7.2.6.7	LFBB Simulation Requirements, Assumptions, and Implications (full mission)	147
7.2.6.8	Options and Configurations Modeled	147
7.2.6.9	Schedule	149
7.3	MSFC Facilities	151
8	Space Shuttle Impacts	152
8.1	Orbiter Impacts	152
8.1.1	Orbiter Hardware Impacts	152
8.1.2	Orbiter Flight Software Impacts	152
8.1.2.1	Primary Avionics System Software	152
8.1.2.1.1	Assumptions	152
8.1.2.1.2	Transport Lag	153
8.1.2.1.3	I/O Handling and Capacity	153
8.1.2.1.4	Abort Mode Processing SLOC Estimate	153

Contents (continued)

Section		Page
8.1.2.1.5	Overall SLOC Estimate	154
8.1.2.2	Back-Up Flight Software (BFS)	154
8.2	ET Impacts	154
9	Safety, Reliability, and Risk Analysis	155
9.1	Development and Construction Risk Assessment	155
9.1.1	Risk Categories	155
9.1.1.1	State of Technology	156
9.1.1.2	Design Engineering Difficulty	156
9.1.1.3	Manufacturing Process Difficulty	156
9.1.1.4	Production Equipment Status	156
9.1.1.5	Personnel Resource Status	157
9.1.1.6	Test Resource Status	157
9.1.2	Risk Measurements	157
9.1.2.1	Vehicle Development and Construction	157
9.1.2.1.1	Structures	158
9.1.2.1.2	TPS/Insulation (system)	158
9.1.2.1.3	Ascent Propulsion	158
9.1.2.1.4	RCS Propulsion	158
9.1.2.1.5	Separation Propulsion	158
9.1.2.1.6	Air-Breathing Propulsion	158
9.1.2.1.7	Power Systems	158
9.1.2.1.8	Control Actuation	158
9.1.2.1.9	Integrated Avionics	158
9.1.2.1.10	Thermal Control	158
9.2	Safety and Reliability	158
9.2.1	Launch Through Separation	158
9.2.1.1	Case 1: Two RD-170s per Booster	159
9.2.1.2	Case 2: Three RD-180s per Booster	163
9.2.1.3	Case 3: Four RD-180s per Booster	164
9.2.2	After Separation Through Recovery	170
9.3	Conclusions and Recommendations	171
9.3.1	Development and Construction	171
9.3.2	Safety and Reliability	171
9.3.3	Issues and Future Work	171
10	Test and Verification	173
10.1	Introduction	173
10.2	Test and Verification Purpose	173
10.3	Test and Verification Background	173
10.4	Assessment Plan of Action	174
10.5	Assessment Findings	174
10.6	Test and Verification Conclusions and Recommendations	178
11	Growth Paths	179
11.1	Growth Path Options	179
11.2	Preliminary Definition and Sizing	181
11.3	Trajectory and Performance Analysis	182
11.4	Summary and Conclusions	184

**Contents
(continued)**

Section		Page
12	Conclusions and Recommendations.....	185
12.1	Results	185
12.2	Conclusions.....	185
12.3	Recommendation	185

Appendix A - Issues List

Appendix B - Issues Rationale Statements

Appendix C - Trade List

Appendix D - Mass Properties and Design Details

Appendix E - Test & Verification Prime Wrap Factor Definitions

Appendix F - Test & Verification Subsystem and Discipline Findings Details

**Contents
(continued)**

Figures

Figure		Page
2.1.3-1	Boosters utilizing single F-1A engines.	5
2.1.3-2	Boosters utilizing single RD-170 engines.	5
2.1.3-3	Boosters utilizing two F-1A engines.	6
2.1.3-4	Boosters utilizing two RD-170 engines.	6
2.2.2-1	Shuttle performance with LFBB (150' x16', 2 RD-170).	13
2.2.3-1	Single SSME failure abort regions.	15
2.2.3-2	RD-170 failure abort regions.	15
2.2.3-3	RD-180 failure abort regions.	16
2.3.1-1	Three-dimensional left booster trajectory trace timeline.	17
2.3.2-1	Heat rate vs normal acceleration.	18
2.3.2-2	Normal acceleration vs time.	19
2.3.2-3	Drag acceleration reference and actual drag acceleration.	21
2.3.2-4	Commanded α vs time.	22
2.3.2-5	Commanded bank angle vs time.	22
2.3.3-1	Thrust vs time.	23
2.3.3-2	Altitude vs time.	24
3.2.2-1	Fixed service structure and umbilical geometry.	30
3.2.2-2	Mobile launch pad and Shuttle geometry.	30
3.3-1	LFBB configuration options.	33
3.4-1	LFBB with Shuttle.	34
3.4-2	LFBB ascent dimensions.	35
3.4-3	LFBB landing dimensions.	36
3.4-4	LFBB cross sections.	37
3.4-5	LFBB exploded view.	38
4.2.2-1	Space Industries, Inc., LFBB concept.	42
4.2.2-2	Fixed wing/deployable canard LFBB concept.	42
4.2.2-3	Fixed wing/deployable canard LFBB launch configuration.	43
4.2.2-4	Pre-Phase A LFBB baseline configuration.	44
4.2.3-1	Wing area vs vehicle weight as function of C_{Lmax}	45
4.3.1-1	LFBB estimated maximum L/D.	46
4.4.1-1	LFBB Y-Z and X-Y plane geometric area projections.	48
4.4.1-2	LFBB ascent aerodynamic evaluation - axial force vs Mach.	49
4.4.1-3a	LFBB impacts to Shuttle aerodynamics @ Mach 1.25 - axial force.	50
4.4.1-3b	LFBB impacts to Shuttle aerodynamics @ Mach 1.25 - normal force.	50
4.4.1-3c	LFBB impacts to Shuttle aerodynamics @ Mach 1.25 - pitching moment.	50
4.4.2-1	Shuttle with LFBBs "packaged" CFD model surface geometry.	51
4.4.2-2a	Shuttle with LFBBs ascent aero Orbiter wing load impacts—shear force.	52
4.4.2-2b	Shuttle with LFBBs ascent aero Orbiter wing load impacts—bending moment.	52
4.4.2-2c	Shuttle with LFBBs ascent aero Orbiter wing load impacts—torsion moment.	52
4.5.1-1	Altitude/velocity profile for LFBB ascent and 62° α entry.	56
4.5.1-2	Mach number and 1-ft reference sphere heating profile for LFBB ascent and 62° α entry.	56
4.5.2-1	LFBB vs generic certification ascent trajectory.	56
4.5.2-2	Reference heating comparison between LFBB and generic certification ascent.	56
4.5.2-3	Maximum ET circumferential heating rate comparison.	57
4.5.2-4	Maximum ET circumferential total heat load comparison.	57

Contents (continued)

Figures

Figure		Page
4.5.3-1	Body point locations on the LFBB forebody.	57
4.5.3.3-1	LFBB forebody heating to BPs 1-3, ascent and 62° α entry trajectory.	57
4.5.3.3-2	LFBB forebody heating to BPs 4, 6, and 8, ascent and 62° α entry trajectory.	57
4.5.3.3-3	LFBB forebody heating to BPs 5, 7, and 9, ascent and 62° α entry trajectory.	58
4.5.3.3-4	LFBB wing leading edge heating during 62° α entry.	58
4.5.3.3-5	Schematic of bow shock/wing shock interaction on the LFBB.	58
4.5.3.4-1	Entry trajectory comparison. (30° α vs 62° α)	58
4.5.3.4-2	LFBB forebody heating to BPs 1-3, ascent and 30° α entry trajectory.	58
4.5.3.4-3	LFBB forebody heating to BPs 4, 6, and 8, ascent and 30° α entry trajectory.	58
4.5.3.4-4	LFBB forebody heating to BPs 5, 7, and 9, ascent and 30° α entry trajectory.	59
4.5.3.4-5	LFBB wing leading edge heating during 30° α entry.	59
5.2-1	Flyback booster ascent surface temperatures: Mach 6 trajectory / 350°F wall.	68
5.2-2	Flyback booster entry surface temperatures: Mach 6 trajectory / 350°F wall.	68
5.2-3	NASA/Ames TABI elements.	70
5.2-4	Flyback booster (TABI/1.0 in. Rohacell) (8 hr on the pad) 90°F hot day.	71
5.3.1-1	LFBB main propulsion system schematic.	73
5.3.1-2	Shuttle flyback booster main propulsion system (RP-1 tank and feed line)	74
5.3.1-3	Shuttle flyback booster main propulsion system (LO ₂ tank and feed line)	75
5.3.1-4	Booster acceleration vs time from liftoff.	78
5.3.1-5	Engine power level vs time.	78
5.3.1-6	Fuel tank ullage pressure.	79
5.3.1-7	RP-1 tank bottom pressure.	79
5.3.1-8	Fuel NPSP vs mass.	81
5.3.1-9	LO ₂ tank ullage pressure.	81
5.3.1-10	LO ₂ tank bottom pressure.	82
5.3.1-11	LO ₂ NPSP vs mass.	82
5.4.2.2-1	RCS thruster configuration.	84
5.4.2.2-2	Manifold and thruster layout.	85
5.4.3.3-1	GO ₂ /RP-1 schematic.	87
5.4.3.3-2	NTO/MMH schematic.	89
5.6.3-1	High and ultra-high bypass air-breathing engines.	94
5.7.2-1	28 VDC battery management and distribution system.	98
5.7.2-2	270 VDC battery management and distribution system.	99
5.9.1.2-1	LFBB integrated avionics architecture.	103
5.9.2.2-1	LFBB GN&C schematic.	107
5.9.3.1-1	LFBB avionics functional architecture.	108
5.9.4.2-1	LFBB communications subsystem architecture.	110
5.11.1-1	Mass properties definition process.	116
5.11.2-1	LFBB design mass summary.	114
5.11.3-1	Vehicle launch conditions during mission phases.	115
6.2-1	LFBB operations concept.	118
6.3-1	LFBB approach to KSC SLF runway 15.	120
6.3-2	LFBB approach to CCAFS skid strip runway 31.	120
6.3.2-1	Onboard command and control concept.	122
6.4-1	Ascent timeline.	124
6.4-2	LFBB mission timeline.	125
6.5-1	Launch site flow of LFBBs.	126
6.5.5-1	LFBB processing operations (mature operations).	129
6.5.5-2	Space Shuttle processing flow (mature operations).	130
6.5.6-1	LFBB transition planning.	131

**Contents
(continued)**

Figures

Figure		Page
7.1-1	LFBB facilities schedule.	134
7.1.1-1	Launch pad with the LFBB.	135
7.1.2-1	Mobile launcher platform deck.	136
7.2.1.2-1	Integrated ascent command and control architecture requirements and interfaces.	139
7.2.1.2-2	LFBB flyback command and control architecture requirements and interfaces.	140
7.2.5-1	LFBB command and control.	144
7.2.6.8-1	LFBB training concept.	148
7.2.6.8-2	LFBB training synergy concept.	149
7.2.6.9-1	LFBB simulation development schedule.	150
8.1.2.1.1-1	Primary avionics system software architecture.	153
9.2.1.1-1	Booster fault tree - two RD-170s per booster.	160
9.2.1.1-2	Two-booster reliability - two RD-170s per booster launch to separation, high-end estimate.	162
9.2.1.1-3	Two-booster reliability - two RD-170s per booster launch to separation, low-end estimate.	162
9.2.1.2-1	Booster fault tree - three RD-180s per booster.	163
9.2.1.2-2	Two-booster reliability - three RD-180s per booster launch to separation, high-end estimate.	164
9.2.1.3-1	Booster fault tree - four RD-180s per booster.	165
9.2.1.3-2	Booster fault tree - four RD-180s per booster.	166
9.2.1.3-3	Booster fault tree - four RD-180s per booster.	167
9.2.1.3-4	Booster fault tree - four RD-180s per booster.	168
9.2.1.3-5	Two-booster reliability - three RD-180s per booster launch to separation, high-end estimate.	169
9.2.1.3-6	Two-booster reliability - three RD-180s per booster launch to separation, low-end estimate.	170
11.1-1	Growth paths.	180
11.2-1	Estimated payload vs ideal delta-V.	181
11.3-1	Altitude vs range for growth path options.	183
11.3-2	Mach number vs range for growth path options.	184

Contents (concluded)

Tables

Table		Page
2.1.2-1	Performance Parameters for F-1A, RD-170, and RD-180 Engines	4
2.1.3-1	LFBB Sizing Data	8
3.3-1	Matrix of LFBB Wing Areas	31
4.3.1-1	LFBB Baseline Configuration Lift and Drag Aerodynamic Characteristics.....	46
4.4.1-1	Ascent Aerodynamic F&M Factors, LFBB-Induced	48
4.6-1	Additional Ascent Trajectory Design Ground Rules for LFBB	60
4.6-2	Ascent Vehicle Rate and Acceleration Limits	61
5.1.2-1	Estimated Load Factors	63
5.1.5-1	TPS-Structure Configuration Options.....	64
5.1.9.1-1	Aft Booster/ET Strut Loads	66
5.1.9.1-2	Forward Attach Booster/ ET Attach Loads	66
5.2-1	Anodized Aluminum (Emissivity - 0.6)	69
5.2-2	Titanium (Emissivity - 0.6).....	69
5.2-3	Anodized Aluminum (Emissivity - 0.6), 30% Uncertainty	69
5.2-4	LFBB Thermal Protection System Weight.....	70
5.3.1-1	LFBB Preliminary Part List	76
5.3.1-2	RD-170 Operating Data	77
5.3.1-3	Booster (RD-170) Propellant Inventory Summary	80
5.4.2.1-1	RCS Pre-Phase A Requirements and Assumptions	84
5.4.3.1-1	RCS Propellant Combinations Considered	85
5.4.3.1-2	Comparison of Leading Propellant Combinations.....	86
5.4.3.3-1	GO2/RP-1 Mass Breakdown.....	88
5.4.3.3-2	NTO/MMH Mass Breakdown	90
5.6.3-1	Estimated ABE Thrust vs Altitude and Mach Number.....	93
5.6.3-2	Estimated ABE TSFC vs Altitude and Mach Number	93
5.7-1	LFBB Power Requirements.....	98
5.8.2.2-1	LFBB Aerosurface Actuator Definition	101
5.8.2.3-1	LFBB Landing Gear Actuation Definition	101
5.8.2.4-1	Wing and Canard Deployment Actuation Definition	101
5.10.2-1	LFBB Component Characteristics	112
5.10.4-1	Thermal Analysis Results	113
7.2.2.1.1-1	Conceptual Integrated Ascent Flight Control Team Structure	141
7.2.4-1	Facilities Supported by Reconfiguration.....	143
8.2-1	Potential ET Structural Locations Requiring Modification	154
11.3-1	Growth Applications Table	182

Acronyms

ABE	air-breathing engine
ADTA	air data transducer assembly
ALT	approach & landing test
α	angle of attack
APAS II	Aerodynamic Preliminary Analysis System II
APU	auxiliary power unit
ARF	Assembly and Refurbishment Facility
ASRM	advanced solid rocket motor
ATO	abort-to-orbit
ATP	Authority To Proceed
β	angle of sideslip
BECO	booster engine cut-off
BFS	back-up flight software
BMAD	battery management and distribution
BP	body point
BSM	booster separation motor
C&T	Communication and Tracking
CAD	computer-aided design
CBT	computer-based training
CCAFS	Cape Canaveral Air Force Station
CCF	Consolidated Communications Facility
CCF	catastrophic correlation factor
CFD	computational fluid dynamics
CL	coefficient of lift
DED	design engineering difficulty
DMS	data management system
EIU	engine interface unit
EMA	electromechanical actuation
EPS	electrical power subsystem
EQI	Production Equipment Status
ET	external tank
F&M	force and moment
FBPF	flyback booster processing facility
FCR	fault containment region
FCR	flight control room
FCT	flight controller trainer
FDIR	fault detection, isolation, and recovery
FEU	flight equivalent unit
FRF	flight readiness firing
F.S.	factor of safety
FSS	fixed service structure
FTE	full-time equivalent
GAP	general avionics processor
GEO	geosynchronous orbit
GN&C	Guidance Navigation and Control
GPC	general purpose computer
GPS	global positioning system
GSE	ground support equipment
GTS	GN&C test station

Acronyms (continued)

HGDS	hazardous gas detection system
HLLV	heavy-lift launch vehicle
HW/SW	hardware/software
ICD	interface control document
IFMU	integrated flight management unit
IGES	initial graphics exchange standard
INS	inertial navigation system
IOC	initial operational capability
JSC	Johnson Space Center
KATS	Kennedy avionics test set
KSC	Kennedy Space Center
L/D	lift-to-drag ratio
LCC	Launch Control Center
LCC	life cycle cost
LEO	low Earth orbit
LFBB	liquid flyback booster
LPS	launch processing system
LRB	liquid rocket booster
LTS	LFBB test station
MCC	Mission Control Center
MDM	multiplexer/demultiplexer
MECO	main engine cut-off
MLG	main landing gear
MLP	Mobile Launch Platform
MPD	manufacturing/operations process difficulty
MPS	main propulsion system
MPSR	multi-purpose support room
MSFC	Marshall Space Flight Center
NASCOM-DB	NASA cost model data base
NEC	National Electric Code
NEOM	nominal-end-of-mission
NGP	National Grid Project
NLG	nose landing gear
NPSP	net positive suction pressure
Nz	normal acceleration
OI	operational instrumentation
OMDP	operations and maintenance down period
PASS	primary avionics system software
PCMMU	pulse code modulation master unit
PER	personnel resource status
QUADPAN	Quadrilateral Element Panel Method

Acronyms (concluded)

RCS	reaction control system
RPSF	Receiving, Processing, and Storage Facility
RSLs	redundant set launch sequencer
RSRM	redesigned solid rocket motor
RSS	rotating service structure
RTLS	return-to-launch-site
SAIL	Shuttle Avionics Integration Laboratory
SCA	shuttle carrier aircraft
SCOM	Shuttle Crew Operations Manual
SLF	Shuttle Landing Facility
SLOC	source lines of code
SMTF	Shuttle Mission Training Facility
SOT	state of technology
SSME	Space Shuttle Main Engine
SSTO	single stage to orbit
STDN	spaceflight tracking and data network
T&V	test and verification
T/W	thrust-to-weight
TABI	tailored advanced blanket insulation
TAL	trans-oceanic abort landing
TDRSS	tracking and data relay satellite system
TEST	test resource status
TO	liftoff
TPS	thermal protection system
TSFC	thrust specific fuel consumption
TSM	tail service mast
TSTO	two-stage to orbit
TVC	thrust vector control
UDF	unducted fan
VAB	Vehicle Assembly Building
VHM	vehicle health monitoring
VHMS	vehicle health management system
WBS	work breakdown structure

SECTION 1 INTRODUCTION

1.1 Background

The concept of a flyback booster has been around since early in the Shuttle program. The original two-stage Shuttle concepts utilized a manned flyback booster. The booster concepts were very large and the development was estimated to be costly. Requirements changed along with funding availability, which eliminated the flyback boosters from the Shuttle program. Today's Shuttle uses two redesigned solid rocket motors (RSRMs) during the boost phase in addition to the three Space Shuttle main engines (SSMEs) on the Orbiter vehicle. The RSRMs are recovered and refurbished after each flight. Refurbishment of the RSRMs, while less expensive than expending them, is one of the major recurring costs in the Shuttle program. Refurbishment of the RSRMs is nearly twice as expensive as the \$40M external tank (ET) that is expended during each Shuttle flight.

Replacement options for the RSRMs have been studied over the past ten years. The options include liquid rocket boosters (LRBs), hybrid rocket boosters, and flyback boosters. During the Access to Space Study performed in 1993, modifications to the current RSRMs were addressed, as well as replacement boosters. The conclusion made by Team 1 of this study was that the only boosters competitive to the RSRMs from a life cycle cost perspective were flyback boosters. Expendable LRBs and hybrids, although they offered possible safety improvements, were much more expensive. Team 1 recommended that a feasibility study on liquid flyback boosters (LFBBs) for the Shuttle Program be conducted¹. Space Industries, Inc., has also advocated the benefits of LFBBs and has presented a concept to NASA².

1.2 Study Purpose/Goals

The purpose of this study was to assess the feasibility and practicality of LFBBs. The study provides an expansion of the recommendations made by Team 1 of the Access to Space Study. The study went to sufficient depth to make an assessment of the proposed concept. Although a detailed configuration was developed, this vehicle concept and its selected systems should be reevaluated in a more comprehensive follow-on study.

The primary benefits provided by LFBBs are the potential for enhanced reusability and a reduction of recurring costs. The development of the boosters would require a funding wedge, but the potential savings in vehicle turnaround could offset the up-front costs. Development of LFBBs for the Shuttle assumes commitment to the Shuttle Program for 20 to 30 years. LFBBs would aid in the development of upgrades supporting a long-term Shuttle evolution strategy.

LFBBs also offer enhanced safety and abort capabilities. Currently, there are no intact abort capabilities during the burn of the RSRMs. Any failure of an RSRM can be considered catastrophic. A liquid system offers more benign propulsion system failures. Although catastrophic failures will exist, many failures can be recovered from. Engine selection may even allow engine out capability, thus providing a higher probability of mission success.

Additional performance is also a goal of the LFBB design. The performance capability of the Shuttle system is currently limited by the lift capability of the propulsion elements. LFBBs sized for increased performance over the RSRMs can use the additional performance to eliminate RTLS or trans-oceanic abort landing (TAL) abort modes, reduce the SSME's maximum throttle setting, increase yaw steering reserve for high inclination launch windows, increase launch probability by flying lower maximum dynamic pressure, and increase design margins. A goal of the LFBB study was to not allow the boosters to be the performance-limiting element of the Shuttle. Therefore, the performance goal of the LFBBs was to lift a fully loaded Orbiter, which would land at the predicted nominal end-of-mission weight limit of 248,000 lb, to an altitude of 220 nmi at an inclination of 51.6°.

A final benefit of LFBBs is the availability of growth paths for applications other than Shuttle. LFBBs can be used as the first stage for alternate low Earth orbit (LEO) and geosynchronous orbit (GEO) transportation systems. LFBBs can be used as strap-on boosters for a heavy-lift booster to support future manned lunar and planetary exploration missions. LFBBs can also provide an interim capability between today's Shuttle system and a fully reusable next generation system. The technology gained in developing an LFBB can be used to develop a fully reusable two-stage-to-orbit (TSTO) system or, eventually, a single-stage-to-orbit (SSTO) system.

1.3 Approach/Scope

The approach used by the NASA team for assessment of LFBBs was to conduct a top-level study that addressed the benefits of LFBBs. This study phase was conducted at a Pre-Phase A level for a period of 4 months. This goal of this study phase was to determine the feasibility of using LFBBs for the Shuttle Program. This document details the findings of the Pre-Phase A study.

The products of this initial effort were preliminary requirements definition; conceptual booster sizing and design; preliminary trade study analyses; system benefit determination (e.g., cost, safety, performance, margin); determination of growth paths; ascent performance and abort capabilities; modifications to Orbiter, ET, and facilities; and top-down cost (Volume 3). Volume 1 includes Sections 1 through 5. Volume 2 includes Sections 6 through 12, plus appendixes. Also, a recommendation on the desirability of proceeding to a more detailed study was requested.

Study participation involved the Johnson Space Center (JSC), Kennedy Space Center (KSC), and the Marshall Space Flight Center (MSFC). In-house personnel were used to the maximum extent possible and were augmented by contractor personnel in some of the discipline areas. JSC was responsible for study direction, requirements, initial booster sizing, integrated vehicle ascent performance, entry and landing system design and performance, and costing. KSC was responsible for the maintainability and operability of the vehicle concept, ground operations processing timelines, modifications and integration to the vehicle assembly building (VAB), mobile launch platform (MLP), launch pad, and facilities. KSC was also responsible for determining the timeline to transition from RSRMs to LFBBs. MSFC supplied analyses and expertise on main engine selection, engine performance characteristics, detailed propulsion system design, and potential modifications to the ET. MSFC also played an active role in determining the test and verification requirements required in LFBB development.

If a determination is made that a more detailed study is warranted, a year-long Phase A study would be initiated. Goals of the Phase A study would be to obtain baseline requirements for progression into Phase B, perform detailed vehicle designs and trades, and develop a reference concept with bottoms-up cost.

1.4 Groundrules

Several groundrules were documented at study initiation in order to bound the range of vehicles for consideration. The first groundrule was that the boosters would be designed for use with the Shuttle and, therefore, had to be compatible with the Orbiter and ET. Modifications to the Orbiter and ET must also be minimized. This holds true for the launch and processing facilities as well.

Current Shuttle ascent constraints were used to shape the ascent trajectories of the Shuttle with LFBBs. The LFBB ascent propulsion system was constrained to liquid propellants. Liquid propellants have more potential for a quick turnaround at the launch site. KSC does not have the capability to pour solids on site, and disassembly of the vehicle for remote processing was not seen as a viable concept. Liquid oxygen (LO₂) and RP-1 were selected for propellant at study initiation due to the availability of engines. An engine with a high thrust rating is required and F-1As and RD-170s were seen as the only viable engine candidates due to their near-term availability.

Implementation of the LFBBs will not reduce the payload performance of the Space Shuttle. Sizing the LFBBs for increased performance to achieve Orbiter maximum landing weight to a 51.6° inclination and a 220 nmi altitude was seen as highly desirable. Other design groundrules include technology readiness

levels of 6 by 1998, hazardous material and fluid avoidance, and minimal environmental effects to the launch and landing areas. Booster designs should also maximize operability and maintainability, provide optimum turnaround time, and reduced operations cost.

Several development schedule groundrules were also made. It is assumed that development of the LFBBs will not affect the Space Station schedule. The LFBB program will begin Phase B in 1997 and Phase C/D in 1998. The initial operational capability (IOC) date is assumed to be 2003.

1.5 Requirements

The following are the top level requirements derived from study groundrules and assumptions for the LFBB study:

Orbiter Modifications - Orbiter downtime allows 8 flights per year.

Launch Site/Facilities Modifications - Downtime for the launch site and processing facilities allows 8 flights per year.

Booster Life Cycle Cost - Shall be \leq projected remaining RSRM Life Cycle Cost.

Unmanned Operations - The booster shall operate in an unmanned configuration.

Return - Booster shall return to launch site.

Landing - Booster shall land autonomously on a runway.

IOC Date - The IOC date is assumed to be 2003.

Abort Capability - The booster shall not reduce the Orbiter abort capability.

Guidance - Ascent guidance shall remain on the Orbiter. Flyback guidance begins at separation.

Safety - Booster safety shall be \geq RSRM safety throughout powered ascent & separation.

Reliability - Booster reliability shall be \geq RSRM reliability throughout powered ascent & separation.

References

¹Access to Space Option 1 Team Summary Report; August 31, 1993; JSC White Paper.

²Access to Space Study; July, 1993; Space Industries, Inc., Rockwell Purchase Order M3D8XXL-453332M.

SECTION 2 BOOSTER SIZING AND PERFORMANCE

2.1 Sizing Methodology and Results

2.1.1 Sizing Model Description

An integrated vehicle sizing model was developed early to estimate LFBB performance and mass. The sizing model contains mathematical mass estimating relationships for the various booster subsystems such as body, wing, and canard structure, thermal protection, main and auxiliary propulsion elements, landing gear, and air-breathing propulsion systems. The mass estimating relationships used were obtained from historical data, previous studies, and reference 3. Masses for avionics, power generation, and other miscellaneous systems were estimated separately and were inputs to the sizing model.

The integrated sizing model was used to rapidly estimate LFBB performance and mass sensitivities to various parameters, including the number and type of main engines, LFBB geometry, landing speed, and the number and type of air-breathing engines. With this information, the most promising booster configuration options were selected for further analysis with a trajectory simulation program. With the updated performance provided by the trajectory simulation program, the configurations, performance, and mass properties are used as the starting point for more detailed subsystem design and analysis.

2.1.2 Booster Sizing Constraints

A maximum booster geometry of 18 ft in diameter and 170 ft in length was established for the sizing and performance analysis. The 18-ft-diameter limit was based upon MSFC wind tunnel data of maximum dynamic pressure versus booster diameter. This data indicated that above an 18-ft diameter, the allowable wing loading on the Orbiter would be exceeded. The data also showed that above 16 ft in diameter, the maximum dynamic pressure allowed during Shuttle ascent would have to be reduced to keep loads on the Orbiter's wings within limits. The booster length limit of 170 ft was based upon previous Shuttle LRB studies that noted several design breakpoints versus booster length based upon facility constraints and Shuttle aerodynamic interference factors. Booster lengths greater than 170 ft would require modification of the launch pad GO₂ vent arm. Booster lengths greater than the current RSRM length (149.2 ft) would significantly change the shock wave patterns and aerodynamic heating on the Shuttle during ascent.

The F-1A and RD-170 engines were baselined as the only candidates to be considered for the booster main engines due to their near-term availability. Boosters with 1 and 2 engines were investigated. The RD-180 engine was subsequently considered for engine-out and abort considerations. An RD-180 has two combustion chambers compared to four chambers for the RD-170. The RD-180 delivers half of the thrust of an RD-170 engine. Boosters with two, three, and four RD-180 engines were also investigated. The performance parameters assumed for the engines are shown in table 2.1.2-1 below:

Table 2.1.2-1 Performance Parameters for F-1A, RD-170, and RD-180 Engines

Parameter	F-1A	RD-170	RD-180
Vac. Thrust (lbf)	2,022,700	1,777,000	888,500
Vac. Isp	303.1	337	337
S.L. Isp	269.7	309	309
Dry Mass (lbm)	19,000	26,600	13,300

2.1.3 Results and Selection of Reference Configuration

The vehicle sizing model was used to estimate booster mass and Shuttle performance for one and two engine boosters, varying in diameter from 16 to 18 ft, and in length from 120 to 170 ft. The results of this analysis are shown in figures 2.1-1 through 2.1-4.

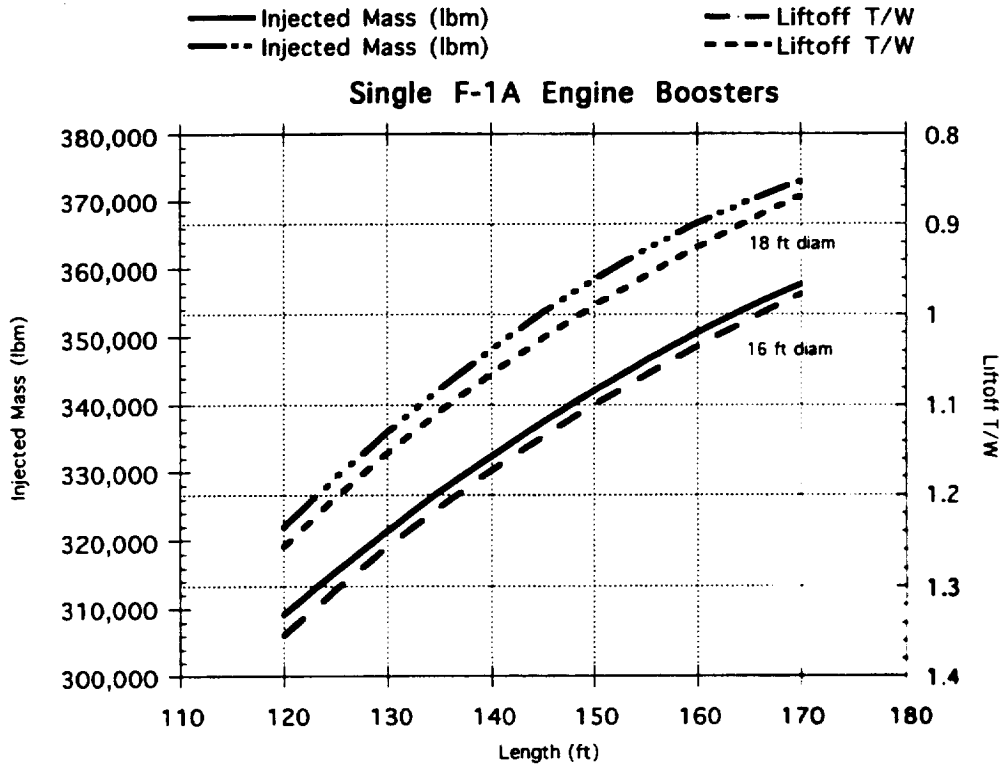


Figure 2.1.3-1 Boosters utilizing single F-1A engines.

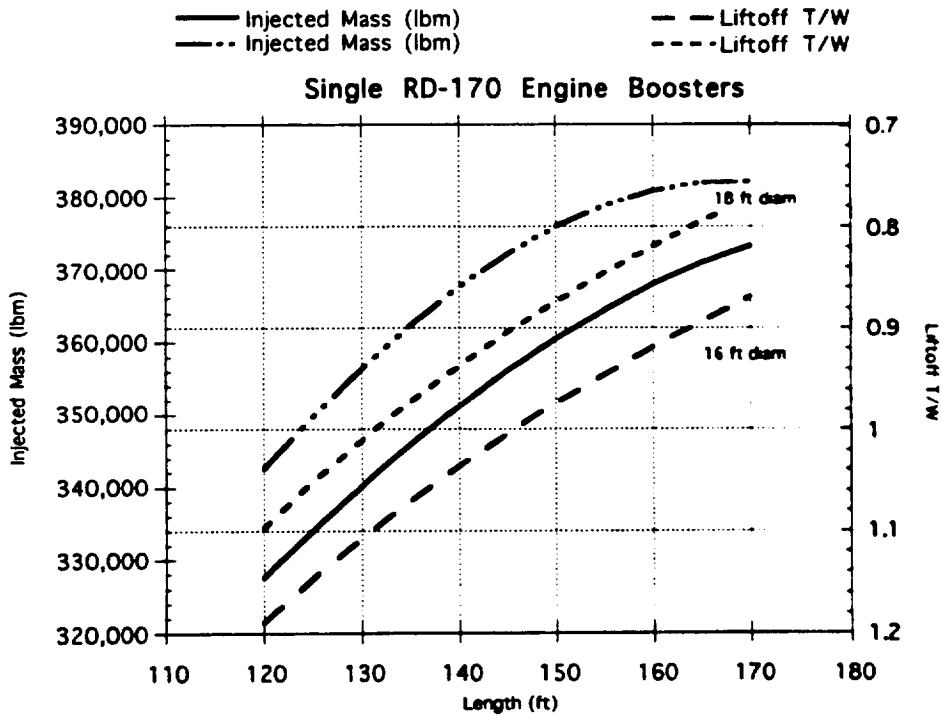


Figure 2.1.3-2 Boosters utilizing single RD-170 engines.

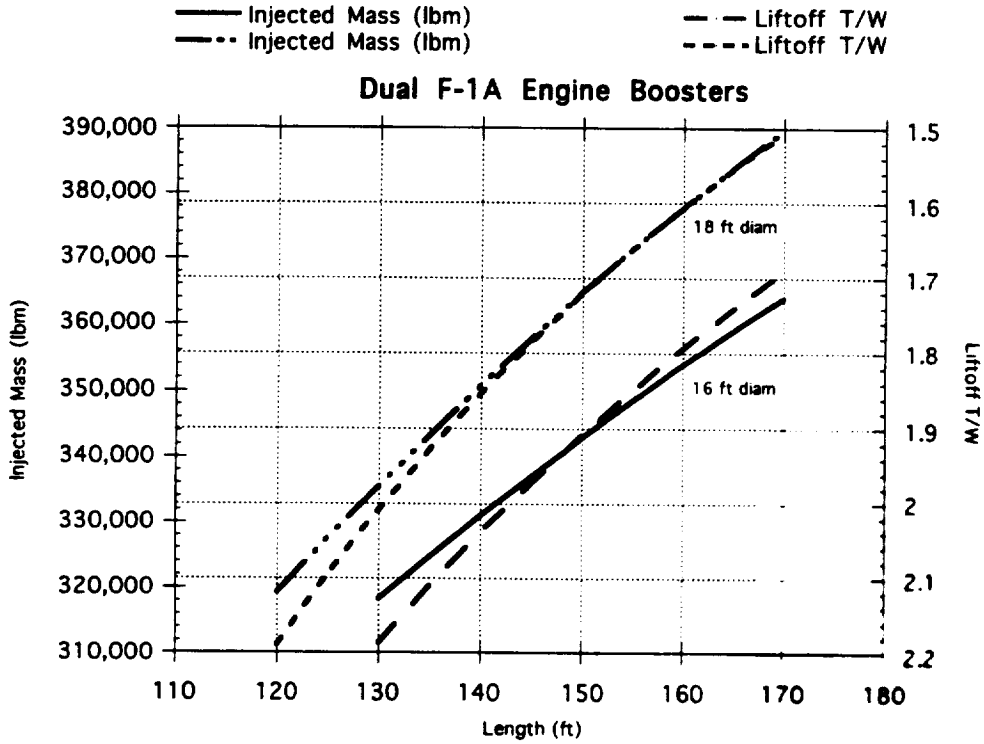


Figure 2.1.3-3 Boosters utilizing two F-1A engines.

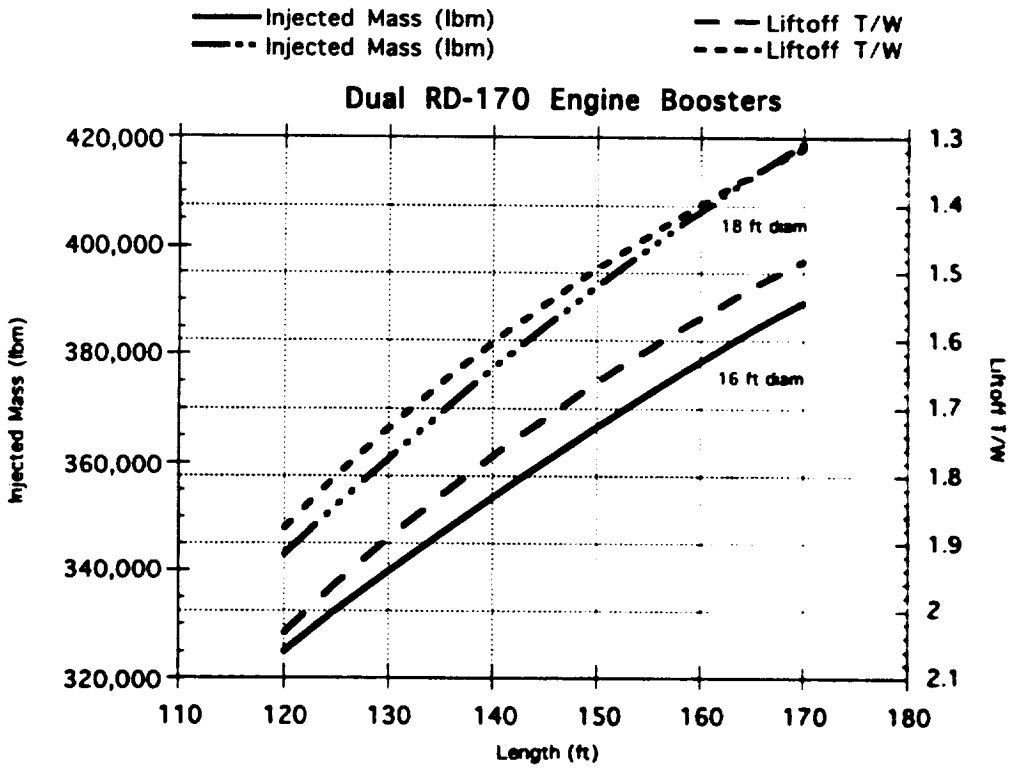


Figure 2.1.3-4 Boosters utilizing two RD-170 engines.

Performance of the single-engine booster configurations was deemed unacceptable since none of these configurations provided a liftoff thrust-to-weight (T/W) ratio greater than 1 with injected mass capability equal to or greater than the Shuttle's current capability. Therefore, single-engine boosters were dropped from further consideration.

Six 2-engine booster configurations were selected for further analyses using SORT. A detailed listing of the sizing model output for these configurations is shown in table 2.1.3-1. All of these configurations provide greater injected mass capability than the current Shuttle. As can be seen, the boosters using the RD-170 engine provide higher injected mass capability than boosters of the same geometry using the F1-A engine. For a 16-ft-diameter booster, a length of 170 ft with F1-A engines is required to match the performance of the 150-ft RD-170 engine booster.

Ascent trajectory analysis confirmed that booster configurations using the RD-170 engine provide better performance than those using the F-1A. Therefore, the RD-170 engine was selected for this phase of the LFBB study. This decision may be revisited in future studies, and a selection made based on criteria that also includes operability, maintainability, reliability, and cost.

A design geometry of 16 ft in diameter and 150 ft in length was selected as the reference LFBB configuration. The 150-ft length is only slightly longer than the current RSRM, and MSFC wind tunnel data showed that a 16-ft diameter does not require any reduction in allowable maximum dynamic pressure during ascent. Therefore a booster with these dimensions should cause a minimum of impacts to Shuttle ascent loads and aerodynamics. With 16x150-ft dimensions and two RD-170 engines per LFBB, the Shuttle/LFBB would have approximately 372 Klbm injected mass capability, compared to the current Shuttle/RSRM capability of 319 Klbm.

Table 2.1.3-1 LFBB Sizing Data

Number & Type of Engines	2 F-1A	2 RD-170	2 F-1A	2 RD-170	2 F-1A	2 RD-170	
Booster Diameter	18 ft	18 ft	16 ft	16 ft	16 ft	16 ft	
Booster Length	170 ft	170 ft	170 ft	170 ft	150 ft	150 ft	units
DELTA V							
ideal dV for stage 2	20,591	18,594	21,935	20,213	23,028	21,446	ft/s
ideal dV for stage 1	10,009	12,006	8,665	10,387	7,572	9,154	ft/s
total ideal dV	30,600	30,600	30,600	30,600	30,600	30,600	ft/s
VEHICLE THRUST/WEIGHT							
vehicle liftoff thrust to weight	1.47	1.28	1.65	1.44	1.86	1.62	
stage 1 separation thrust to weight	0.88	0.94	0.85	0.90	0.83	0.87	
MASS PROPERTIES *****							
STAGE 1 MASS							
mass of wing + elevons	18,395	20,116	18,891	20,482	8,194	9,130	lbm
mass of winglets	2,671	2,844	2,631	2,789	1,342	1,434	lbm
mass of canards	0	0	0	0	188	200	lbm
mass of fuel tank	14,406	13,150	14,975	13,551	10,539	9,709	lbm
mass of oxidizer tank	28,609	30,055	29,260	30,115	20,850	22,155	lbm
mass of forward skirt	2,610	2,471	2,333	2,202	2,026	1,925	lbm
mass of intertank adaptor	6,039	5,719	5,490	5,183	4,768	4,530	lbm
mass of aft adaptor	5,219	4,943	4,665	4,404	4,052	3,849	lbm
mass of cone	2,495	2,495	1,971	1,971	1,971	1,971	lbm
mass of thrust structure	16,182	14,216	16,182	14,216	16,182	14,216	lbm
TOTAL STRUCTURE	96,626	96,010	96,398	94,915	70,112	69,118	lbm
mass of fuel tank insulation	0	0	0	0	0	0	lbm
mass of oxidizer tank insulation	898	982	823	899	686	756	lbm
TOTAL PROTECTION	898	982	823	899	686	756	lbm
mass of main engines	37,999	53,204	37,999	53,204	37,999	53,204	lbm
mass of gimbal mechanism	5,219	4,585	5,219	4,585	5,219	4,585	lbm
mass of purge system	2,080	2,080	2,080	2,080	2,080	2,080	lbm
mass of engine mounts	809	711	809	711	809	711	lbm
mass of propellant system	16,182	14,216	16,182	14,216	16,182	14,216	lbm
mass of base heat shield	1,912	1,831	1,912	1,831	1,912	1,831	lbm
Dry mass of main propulsion system	64,201	76,626	64,201	76,626	64,201	76,626	lbm
Dry mass of RCS	1,863	1,904	1,853	1,891	1,739	1,775	lbm
TOTAL PROPULSION	66,064	78,530	66,054	78,517	65,939	78,402	lbm
mass of power generation system	640	640	640	640	640	640	lbm
mass of EPDC system	2,614	2,614	2,549	2,549	2,233	2,233	lbm
TOTAL POWER	3,254	3,254	3,189	3,189	2,873	2,873	lbm
mass of wing deployment mechanism	0	0	0	0	0	0	lbm
mass of canard actuation system	0	0	0	0	56	60	lbm
mass of aerosurface actuators	1,600	1,800	1,600	1,600	1,600	1,600	lbm
TOTAL CONTROL	1,600	1,800	1,600	1,600	1,656	1,660	lbm

Table 2.1.3-1 LFBB Sizing Data
(continued)

Number & Type of Engines	2 F-1A	2 RD-170	2 F-1A	2 RD-170	2 F-1A	2 RD-170	
Booster Diameter	18 ft	18 ft	16 ft	16 ft	16 ft	16 ft	
Booster Length	170 ft	170 ft	170 ft	170 ft	150 ft	150 ft	units
I mass of guidance, navigation, & cont	350	350	350	350	350	350	lbm
I mass of communication system	200	200	200	200	200	200	lbm
I mass of data management system	220	220	220	220	220	220	lbm
mass of instrumentation	1,030	1,030	1,010	1,010	910	910	lbm
TOTAL AVIONICS	1,800	1,800	1,780	1,780	1,680	1,680	lbm
TOTAL ENVIRONMENT	0	0	0	0	0	0	lbm
mass of air-breathing engines	8,850	8,850	8,850	8,850	8,850	8,850	lbm
mass of air-breathing engine mount	230	230	230	230	230	230	lbm
mass of air-breathing engine pylon	6,100	6,100	6,100	6,100	6,100	6,100	lbm
mass of ABE nacelles	1,188	1,188	1,188	1,188	1,188	1,188	lbm
mass of ABE fuel distribution syst	30	30	30	30	30	30	lbm
mass of ABE firewalls & fireseals	200	200	200	200	200	200	lbm
mass of ABE air induction ducts	260	260	260	260	260	260	lbm
mass of ABE air induction controls	150	150	150	150	150	150	lbm
mass of ABE controls	33	33	33	33	33	33	lbm
mass of ABE exhaust system	320	320	320	320	320	320	lbm
mass of ABE water injection system	300	300	300	300	300	300	lbm
mass of ABE fuel tanks (total)	103	103	103	103	103	103	lbm
Dry mass of ABE systems	17,763	17,763	17,763	17,763	17,763	17,763	lbm
mass of body structure impacts for	1,216	1,290	1,199	1,267	1,029	1,099	lbm
total mass of main landing gear	6,250	6,628	6,163	6,509	5,287	5,647	lbm
total mass of nose landing gear	3,455	3,670	3,406	3,602	2,911	3,114	lbm
total mass of landing gear and struc	10,922	11,588	10,768	11,378	9,227	9,859	lbm
mass of ET attach structure	4,500	4,073	4,500	4,073	4,500	4,073	lbm
I mass of recovery sys	0	0	0	0	0	0	lbm
mass of separation system	2,368	2,510	2,362	2,493	2,031	2,168	lbm
mass of range safety system	145	145	145	145	145	145	lbm
TOTAL OTHER	35,698	36,080	35,537	35,852	33,665	34,008	lbm
dry mass of stage 1 without growth	205,939	218,255	205,381	216,752	176,612	188,496	lbm
GROWTH	30,891	32,738	30,807	32,513	26,492	28,274	lbm
DRY MASS of stage 1 (w/growth)	236,830	250,993	236,188	249,264	203,104	216,771	lbm
mass of residual fuel	4,835	4,712	3,947	3,849	3,197	3,161	lbm
mass of residual oxidizer	10,976	12,251	8,959	10,007	7,258	8,219	lbm
mass of residual propellant	15,811	16,963	12,906	13,856	10,455	11,381	lbm
mass of reserve & resid ABE fuel	639	639	639	639	639	639	lbm
mass of reserve & resid RCS prop	127	134	125	132	104	111	lbm
TOTAL NONCARGO	16,577	17,736	13,670	14,627	11,199	12,131	lbm
INERT MASS of stage 1	253,407	268,729	249,858	263,892	214,303	228,901	lbm
TOTAL NONPROPELLANT	0	0	0	0	0	0	lbm

Table 2.1.3-1 LFBB Sizing Data
(continued)

Number & Type of Engines	2 F-1A	2 RD-170	2 F-1A	2 RD-170	2 F-1A	2 RD-170	
Booster Diameter	18 ft	18 ft	16 ft	16 ft	16 ft	16 ft	
Booster Length	170 ft	170 ft	170 ft	170 ft	150 ft	150 ft	units
mass of usable ABE fuel	6,393	6,393	6,393	6,393	6,393	6,393	lbm
mass of usable RCS propellant	2,536	2,685	2,501	2,638	2,083	2,216	lbm
mass of startup fuel	24,489	17,577	24,489	17,577	24,489	17,577	lbm
mass of startup oxidizer	55,591	45,699	55,591	45,699	55,591	45,699	lbm
mass of startup propellant	80,081	63,276	80,081	63,276	80,081	63,276	lbm
mass of usable ascent fuel	483,522	471,184	394,666	384,896	319,734	316,130	lbm
mass of usable ascent oxidizer	1,097,595	1,225,078	895,891	1,000,730	725,797	821,937	lbm
mass of usable ascent prop	1,581,117	1,696,262	1,290,556	1,385,626	1,045,531	1,138,067	lbm
TOTAL PROPELLANT	1,670,126	1,768,616	1,379,530	1,457,933	1,134,087	1,209,951	lbm
GROSS MASS (of 1 fly back booster)	1,923,533	2,037,345	1,629,389	1,721,825	1,348,390	1,438,853	lbm
inert mass of stage 2	272,949	272,949	272,949	272,949	272,949	272,949	lbm
mass of propellant in stage 2	1,587,240	1,587,240	1,587,240	1,587,240	1,587,240	1,587,240	lbm
mass of stage 2 at lift off	1,860,189	1,860,189	1,860,189	1,860,189	1,860,189	1,860,189	lbm
G mass of payload (payload + oms)	119,011	147,753	93,950	119,332	75,384	99,779	lbm
COMPLETE VEHICLE MASS							
gross mass of vehicle	5,826,267	6,082,633	5,212,916	5,423,170	4,632,354	4,837,674	lbm
inert mass	5,666,106	5,956,081	5,052,755	5,296,618	4,472,193	4,711,122	lbm
mass just before separation	2,135,059	2,062,805	2,170,606	2,116,316	2,137,249	2,099,021	lbm
mass just after sep of stage 1	1,610,388	1,507,191	1,653,103	1,570,472	1,691,692	1,624,001	lbm
mass at stage 2 burnout	391,960	420,702	366,899	392,281	348,333	372,728	lbm
injected mass	391,960	420,702	366,899	392,281	348,333	372,728	lbm
booster mass post entry (RCS burnout)	259,800	275,122	256,251	270,284	213,437	227,075	lbm
booster landing weight	253,407	268,729	249,858	263,892	207,045	220,682	lbm

2.2 Ascent Performance

2.2.1 Ascent Constraints

For the most part, the ascent trajectory constraints assumed for the LFBB study were those in use for Shuttle/RSRM flight design during the time this study was conducted. The initial ascent trajectory was derived using these constraints with the intention of establishing a baseline for integrated vehicle ascent and separated booster flyback loads analyses. It was anticipated that the results of these loads analyses would either confirm the use of current ascent constraints or derive new limits to be used in successive flight design iterations.

Ascent trajectory constraints based on current Shuttle flight design constraints included:

Launch month:	June
Max-q:	670 psf
Max acceleration:	3 g
Q-alpha limit:	-3250 psf-deg

Attitude Rates:

Stage 1

Angular Rate Limit:	15.0° per sec
Angular Acceleration Rate Limit:	5.0° per sec ²

Stage 2

Angular Rate Limit:	5.0° per sec
Angular Acceleration Rate Limit:	1.5° per sec ²

High Loads Region (Mach 0.6 to Mach 2.3)

Side Slip Angle: 0° from Mach 0.6 to staging

Roll Angle: 180° (Boost Reference frame) from the end of single-axis roll to staging

Angle of Attack: From Mach 0.6 to approximately Mach 2.3, alpha was computed to yield desired Q-alpha as a function of Mach. Near Mach 2.3, the commanded angle of attack (α) reaches 2.0° and was set to a constant value of 2.0° until staging. From staging until an altitude of 200,000 ft, the total α was limited to 2.0 +/- 5.0°.

The booster-to-ET shear attach loads used in this study were derived in previous LRB studies. The attach shear loads were established to maintain a minimum oxygen and hydrogen tank dome dynamic clearance of 0.6 inches. For conservatism, study attach shear loads which were less than allowable loads were assumed. The loads assumed for this study were greater than those in use for Shuttle/RSRM flight design. The Shuttle/RSRM ascent attach load limits were established to protect for 3-sigma hot RSRMs. It is difficult to predict the burn rate of a solid for any given day of launch. Conversely, a liquid engine can be test fired pre-flight and its performance can be measured. Therefore, the shear attach loads established for this study were felt to be within reason for use with a LFBB. Further analysis of these constraints is recommended for Phase A.

The ET forward thrust beam design loads were:

Allowable RSRM-ET attach shear loads:	1.646E06 in-lbf compression 1.780E05 in-lbf tension
Nominal RSRM-ET attach shear loads:	1.460E06 in-lbf compression 1.030E05 in-lbf tension
LFBB-ET study attach shear loads:	1.600E06 in-lbf compression 1.650E05 in-lbf tension

Current Shuttle/RSRM separation constraints:

Alpha : +2.0° - This was done to minimize the amount of aerodynamic heat soak the ET would experience during boost ascent.

Beta: 0.0° - Flight design ground rule for side slip angle.

Dynamic Pressure: <75.0 lbf/ft² - Shuttle/RSRM flight design value including knock-downs for 3-σ cold RSRM protection.

Thrust: LFBB engine thrust was zero pounds force at booster separation.

Engine performance parameters were as follows:

SSME specifications:

Thrust level: 364 Klbf - Sea Level
470 Klbf - Vacuum
Throttle range: 104%-67%

F-1A specifications:

Thrust level: 1.80 Milbf - Sea Level
2.02 Milbf - Vacuum
Throttle Range: 100% & 75% (Step)
100% - 69.4% (Continuous)
Gimbal Limit: ± 8°

RD-170 specifications:

Thrust level: 1.632 Milbf - Sea Level
1.777 Milbf - Vacuum
Throttle Range: 100% - 50% (Continuous)
Gimbal Limit: ± 8°

RD-180 specifications:

Thrust level: 827 Klbf - Sea Level
900 Klbf - Vacuum
Throttle Range: 100% - 50% (Continuous)
Gimbal Limit: ± 8°

2.2.2 Ascent Performance

The ascent performance analyses conducted for this study used the established ascent constraints while attempting to maximize the payload delivery capability of the Shuttle/LFBB ascent vehicle. The ascent trajectories derived represent a baseline from which future analyses would be incremented.

The baseline trajectory assumed that the SSMEs were brought to 100% throttle on the pad and were throttled to 104% once the vehicle achieved 60 ft/second of velocity during ascent. The SSMEs were not throttled down until necessary in the second stage to stay within the 3-g acceleration constraint. Elimination of SSME throttle bucket during first stage reduces the failure mode associated with SSME throttle-up. Booster engines were throttled during first stage for dynamic pressure, attach load and acceleration regulation. Figure 2.2.2-1 depicts the throttle profiles for the SSMEs and RD-170s. Reducing the maximum SSME throttle setting would be possible given the added performance of the baseline LFBBs and should be the subject of a trade study in Phase A.

STS PERFORMANCE w/LFBB

(150'x16' 2 RD-170 Configuration)

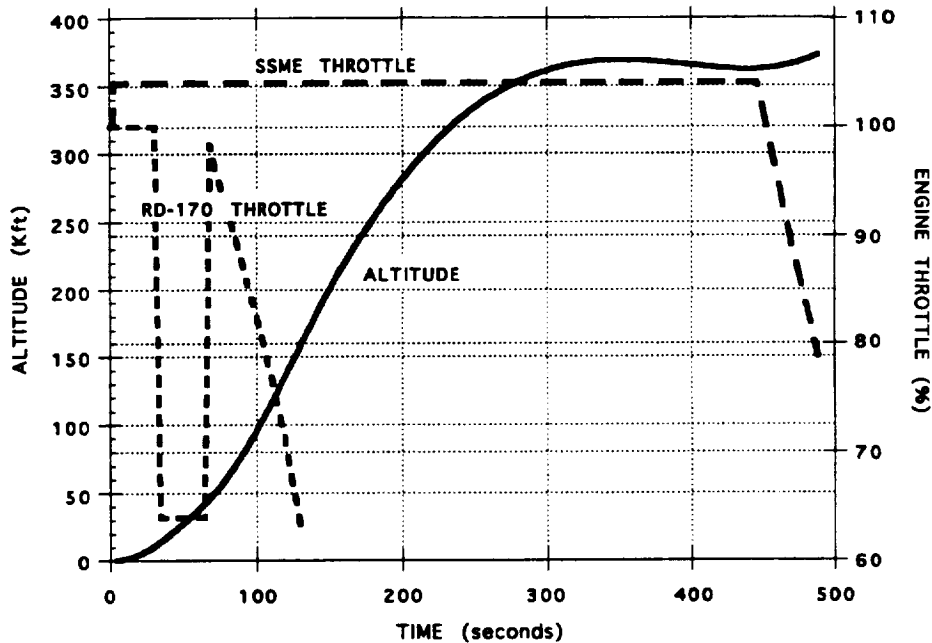


Figure 2.2.2-1 Shuttle performance with LFBB (150' x 16', 2 RD-170).

The baseline dual-engine booster configuration (150 ft tall x 16 ft diameter, using two RD-170 engines) provided an additional 56,000 lb of injected mass capability versus Shuttle/RSRM capability. The remaining study dual-engine configurations and the additional injected mass capability achieved by each is as follows:

170' x 18' step throttled F-1A	36,000 lb
170' x 16' step throttled F-1A	12,000 lb
170' x 18' continuous throttle F-1A	56,000 lb
170' x 16' continuous throttle F-1A	33,000 lb
170' x 18' RD-170	93,000 lb
170' x 16' RD-170	71,000 lb

The ascent performance capability of the baseline LFBB provided sufficient lift capability to meet the desired insertion of a nominal-end-of-mission Orbiter landing at 248,000 lb. This resulted in an Orbiter lift capability (i.e., payload) of approximately 56,000 lb and an orbital maneuvering system propellant loading of approximately 21,000 lb. In addition, approximately 24,000 lb of excess ascent lift capability resulted for the reference mission, to 220 nmi. at 51.6° inclination.

Baseline LFBB configuration nominal staging conditions were:

Time:	142 seconds after liftoff
Velocity:	Mach 5.8, 6300 ft/sec
Altitude:	185,000 ft
Dynamic pressure :	17 psf
Flight path angle:	20.3°

2.2.3 Abort Performance

A goal of the LFBB design study was the elimination of TAL intact aborts. A requirement was made that there be no time gaps between the intact abort modes. The combination of booster performance and baseline ascent trajectory made it possible to accomplish both objectives. The ability to control the throttle settings of the booster liquid rocket engines made it possible to establish abort mode initial boundary times which were earlier than could be achieved using RSRMs. Abort performance analyses were performed for the baseline LFBB using RD-170 and RD-180 engines only.

Given the LFBB design characteristics, it was feasible to achieve single SSME failure intact aborts or single booster engine failure intact aborts. It was assumed that for single booster engine failures, a simultaneous shutdown or throttle down of the opposing booster engine(s) would be accomplished to avoid prolonged exposure to asymmetric thrust. Combinations of SSME and booster engine failure scenarios were not considered during this study. Further study of all Shuttle/LFBB engine out abort scenarios would be required during Phase A.

It is important to note that if the two RD-170 engines on the LFBB were to be replaced by four RD-180 engines, single booster engine failures could be tolerated while still on or near the launch pad. Such failures would result in intact aborts ranging from return to launch site (RTLS) to press to main engine cutoff (MECO). For the same design scenario, two engines could fail approximately 24 seconds or later into the first stage of ascent with intact abort capability coverage.

The abort timeline for the baseline LFBB was as follows (figs. 2.2.3-1 through 2.2.3-3):

Single SSME failure options:

RTLS and TAL	capabilities existed for an SSME failure at liftoff
earliest abort to orbit (ATO)	MET = 2:37
negative RTLS	MET = 3:06
earliest press to MECO	MET = 3:57

Single RD-170 engine failure options (required opposite LFBB engine[s] throttling or shutdown):

earliest RTLS	MET = 0:24
earliest TAL	MET = 0:49
earliest ATO	MET = 1:07
earliest press to MECO	MET = 1:14

Single RD-180 engine failure options (required opposite LFBB engine[s] throttling or shutdown):

earliest RTLS	MET = 0:00
earliest TAL	MET = 0:00
earliest ATO	MET = 0:00
earliest press to MECO	MET = 0:02

Two RD-180 engine failure options: Times were the same as single RD-170 engine failure times.

Single SSME Failure Abort Regions (LFBB vs STS-63)

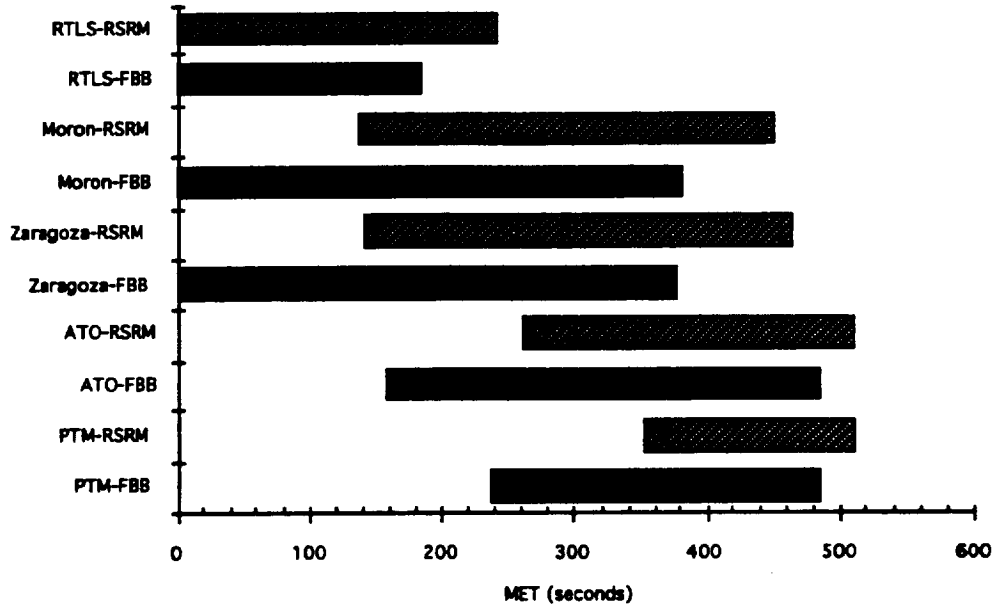


Figure 2.2.3-1 Single SSME failure abort regions.

LFBB RD-170 Engine Failure Abort Regions

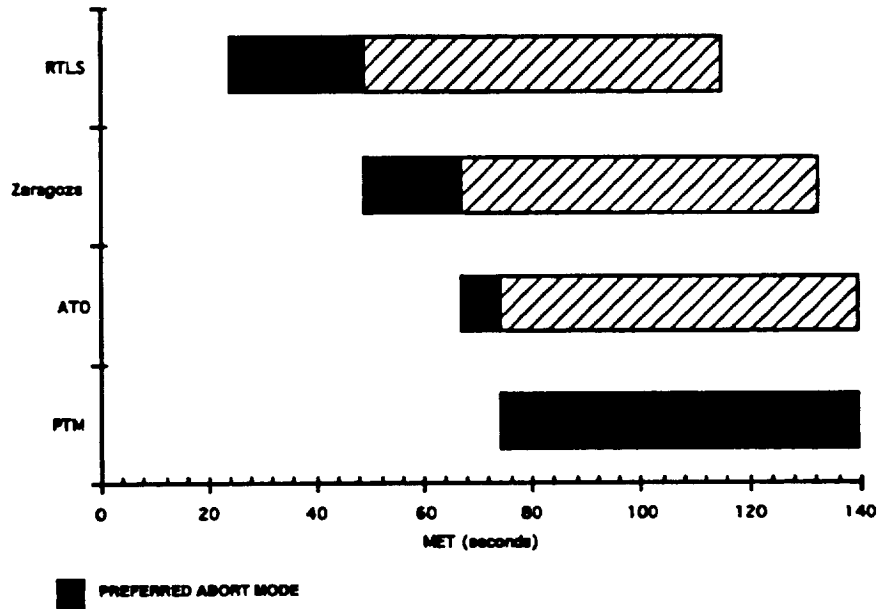


Figure 2.2.3-2 RD-170 failure abort regions.

LFBB RD-180 Engine Failure Abort Regions

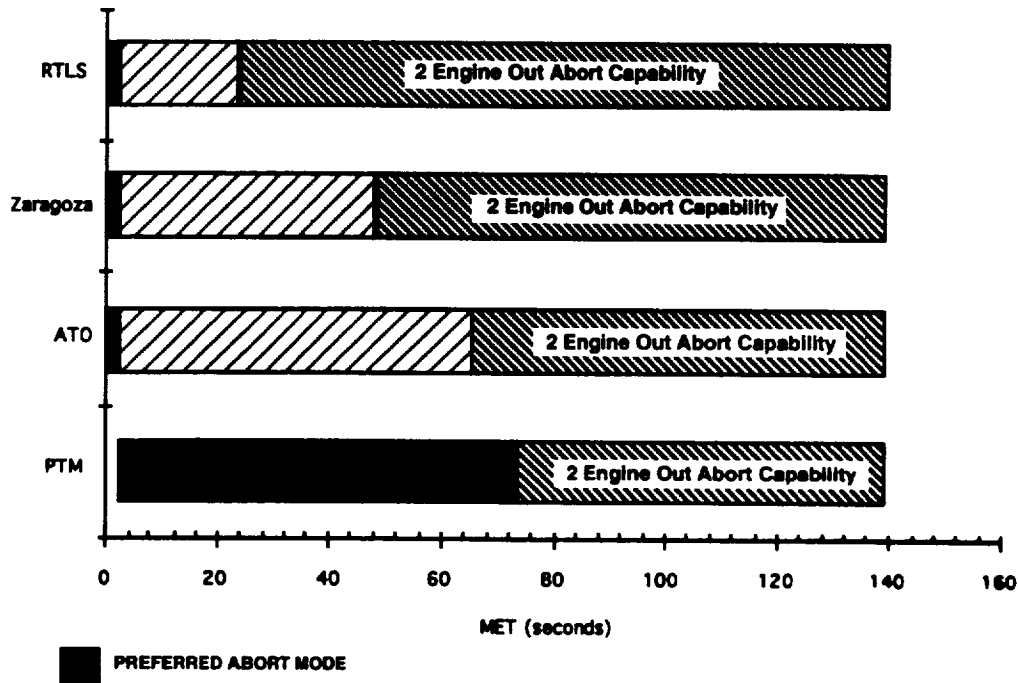


Figure 2.2.3-3 RD-180 failure abort regions.

An issue not addressed in this study was Orbiter landing weight constraints for high inclination intact aborts. At the time this study was conducted, the TAL abort landing weight constraint for a high inclination (51.6°) mission was 233,000 lb. The Orbiter would have to be recertified to a higher landing weight limit to accommodate the mission objectives for this study. Orbiter impacts will need to be addressed in Phase A. The nominal ascent trajectory for the baseline LFBBs has sufficient performance and ascent shaping to allow for the elimination of TAL aborts if so desired.

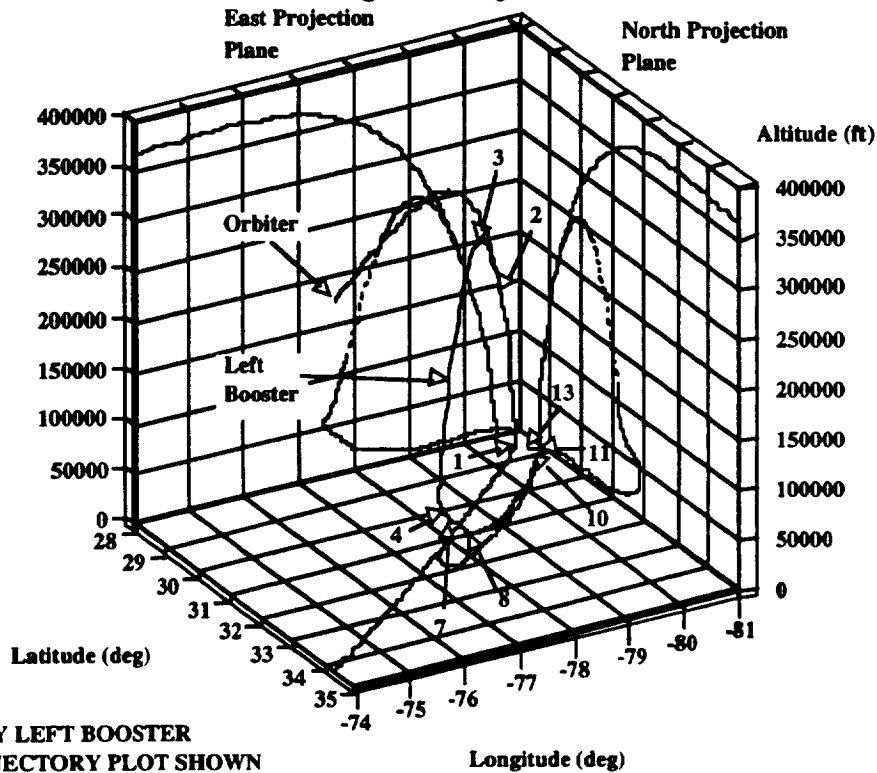
2.3 Post-Separation/Return Performance

2.3.1 LFBB Trajectory Design

The objective of the LFBB trajectory design is to return the boosters to a desired landing area while satisfying operational constraints, maximizing mission flexibility, and maintaining abort capability. Aerodynamic heating and loads were considered in the trajectory design to reduce thermal protection system and vehicle structure requirements.

Figure 2.3.1-1 depicts the three-dimensional groundtrack of the Orbiter and LFBB, and a comparison of the timelines for both left and right boosters; however, only the left LFBB flight path is shown in the figure for clarity. The projections of the trajectory curves onto three orthogonal planes are shown for each vehicle. The projection on the lower plane shows the groundtrack of the vehicles on the surface of the Earth. The East plane and West plane projections show the altitude tracks of the vehicles. Key events are numbered and labeled on the curve and correspond to the numbers on the event timeline. Note that the boosters arrive at the loiter decision point only one minute and nine seconds apart. For this timeline, the right booster is placed into a holding pattern for 15 minutes while the left booster is commanded to KSC runway 15. Once the left booster has cleared the runway, the right booster is commanded to land at the same runway and lands 16 minutes, 43 seconds following the first.

LFBB Trajectory Timeline *



* ONLY LEFT BOOSTER
TRAJECTORY PLOT SHOWN

EVENT	LEFT BOOSTER (mm:ss)	RIGHT BOOSTER (mm:ss)
1. Launch	00:00	00:00
2. Booster Sep	02:16	02:16
3. Max Alt	03:31	03:31
4. Load Relief	05:13	05:13
5. Linear Energy	05:56	05:56
6. Plane Change	06:27	06:27
7. Max D.R.	07:10	07:10
8. ABE Ign (Const Alt)	11:06	11:00
9. Descent on Glide	65:05	63:34
10. Lotter Decision	68:43	67:34
11. Runway Align	72:50	89:28
12. Final Approach	73:50	90:28
13. Land	77:41	94:24

Left Booster touchdown 16:43 before the right booster

Figure 2.3.1-1 Three-dimensional left booster trajectory trace timeline.

2.3.2 Post-Separation Mode

During the first three minutes of flight following separation from the Orbiter, the boosters are executing events in preparation for atmospheric entry. This includes deployment of main wings and maneuvering to entry attitude. To minimize the possibility of recontact following separation, one booster is banked right and the other left. During this time the vehicle maintains a fixed high α required to dissipate excess energy, and a fixed aerodynamic bank angle for turning the vehicle back toward the landing site. Before the maximum normal acceleration (N_z) reference can be selected, the corresponding heat rate must be examined. As shown in figure 2.3.2-1, the maximum heat rate does not significantly decrease above an N_z of 3. Therefore, normal force constraints greater than this value do not have any appreciable effect on thermal protection system (TPS) requirements. For this analysis a value of 2.5 was used for the N_z constraint. This was chosen as a compromise between aerodynamic loads and heating, which affect vehicle structure weight and TPS requirements.

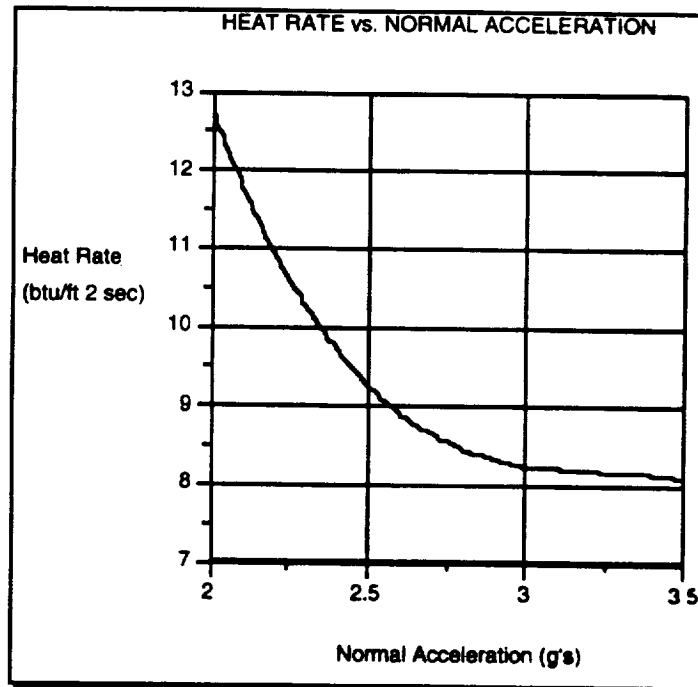


Figure 2.3.2-1 Heat rate vs normal acceleration.

As aerodynamic loads on the vehicle increase during reentry, guidance begins a load relief event (figure 2.3.2-2) that decreases α and controls the N_z . The vehicle maintains a constant bank angle of 20° during load relief. This event continues nominally for about 40 seconds until a minimum α for maintaining load relief is reached. The following equations were used in the load relief logic and produced the following graph (figure 2.3.2-2).

$$\alpha_{\dot{}} = \left[h\dot{} * \left(\frac{1}{hs} + \frac{2 * g}{v^2} \right) + \frac{2 * d}{v * m} \right] * \frac{c_n}{c_{na}} \quad (\text{eq. 2.3.2-1})$$

$$\text{var_}\alpha = xk_1 * (n_z - n_{z_target}) \quad (\text{eq. 2.3.2-2})$$

$$\alpha_{\dot{}}_{\text{cmd}} = \alpha_{\dot{}} + \frac{\text{var_}\alpha}{(4 * dt)} \quad (\text{eq. 2.3.2-3})$$

$$\alpha_{cmd} = \alpha_{cmd} + \alpha_{dot_cmd} * dt \quad (\text{eq. 2.3.2-4})$$

where the gain = $xk_1 = -0.4$, the atmospheric scale height $hs = 23385$ ft, $cn = cn_{\alpha} * \alpha - 0.518$ and $cn_{\alpha} = 0.055$.

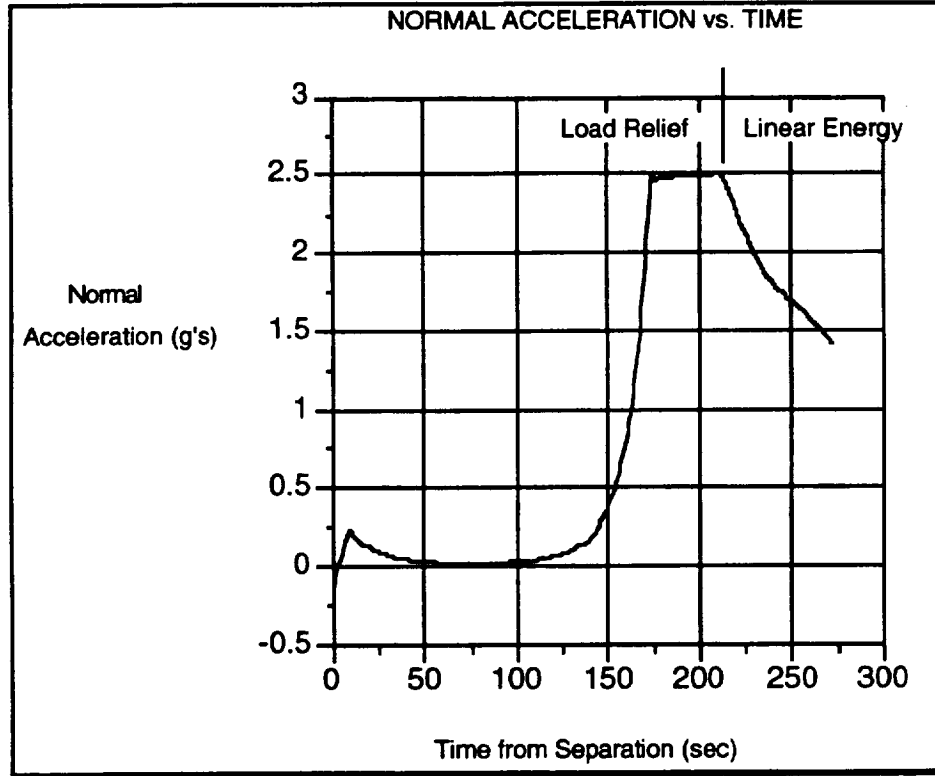


Figure 2.3.2-2 Normal acceleration vs time.

The linear energy event uses a canned α profile and varies the bank angle to achieve a drag acceleration and altitude rate reference. This steering profile is used to reduce long period altitude oscillations (phugoid). Linear energy continues until the velocity drops below Mach two (figure 2.3.2-3). This guidance is similar to the one used on the Orbiter during entry with the range equations removed. The linear energy equations used in the controller are:

$$d_{ref} = c_4 + c_5 * e \quad (\text{eq. 2.3.2-5})$$

where c_4 and c_5 are initialized with respect to drag acceleration and drag acceleration final (d, d_f) and current energy and final energy (e, e_f).

$$c_5 = \left(\frac{d - d_f}{e - e_f} \right), \quad c_4 = d_f - c_5 * e_f \quad (\text{eq. 2.3.2-6})$$

The final energy is defined from the target final altitude (hd_f) and the final target relative velocity (v_f).

$$e_f = g * hd_f + \frac{1}{2} * v_f^2 \quad (\text{eq. 2.3.2-7})$$

The rate of change of drag acceleration is determined from a proportionality with the drag reference.

$$d_dot = -c_5 * d_ref \quad (\text{eq. 2.3.2-8})$$

The altitude rate reference is then defined by:

$$h_dot_ref = -hs \left[2 * \left(\frac{d_ref + g * \sin(\text{gamr})}{v} \right) + \frac{d_dot}{d_ref} \right] \quad (\text{eq. 2.3.2-9})$$

The vertical lift-to-drag reference is defined from the relative velocity (v), the circular satellite velocity (v_{sat}), the flight path angle rate (gam_dot), and the local acceleration of gravity (g).

$$lodv_ref = \frac{g}{d_ref} \left(1 - \frac{v^2}{v_{sat}^2} \right) + \frac{v * \text{gam_dot}}{d_ref} \quad (\text{eq. 2.3.2-10})$$

In the guidance logic, gam_dot is actually an analytical equation which can be found in reference 4. The vertical lift-to-drag command (lodv_cmd) is then given by

$$lodv_cmd = lodv_ref + k_1 * (d - d_ref) + k_2 * (h_dot - h_dot_ref). \quad (\text{eq. 2.3.2-11})$$

The vehicle bank command is then given by the ratio of the commanded and available lift-to-drag,

$$\text{bank_cmd} = \cos^{-1} \left(\frac{\text{lodv_cmd}}{\text{lod}} \right) \quad (\text{eq. 2.3.2-12})$$

where $\text{lod} = \frac{c_l}{c_d}$, and k_1, k_2 are gains for achieving desired performance.

Figure 2.3.2-3 shows the drag acceleration reference and the actual drag acceleration resulting from the above equations.

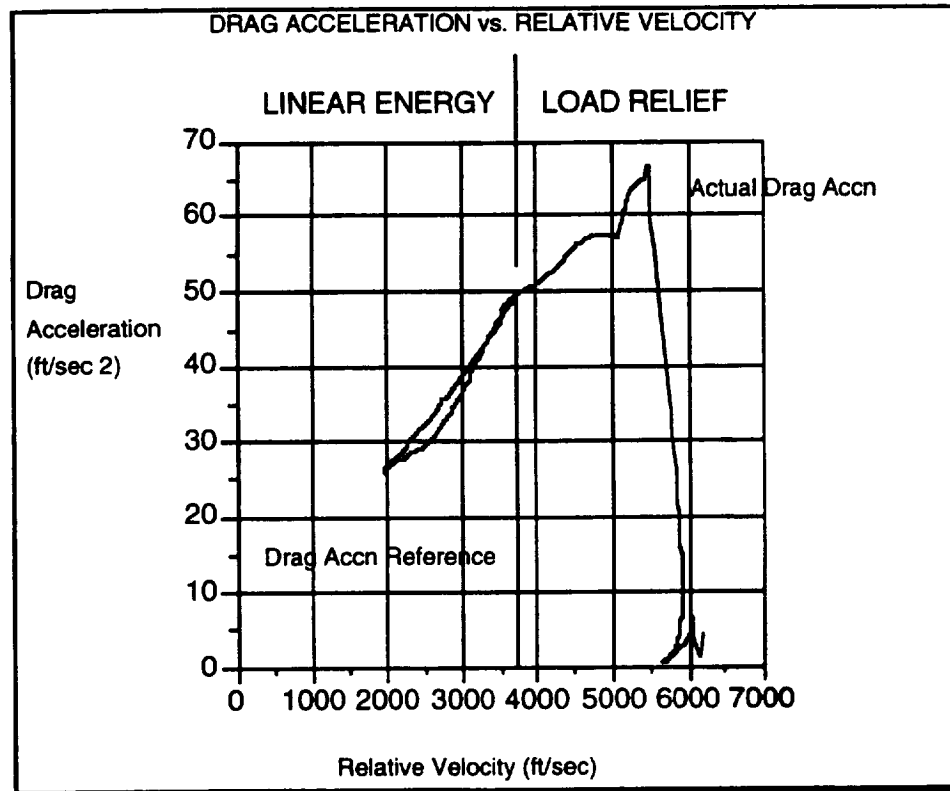


Figure 2.3.2-3 Drag acceleration reference and actual drag acceleration.

The α and aerodynamic bank during load relief and linear energy are presented in figures 2.3.2-4 and 2.3.2-5. Note that early during the reentry, high α s ($\sim 50^\circ$) are commanded to increase the rate at which energy is removed from the vehicle, therefore reducing the peak heat rate that the thermal protection system must absorb. As the load relief event is initiated, deviations from the commanded normal acceleration limit cause a reduction in α . This results in a re-distribution of aerodynamic loads along the vehicle longitudinal axis and reduces structural demands in the normal axis direction. Load relief continues until it would become necessary to command a positive pitch to maintain loads which would induce the altitude oscillations discussed earlier (phugoid). Guidance then transitions to an event that uses bank angle modulation to control altitude rate and drag acceleration. The α is commanded according to a pre-specified profile which continues to reduce the vehicle α and to increase lift-to-drag.

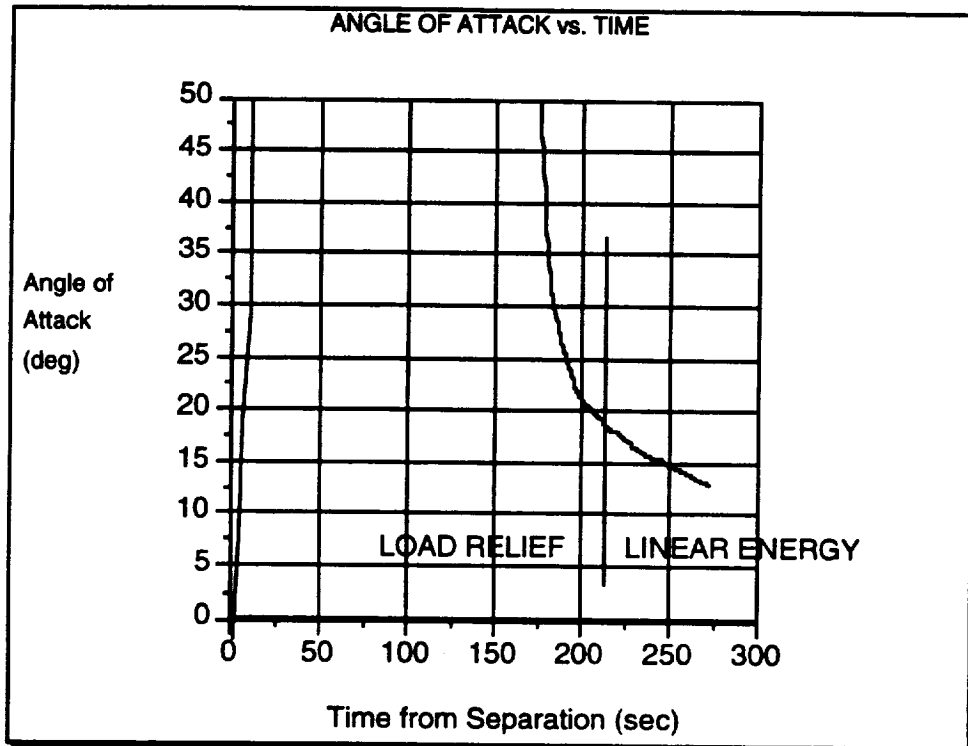


Figure 2.3.2-4 Commanded α vs time.

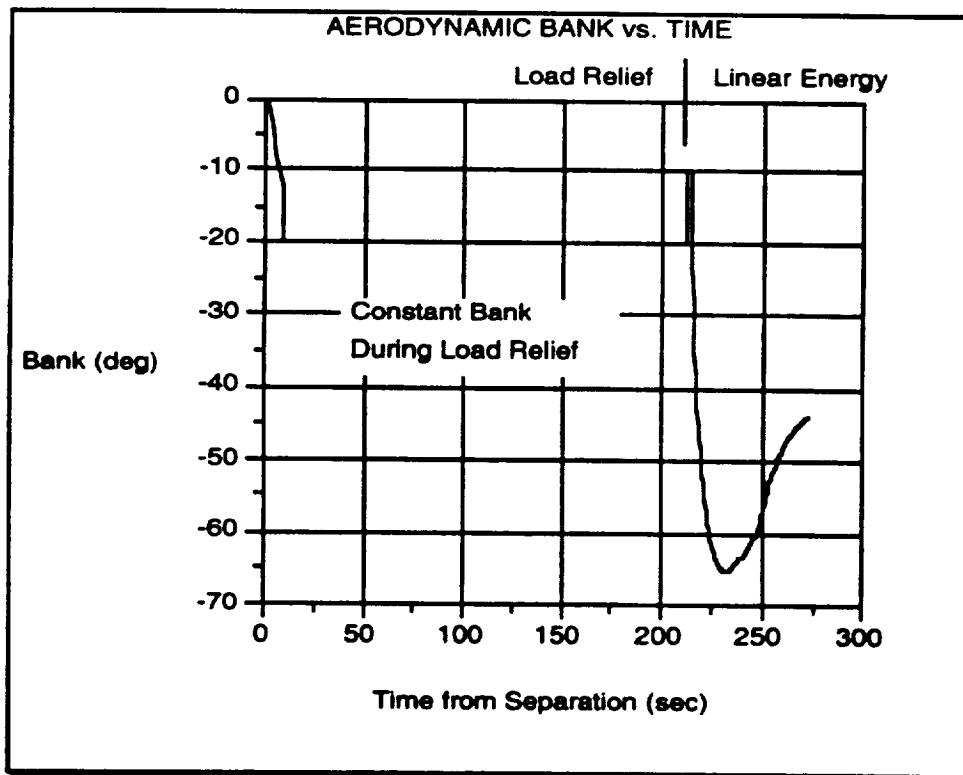


Figure 2.3.2-5 Commanded bank angle vs time.

After the linear energy event a 20° bank is maintained until the desired flyback azimuth is achieved. The turning angle required for this event is approximately 60°.

2.3.3 Cruise Mode

The cruise mode begins just before engine ignition, which occurs at an altitude of 25,000 ft. This altitude was chosen as an assumed upper limit for an air start of the air-breathing engine.

The air-breathing engine is capable of 72,000 lb maximum static sea level thrust with a thrust specific fuel consumption (TSFC) of 0.339 lb/(sec lb). The variation of thrust as a function of time can be seen in figure 2.3.3-1.

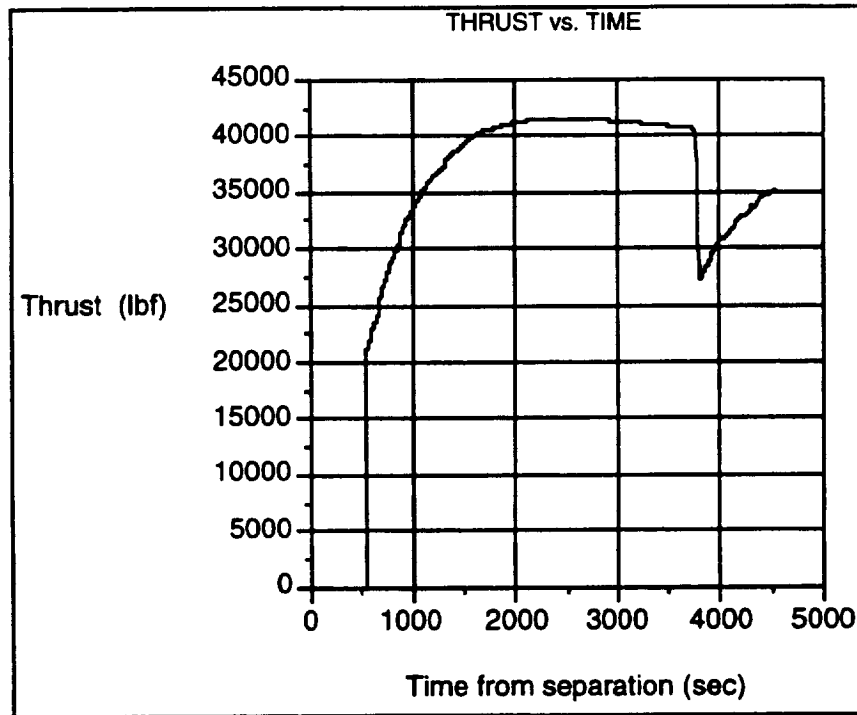


Figure 2.3.3-1 Thrust vs time.

The vehicle descends to the cruise altitude of 8,000 ft (figure 2.3.3-2). This altitude is maintained until a pre-determined range from the runway where the engine is throttled down and the vehicle descends on glide path to the 5,000-ft altitude loiter decision point. At this time the distance from the runway is 25 nm.

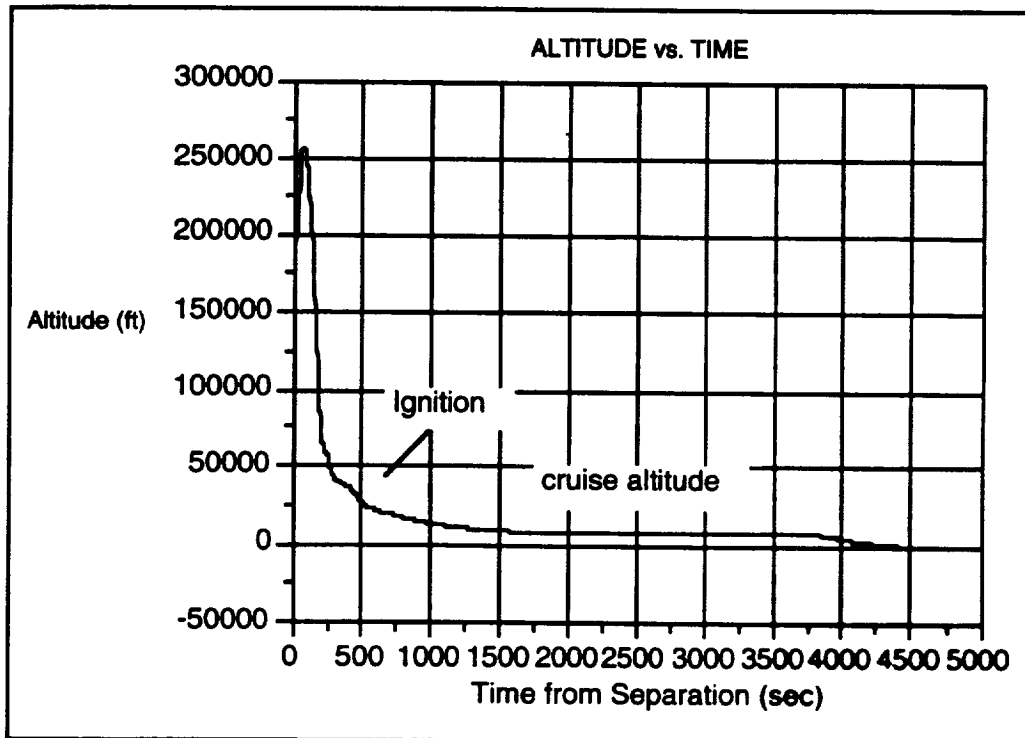


Figure 2.3.3-2 Altitude vs time.

2.3.4 Loiter Mode

At the loiter decision time, the ground can issue a command to continue to the runway. If no command is issued or a loss of communication occurs, the vehicle will enter a pre-determined holding pattern. This holding pattern will be maintained until ground commands a mode transition or an abort mode.

If a holding pattern command is issued, then the vehicle begins a series of pre-defined maneuvers. The holding pattern is defined by a 180° right bank maneuver at 3°/sec, followed by a 1.5-minute leg and then another 180° right bank maneuver. The holding pattern is completed by another 1.5-minute leg. The duration of the entire maneuver is 5 minutes and consumes approximately 1728 lb of propellant.

The vehicle will leave the holding pattern only when a ground command is received.

2.3.5 Landing Mode

The landing mode begins with the vehicle descending on glide slope to a point 15 nm from the runway threshold.

A bank for runway alignment is then executed, followed by final approach to the runway.

The first vehicle will flair, land, rollout, and taxi to a safe position to allow for the second booster to land. The second booster will then be commanded to exit the loiter mode and enter the landing mode.

References

³Wetzel, E. O. and Kotker, D. J., "Conceptual Design and Analysis of Hypervelocity Aerospace Vehicles, Volume 7 - Design Data Base"; AFWAL-TR-87-3056; February 1988.

⁴Harpold, Jon C.; "Analytic Drag Control Entry Guidance System"; JSC Internal Note 74-FM-25; April 15, 1974.

SECTION 3 CONFIGURATION

3.1 Design Goals

Although the LFBB study was focused on the development of a safe and cost-effective upgrade for the existing RSRMs, the strategic and economic importance of LFBB evolutionary paths for commercial and heavy-lift launch vehicle applications was recognized at the inception of the study. Two of the primary study objectives, reduced LFBB operational costs and a high probability of mission success, also benefit the commercial and heavy-lift LFBB evolution paths. Most of the key LFBB design parameters, however, were influenced by Shuttle integration and performance concerns.

The Shuttle application drove the LFBB design by imposing a set of interdependent requirements and constraints involving ascent performance, ascent aerodynamics and vehicle interfaces. For example, the contribution of the LFBB to the Shuttle ascent trajectory is driven by the fuel load, thrust history, mass fraction and Isp of the LFBB. The maximum fuel load, in turn, is related to the external dimensions of the booster. The external dimensions of the LFBB influence the design maximum dynamic pressure for the Shuttle ascent, which is an important factor in ascent performance. Other factors, such as the selection of the LFBB main engine, further complicate the design process by combining multiple performance variables such as Isp and throttle range. External interfaces with KSC processing and launch infrastructure and the Shuttle stack further constrained the LFBB design space.

The plan for the Pre-Phase A LFBB study, dictated by the inflexibility of many of the Shuttle integration factors, was to assess the feasibility of the Shuttle/LFBB concept and then determine the applicability of the Shuttle LFBB design to commercial and heavy-lift launch vehicle applications. Because of the high thrust levels and performance requirements for the Shuttle booster application, it was recognized that the resulting LFBB design would be better suited for medium and heavy-lift launch vehicle applications than for lower payload ranges.

The Pre-Phase A LFBB concept was designed to achieve the following objectives:

- Reduce Shuttle booster operations cost
- Increase Shuttle abort opportunities
- Increase Shuttle performance relative to the current RSRM baseline
- Increase the performance margins on the SSMEs and other Shuttle vehicle elements
- Target technology advancements that can be applied to other NASA programs
- Provide opportunities for alternate vehicle development (LFBB growth paths)
- Minimize required modifications to Shuttle elements
- Minimize the adverse environmental effects to the LFBB launch and landing areas
- Avoid the use of hazardous materials and fluids

3.2 Geometry Constraints

3.2.1 KSC Facilities Considerations (supplied by Roger Mathews/KSC)

KSC personnel identified and ranked Shuttle infrastructure constraints to the LFBB design from the VAB, Launch Pad 39, and the MLPs. The risk rating is a qualitative assessment of the likelihood that the LFBB design will impact the infrastructure constraint. A high risk rating means that it may be difficult to avoid violating the constraint while meeting the LFBB functional requirements, even with major design compromises. The risks are categorized as follows:

- 9 *KSC impact cannot be avoided*
- 7 *KSC impact can be avoided with major constraint to LFBB design*
- 5 *KSC impact can be avoided with constraint to LFBB design*
- 3 *KSC impact can be avoided with minor constraint to LFBB design*
- 1 *KSC impact can be avoided with little or no constraint to LFBB*

For the purpose of conducting trade-offs only at the conceptual stage, potential impacts to KSC facilities are categorized by cost as follows:

LOW	< \$2.0 M
MODERATELY LOW	\$2.0 M - \$10.0 M
MODERATELY HIGH	\$10.0 M - \$25.0 M
HIGH	\$25.0 M - \$50.0 M
VERY HIGH	> \$50.0 M

Vehicle Assembly Building

<u>Risk</u>	<u>Description</u>
7	The LFBB wing span is limited to #90 ft due to the width of the VAB transfer aisle, i.e., interference with the main load-bearing columns (ref. KSC-DD-186, Table 2-1). KSC IMPACT: VERY HIGH
7	The LFBB horizontal height (in tow) is limited to #50 ft due to entrance into VAB through the transfer aisle north door (ref. KSC-DD-186, Fig. 2-5). KSC IMPACT: LOW
7	Width of the overall vehicle stack is limited to #70 ft at an elevation of 60 ft above the MLP deck due to rollout through the VAB high bay east doors. KSC IMPACT: MODERATELY LOW
1	The LFBB must be lifted from the transfer aisle to the VAB high bay through the opening above the 16th floor crossover. The opening is 76' wide by 272' high (the Orbiter is currently rotated 45° for the 78' wing span to clear the 76' width). KSC IMPACT: HIGH
1	The current VAB crane limit is 325 tons. The LFBB and its lifting assembly must weigh less than this limit. KSC IMPACT: MODERATELY LOW

Launch Pad 39

<u>Risk</u>	<u>Description</u>
9	Any increase in diameter of the left-hand booster will interfere with the ET GH ₂ vent arm and supporting structure due to liftoff/drift clearances (ref. KSC-DD-186, Fig. 9-2). A significant increase in booster diameter combined with vehicle drift would interfere with the fixed service structure (FSS). KSC IMPACT: MODERATELY HIGH to VERY HIGH
9	Any increase in distance between the centerlines of the boosters will require some modifications to the flame trench/deflectors. A significant increase between centerlines will require a redesign of the flame trench and launch pad. Also, scale model testing will be required to verify exhaust flows. Gimbaling the booster engines inward from the null position until the vehicle clears the exhaust hole would help alleviate this problem, but may adversely affect vehicle drift. KSC IMPACT: MODERATELY LOW to VERY HIGH
9	Some structural modifications will be required on the rotating service structure (RSS) to allow mating the RSS with the Orbiter. The extent of the modifications will depend on the location of the wings on the LFBB (ref. KSC-DD-186, Fig. 12-2). KSC IMPACT: LOW to MODERATELY LOW

- 9 The drift envelopes for this vehicle must be within existing limits (ref. ICD-2-0A002) or interferences with GSE structure may result. The vehicle configuration combined with corresponding drift must be considered to minimize impacts.
KSC IMPACT: MODERATELY HIGH to VERY HIGH

Mobile Launcher Platform

- | <u>Risk</u> | <u>Description</u> |
|-------------|---|
| 9 | Any change to the boosters will require reconfiguring the exhaust holes in the MLP and redesigning the hold-down and release of the launch vehicle (ref. KSC-DD-186, Fig. 19-1).
KSC IMPACT: HIGH to VERY HIGH |
| 7 | The clearance between the Orbiter elevons and the MLP deck (*20 ft in the vertical orientation) is a constraint to the width of the LFBB aft wings unless they fall either outboard or forward of the Orbiter wings (ref. KSC-DD-186, Fig. 4-4). Locating the wings outboard or forward of the Orbiter wings may impact other areas (tower drift clearance or RSS mate, respectively). Raising the Orbiter relative to the MLP would dramatically change virtually every interface between the vehicle and ground.
KSC IMPACT: MODERATELY HIGH to VERY HIGH |
| 5 | LFBB aft wings will interfere with the tail service masts (TSMs) unless they are located outboard of $Y_0^a \pm 400$ to provide clearance for the TSM between the Orbiter aft umbilical interface and LFBB aft wings (ref. KSC-DD-186, Fig. 19-1).
KSC IMPACT: MODERATELY HIGH |

General Design Guidelines

- Relative position of the Orbiter and ET to the MLP and launch pad should remain unchanged. Any change in position of the vehicle relative to the ground will have extensive impacts to all access and servicing interfaces.
KSC IMPACT: VERY HIGH
- LFBB bending stiffness will have a major effect on vehicle excursions during SSME thrust buildup. If these excursions are larger than the current baselines (ref. ICD-2-0A002), then every umbilical interface will have to be modified and requalified for flight.
KSC IMPACT: MODERATELY HIGH to HIGH
- GOX vent for boosters should be located in a position where overboard dump will not pose ice hazard to Orbiter TPS. Otherwise, GO₂ vent umbilicals will be required for boosters.
KSC IMPACT: MODERATELY HIGH
- Rebound loads due to LFBB engine shutdown are a concern. MLP may require additional support (Apollo extensible columns) or modification. A rough estimate of these loads is needed for an early assessment.
KSC IMPACT: MODERATELY LOW
- Requirements for on-pad access to the LFBBs from the north (-z₀ direction) should be avoided if at all possible. No fixed access currently exists and to provide fixed access from this side of the vehicle would interfere with liftoff because of northerly drift due to canted SSMEs. Some temporary, light access could be provided from the north for contingency operations.
KSC IMPACT: LOW to HIGH
- POGO effects will be of concern for the LFBB. However, any contributions to the POGO effect due to the launch mount will be mitigated by the design of a new hold-down and release system.
KSC IMPACT: NONE

3.2.2 Aerodynamic, Aerothermal, and Performance Considerations

Guidelines from previous aerodynamic analyses were used to establish the maximum LFBB dimensions of 18 ft in diameter and 170 ft in length. The maximum diameter was selected based upon results from MSFC wind tunnel tests, which indicated that the allowable wing loading on the Orbiter would be exceeded for booster diameters greater than 18 ft. The MSFC data also showed that the maximum allowable dynamic pressure during Shuttle ascent would have to be reduced for booster diameters in excess of 16 ft. The booster length limit of 170 ft was based upon previous Shuttle LRB studies that identified several design breakpoints versus booster length based upon facility constraints and Shuttle aerodynamic interference factors. Booster lengths greater than 170 ft would require modification of the launch pad GO₂ vent arm. Booster lengths greater than the current RSRM length (149.2 ft) would significantly change the shock wave patterns and aerodynamic heating on the Shuttle during ascent.

One of the key LFBB configuration decisions, the location and orientation of the wing, is driven by a combination of physical constraints (facilities and Shuttle integration) and performance factors. As the Space Industries, Inc., booster configuration shows, fixed LFBB wings that are oriented normal to the Orbiter wings are severely constrained both in wing chord and in axial location, and protrude into launch pad areas currently occupied by the TSMs and the RSS. At the point where the LFBB wings pass under the Orbiter wings, the LFBB wing chord is limited to approximately 20 ft between the trailing edge of the Orbiter elevons and the MLP deck. The wings must also be located at the extreme aft end of the LFBB, which results in a need for large canards for pitching moment control, even with an aft LFBB center of gravity location. As the wing is rotated about the longitudinal axis of the LFBB to bypass the wing chord constraint, launch tower clearances come into play. The LFBB wing chord must be increased to compensate for the reduction in allowable wing span, which increases the expected interference effects with the Orbiter wing. As the wing is rotated even more to provide clearance between the LFBB wings and the Orbiter wings (towards a parallel Orbiter/LFBB wing orientation), the launch tower further constrains the maximum LFBB wing span and the ET begins to influence the required wing dihedral. A fixed LFBB wing that is "parallel" to the Orbiter wing is severely constrained in span by the proximity of the FSS and by the centerline distance between the two LFBBs (approximately 46 ft). The result is a low-aspect ratio wing with a large root chord, which raises aerodynamic interference concerns with the ET during ascent. For a parallel wing attached to a 16-ft diameter LFBB, the required dihedral for ET clearance is estimated to be in the range of 25° to 30°. Figure 3.2.2-1 depicts the geometry constraints placed on the LFBBs by the FSS and Shuttle.

The orientation of the main engines for a multi-engine booster configuration is closely tied to other LFBB configuration decisions, such as the wing location and orientation relative to the overall Shuttle launch configuration. Landing considerations favor a parallel orientation of the LFBB engines and wings because that orientation minimizes the length of the main landing gear to provide a given tail drag α . The aft flare section also provides separation of the main landing gear for crosswind stability. Finally, a parallel engine/wing orientation reduces the vertical towing height of the booster. From the standpoint of integrating the LFBB with the Shuttle launch configuration, the LFBB engine orientation was not a factor. KSC reviewed two LFBB engine orientations relative to the engine exhaust cutouts on the MLP deck and concluded that both orientations would require significant structural modifications (figure 3.2.2-2).

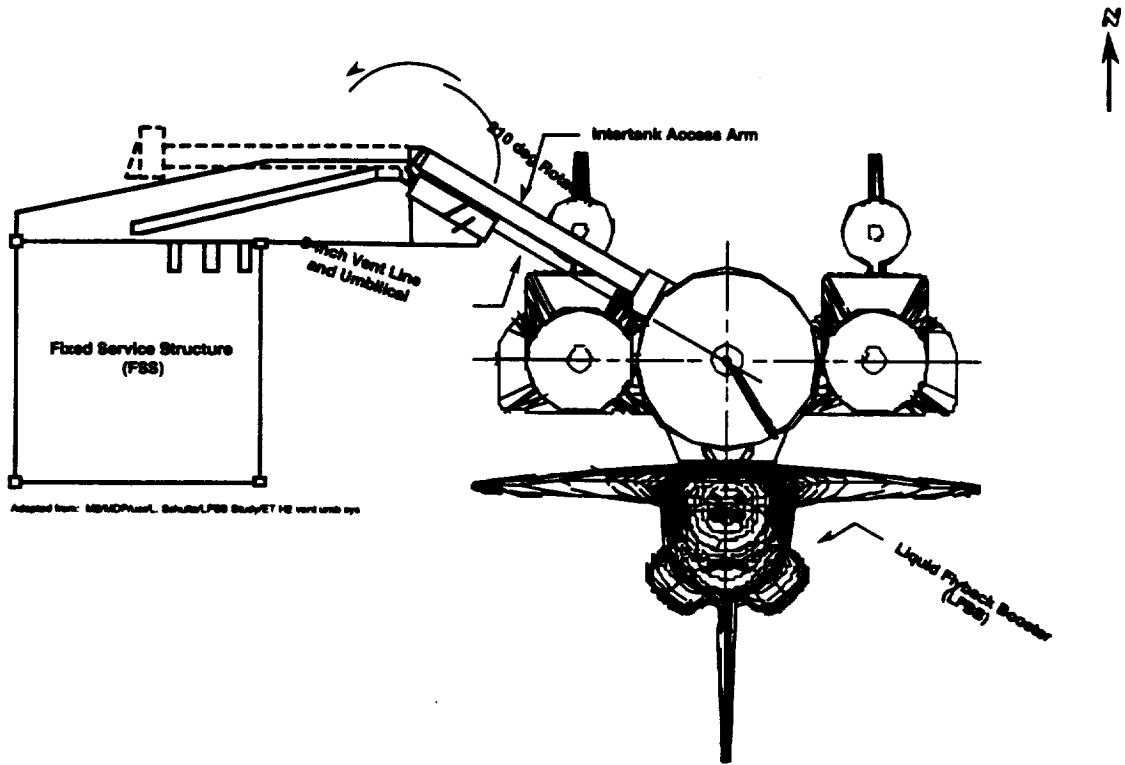


Figure 3.2.2-1 Fixed service structure and umbilical geometry.

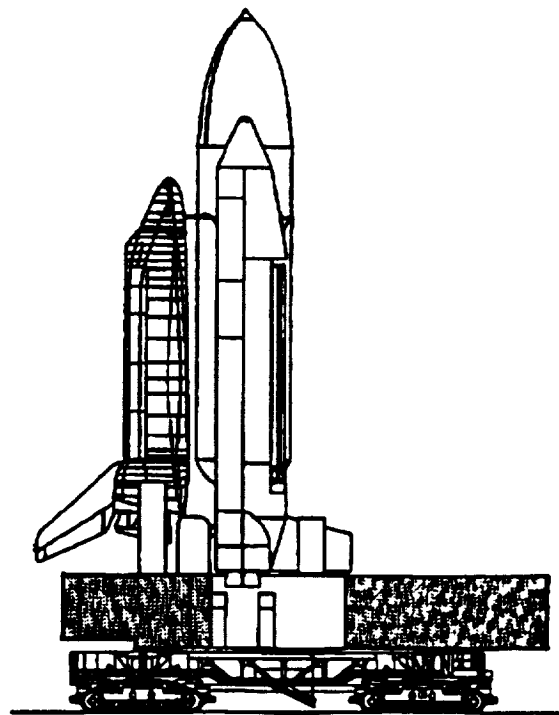


Figure 3.2.2-2 Mobile launch pad and Shuttle geometry.

3.3 Options Considered

A configuration design team, including aerodynamics and trajectory specialists, was assembled early in the study to narrow the range of LFBB configuration options. The following factors were felt to be the primary design drivers for the LFBB aerodynamic configuration:

- Cruise and landing mass properties
- Dynamic pressure at landing, which is a function of:
 - desired landing speed
 - nominal atmospheric conditions at landing
- Coefficient of Lift (CL) at landing, which is primarily a function of:
 - wing geometry
 - landing α
 - lift augmentation devices/strategies
- Lifting surface geometry constraints
- Ascent aerodynamic and aerothermal effects for the integrated vehicle (ET, Orbiter and LFBBs)

One of the key initial design considerations was the size of the LFBB wing in relation to the design landing speed. Note that for commercial aircraft the approach and landing speeds are typically 1.3 and 1.15 times the stall speed, respectively. Assuming a sea level atmosphere, the three primary variables in the lift equation are wing area (S), coefficient of lift (CL) and airspeed (V):

$$\text{Lift} = (1/2 \cdot \rho \cdot V^2) \cdot S \cdot CL \quad (\text{eq. 3.3-1})$$

Using equation (3.3-1) and a design sea level touchdown speed of 170 knots, a matrix of wing area solutions was generated by varying the LFBB design landing weight and lift coefficient (table 3.3-1).

Table 3.3-1 Matrix of LFBB Wing Areas

	W=175,000 lbf	W=200,000 lbf	W=225,000 lbf	W=250,000 lbf
Design Landing CL	LFBB Wing Area (ft ²)			
0.5	3582	4094	4605	5117
0.6	2985	3411	3838	4264
0.7	2559	2924	3290	3655
0.8	2239	2559	2878	3198
0.9	1990	2274	2559	2843
1	1791	2047	2303	2559
1.1	1628	1861	2093	2326
1.2	1493	1706	1919	2132
1.3	1378	1575	1771	1968
1.4	1279	1462	1645	1828
1.5	1194	1365	1535	1706
1.6	1119	1279	1439	1599

The maximum landing CL is driven by several factors including wing geometry, landing α and control surface deflections. Based upon a preliminary aerodynamic assessment of a high-aspect ratio wing configuration, it was felt that a landing CL in the range of 1.3 to 1.6 could be achieved at reasonable angles of attack using simple flaps. The weight of the LFBB at landing was estimated to be approximately 250,000 lbf, which translates to a wing area in the range of 1,600 to 2,000 ft². Later refinements of the LFBB configuration resulted in a selected wing area of 1,750 ft².

A variety of aerosurface options were considered by the configuration team. The options, several of which are illustrated in Figure 3.3-1, fell into four main categories:

- Fixed wing
- Swing wing
- Flexible deployable wing
- Rigid deployable wing

Every effort was made to develop a feasible fixed wing LFBB configuration because of the structural advantages and simplicity of the traditional design approach. The most practical fixed wing configuration closely resembled the Space Industries, Inc., booster, with the LFBB wings oriented perpendicular to the Orbiter wings and located at the aft end of the booster. Unfortunately, the fixed-wing configuration violates several of the geometry constraints identified in section 3.2.2 and also raises serious concerns about ascent aerodynamic loading on the Orbiter and ET. Alternative versions of the fixed wing concept, such as a standoff wing, did not appear to offer any significant advantages.

Because the LFBB must operate in both the supersonic and subsonic flight regimes, the team considered a swing wing design similar to that used on the B-1 and F-14 military aircraft. The swing wing concept was eliminated by the aft center of gravity location of the LFBB during reentry and flyback. Early estimates placed the LFBB center of gravity at 70% to 75% of body length, which was too far aft for an effective swing wing design. The complexity and weight of the swing mechanism, which must operate under aerodynamic load, also outweighed the advantages of the swing wing concept for an LFBB application.

Flexible deployable wings, such as parafoils and parawings, offer superior packaging flexibility and improved Shuttle ascent aerodynamics relative to rigid wing concepts. However, flexible deployable wings also require complex control systems, and are unproven for the soft landing of massive aerospace vehicles. Parafoils and parawings were eliminated from consideration due to their high technical risk.

Several rigid deployable wing concepts were considered including folded wings, ring wings, oblique wings and scissor wings. Folded wings have a hinge line along the wing chord to enable the wing to unfold from a stowed to a deployed position. Ring wings can be considered to be a subset of the folded wing concept in which the wing is wrapped around the vehicle fuselage in the stowed configuration. Ring wings offer the best packaging characteristics of the rigid deployable wing class, but are not appropriate for high-lift, high angle-of-attack applications. The oblique wing concept, a one-piece wing which pivots about a central axis normal to the wing planform, enables alignment of the wing with the LFBB fuselage during ascent to minimize aerodynamic interference. An oblique wing is not applicable to the current LFBB concept, however, because the aft center-of-gravity location of the vehicle severely limits the allowable wingspan. The scissor wing concept, the eventual choice of the configuration team, is a version of the oblique wing concept in which the wing is split into two sections which are both pivoted forward when stowed. Like the oblique wing, the scissor wing concept removes the wings from the Shuttle ascent aerodynamic environment, but at some increase in overall complexity and weight.

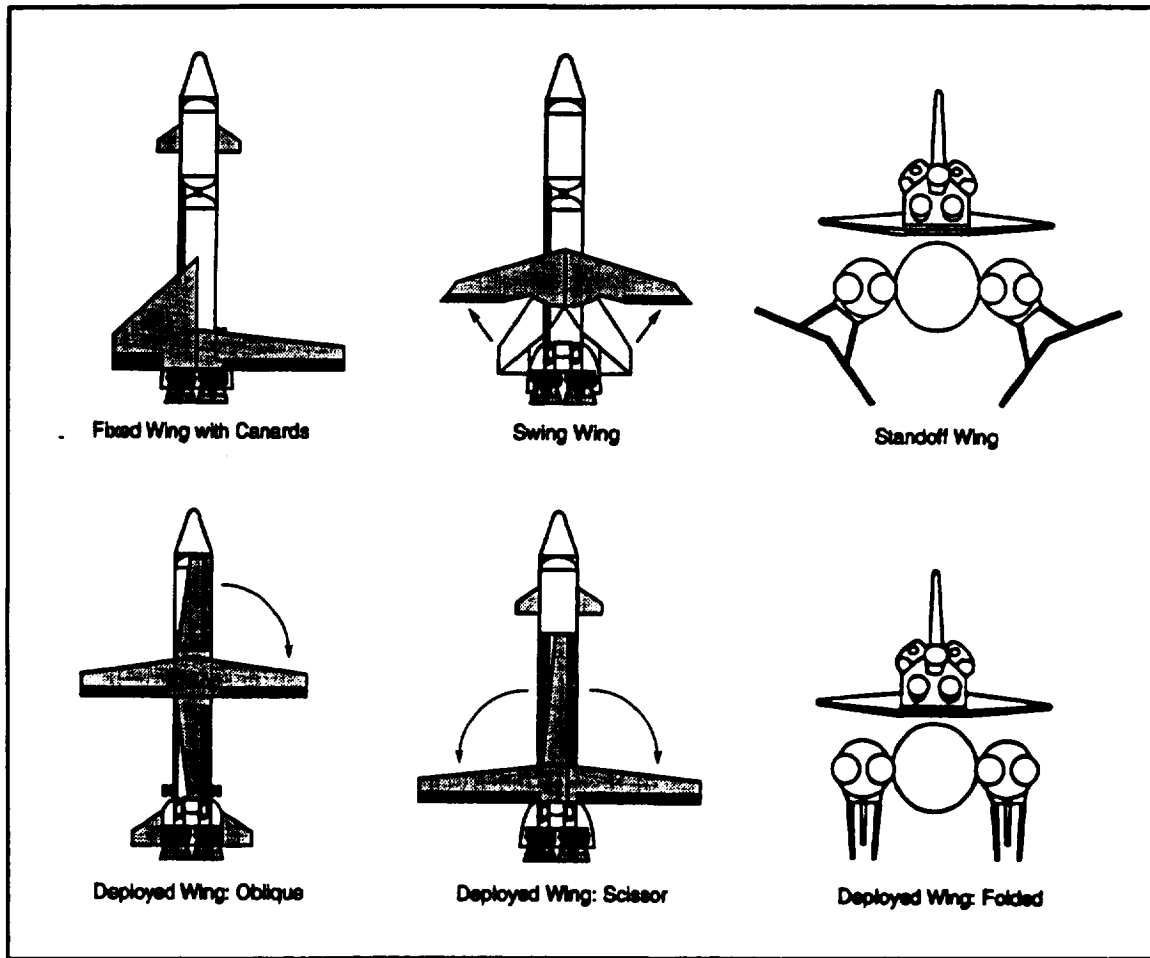


Figure 3.3-1 LFBB configuration options.

A deployed wing has several advantages over a fixed wing for a recoverable booster application, not the least of which is a clean ascent moldline. Stowing the wing along the booster fuselage greatly simplifies the integrated ascent aerodynamics for the launch vehicle and reduces the loads that would otherwise be generated from the exposed wings during ascent. For the Shuttle application, in particular, there were concerns that excessive loads would be transferred from the LFBB to the ET from wind gusts and non-symmetric airflow over the wings during ascent. As a consequence, an LFBB with deployed wings should offer improved launch probability and greater performance margins (e.g., higher allowable maximum dynamic pressure) than a comparable fixed wing booster. A deployed wing also offers packaging efficiency and flexibility, which reduces the resources required to adapt existing ground processing and launch infrastructure to the LFBB.

The desire for a moderate LFBB landing speed led to the requirement for a canard or tail for pitch trim control. Aerospace vehicles without auxiliary pitch trim aerosurfaces (e.g., Shuttle Orbiter) cannot generate high lift coefficients at reasonable landing angles of attack. The addition of a tail or canard for trim control enables an aircraft to use flaps to achieve reduced landing speeds. The aft LFBB center-of-gravity location during flyback and landing strongly favors the use of a canard because the size of the aerosurface is inversely related to the length of the moment arm. In order to preserve the favorable Shuttle ascent aerodynamics provided by the deployable wing concept, the canards are also stowed on top of the LFBB fuselage during ascent. To minimize the effects of the reentry heating environment, the canards are deployed after the LFBB has decelerated to low supersonic speeds.

Because of the physical constraints imposed on the LFBB fixed wing configurations and the uncertainty associated with the potential Shuttle/LFBB ascent aerodynamic interference effects, the decision was made to focus on rigid deployable wing and canard configurations in the Pre-Phase A LFBB feasibility study. The purpose of this study was to gain a better understanding of the LFBB subsystem design requirements and Shuttle/LFBB integration issues, as well as to evaluate the commercial and heavy-lift launch vehicle applications of the resulting LFBB design. A wide range of configurations should be considered in Phase A of the LFBB program.

3.4 Description of Selected Configuration

The LFBB integrated with the Orbiter and ET is shown in figure 3.4-1. When integrated into the Shuttle system, the LFBB's location is similar to the current RSRM's, with the booster's wings and vertical tail facing the -z (ET coordinates) direction. This orientation avoids having any protuberances on the Orbiter side of the ET, and thus minimizes impacts to the aerodynamic loads on the Orbiter during ascent.

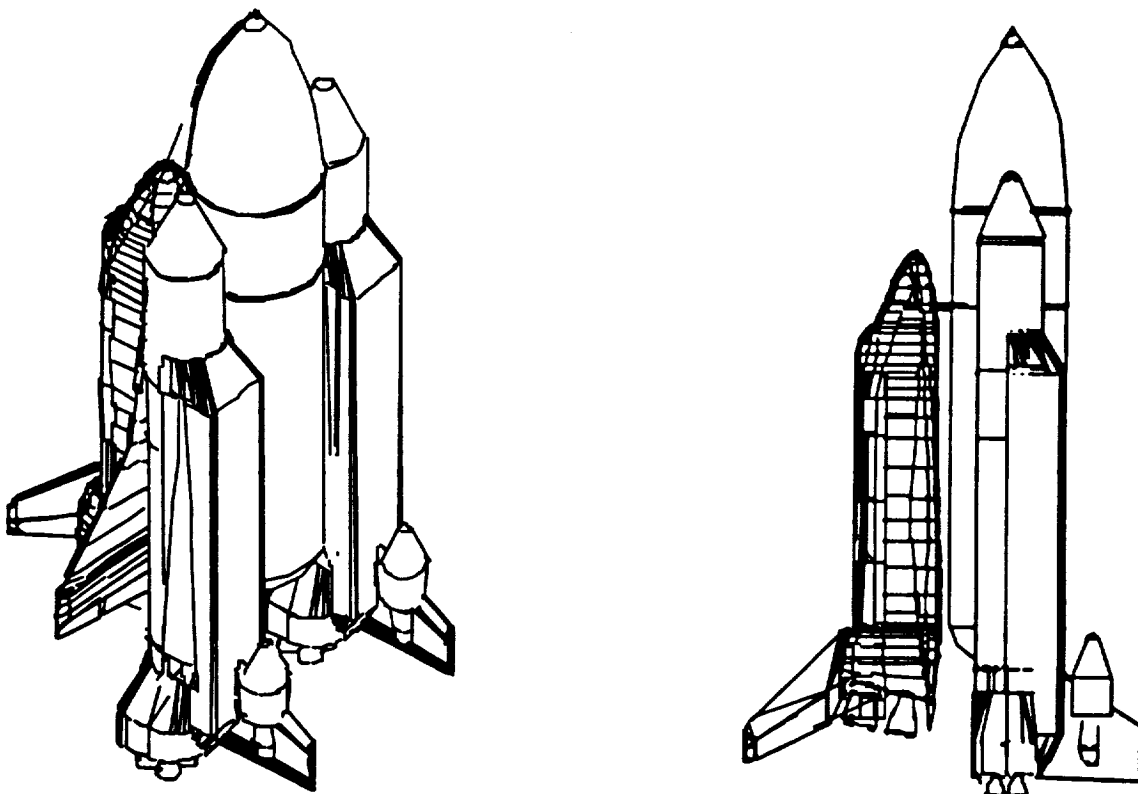


Figure 3.4-1 LFBB with Shuttle.

The LFBB is 150 ft long from its nose to the exit plane of its main engines, and the tank outer diameter is 16 ft. Deployable wings and canards located on top of the booster are covered by an expendable fairing that is jettisoned after booster separation and before wing deployment. A vertical tail with an air-breathing engine is also located on top of the booster. An aft skirt, with a maximum diameter of 25 ft, forms an aft compartment that contains the main engines, thrust structure, and bulk of the booster's subsystems. The basic shape and dimensions of the booster in its ascent configuration are shown in figure 3.4-2.

LFBB Ascent Configuration
All dimensions in inches

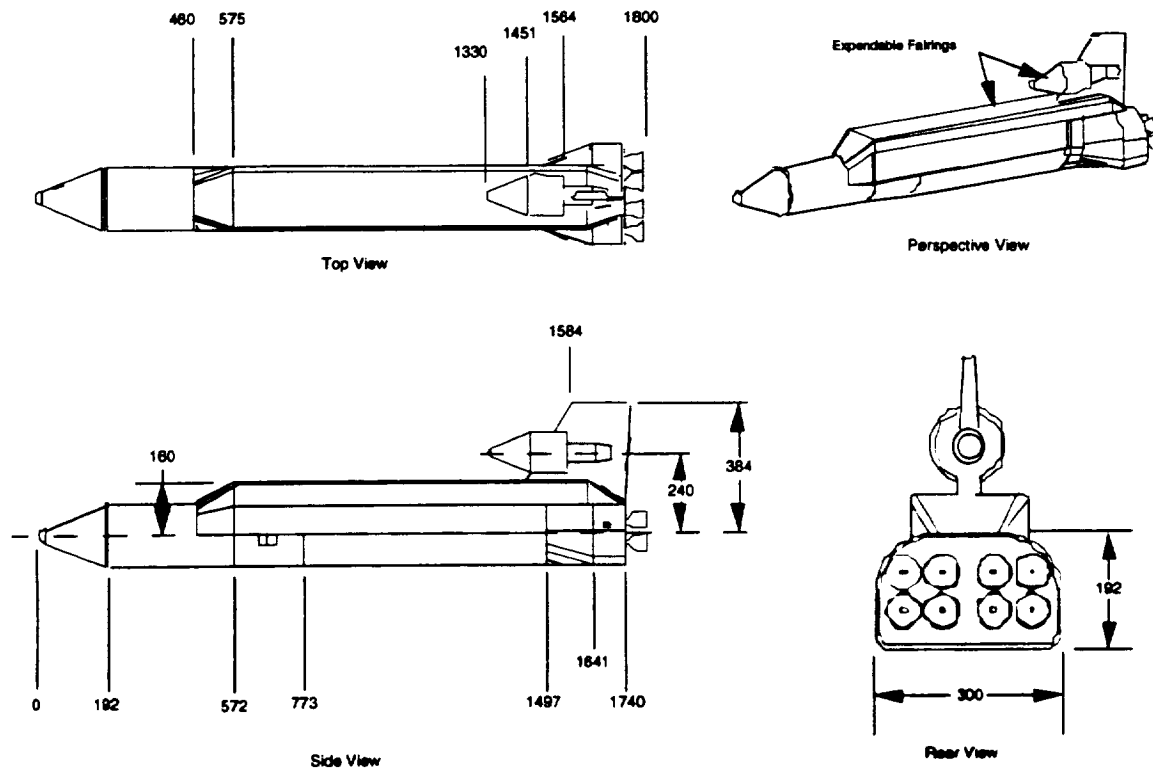


Figure 3.4-2 LFBB ascent dimensions.

After the boosters have provided their ascent impulse, they separate from the Shuttle by explosive bolts and are pushed away from the Shuttle using solid rocket motors located on the booster. The boosters continue upward until they reach a peak altitude, then begin descending. The fairing covering the wings and canards is jettisoned, and the wings are deployed at low dynamic pressure and loading. After reentry into the atmosphere and achieving appropriate flight conditions, the fairing covering the air-breathing engine is ejected, the engine is started, and the vehicle begins its powered return flight to the launch site. Landing occurs on a runway similar to normal aircraft. Figures 3.4-3 and 3.4-4 show the LFBB in its landing configuration, and the cross sections of the booster's body at various stations.

LFBB Landing Configuration
All dimensions in inches

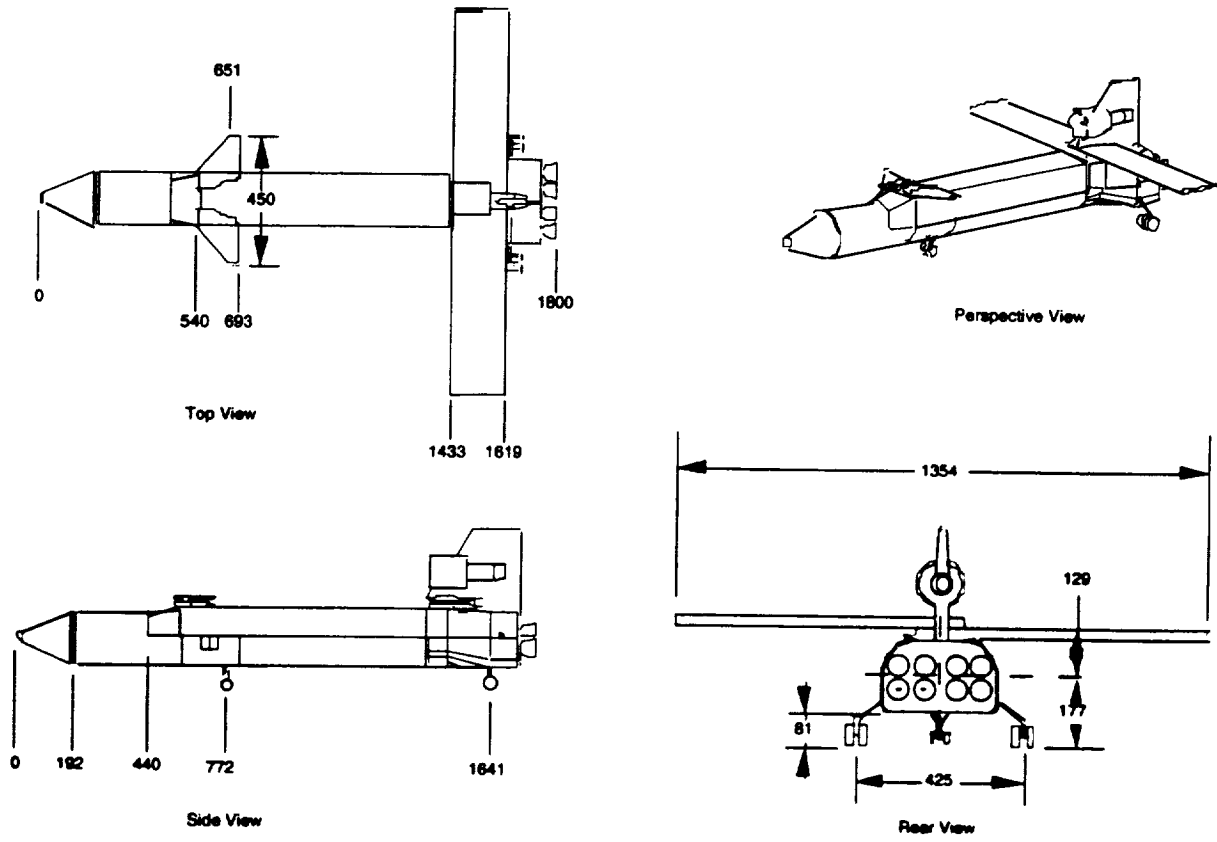


Figure 3.4-3 LFBB landing dimensions.

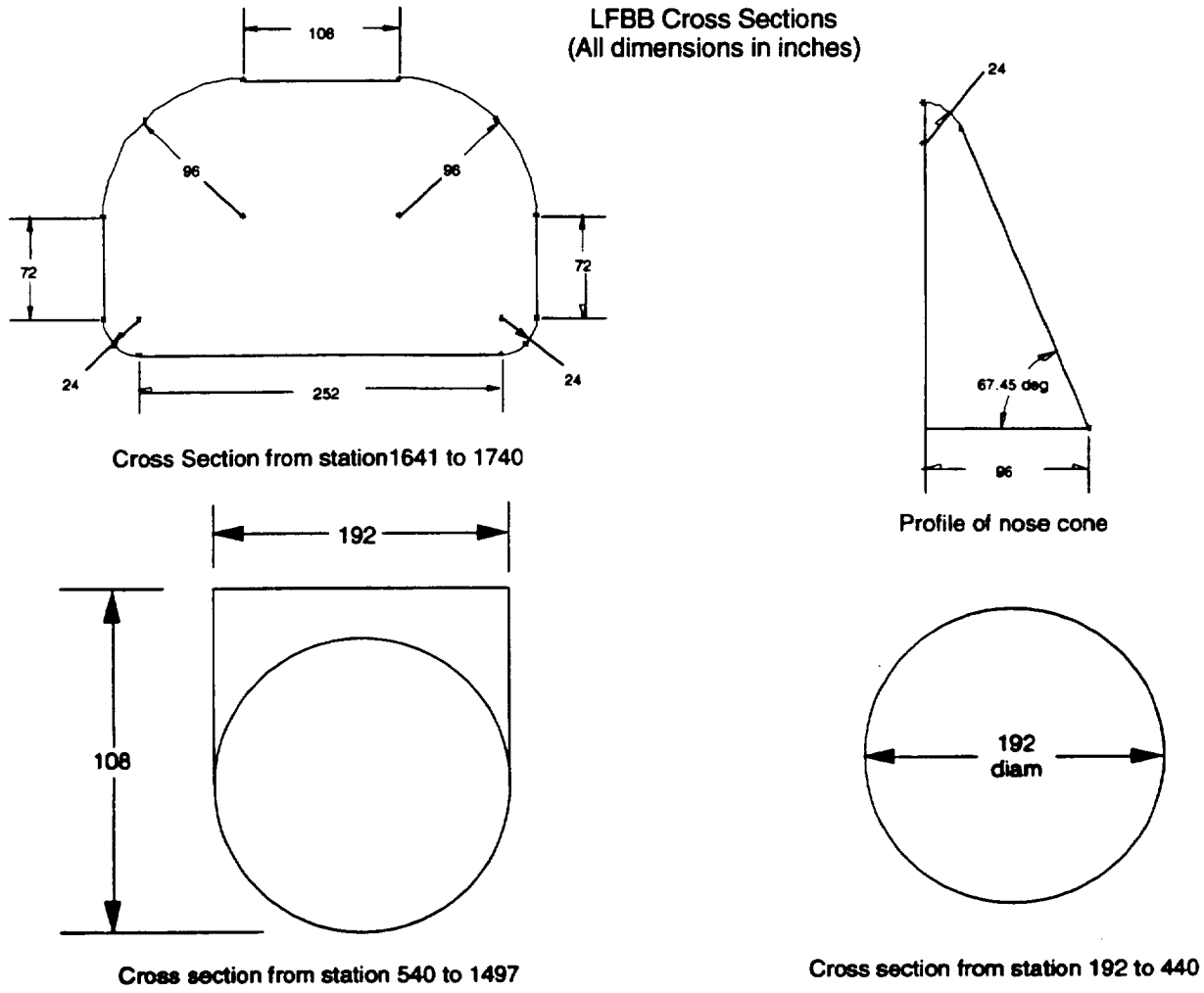


Figure 3.4-4 LFBB cross sections.

The major components of the LFBB include: folding wing and canard assemblies; a vertical tail; primary structure in the form of tanks, an intertank structure, and aft skirt; secondary structure for attachment of aerodynamic fairings; ascent, reaction control, air-breathing, and booster separation propulsion systems; avionics bays; and landing gear. Figure 3.4-5 shows these major components and their relative locations.

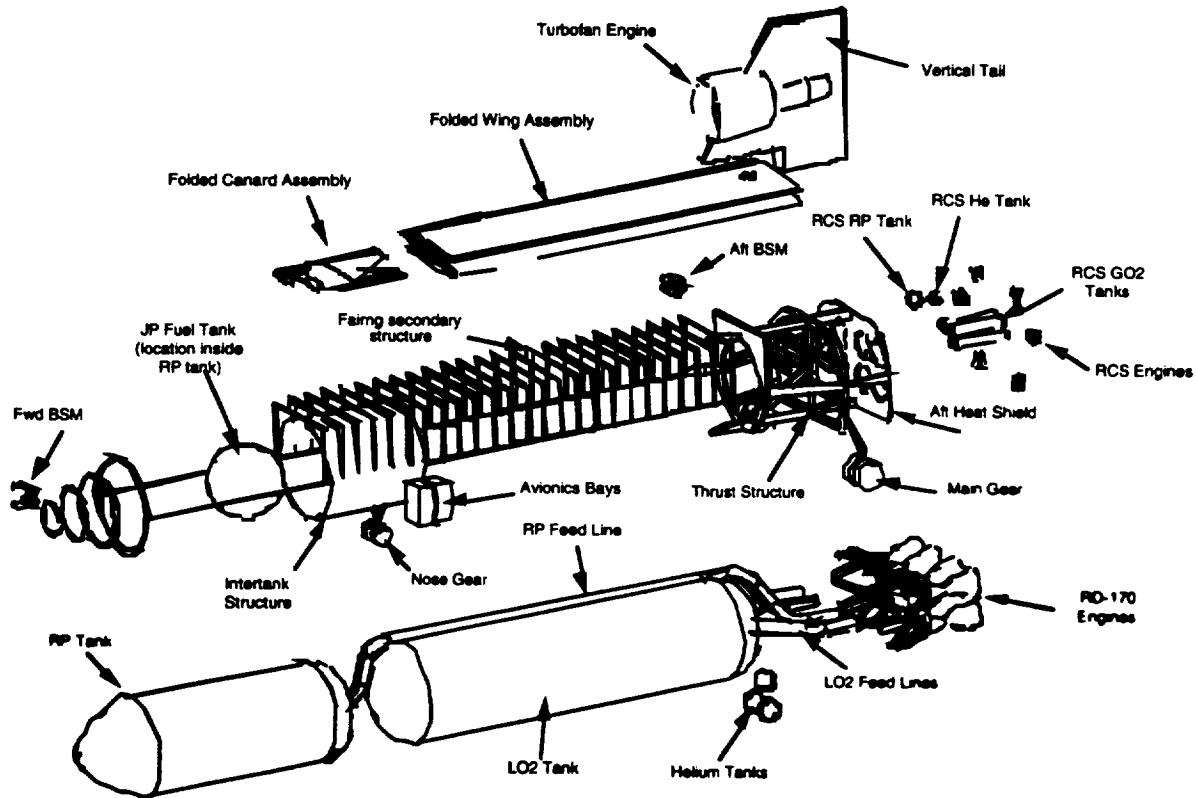


Figure 3.4-5 LFBB exploded view.

A deployable wing assembly is used to minimize impacts to Shuttle ascent aerodynamics and loads. A scissor folding style is used so that the wing is located aft of the booster's cg in its deployed configuration, and located on top of the booster in its stowed configuration. When deployed, the wing has a reference planform area of 1750 sq ft, a constant chord length of 15.5 ft, and span of 112.8 ft. Ailerons, located at the wing's outboard trailing edge, provide roll control. Elevons, located at the wing's inboard trailing edge, can be extended to increase the lift coefficient, thus lowering stall speed. The wing was sized for a landing speed of 170 knots.

Because the booster's cg location is at approximately 75% of the booster's length, a relatively large horizontal tail would be required to provide pitch control during the return flight. A large horizontal tail would interfere with existing Shuttle vehicle geometry, the launch platform, and tower. Therefore, pitch control is provided by canards that have a controllable incidence angle. During ascent, the canards fold together on top of the booster's body. Deployable canards are required in order to avoid serious detrimental effects to the Shuttle ascent aerodynamics that would be caused by protrusions ahead of the Orbiter.

An expendable fairing is used to protect the folded wings and canards during ascent. It may be possible to design the booster such that this fairing is not required. However, this may require an increase in wing structure mass to provide sufficient stiffness during ascent, an increase in wing TPS mass to handle the different heating environment, and possible adverse affects on the ascent aerodynamics of the Shuttle. A study to trade these impacts versus the operations costs associated with an expendable shroud is needed to answer these questions. For this phase of the study, it is assumed that the wing fairing is required.

A vertical tail with controllable rudder located on top of the booster provides lateral stability and yaw control. When the booster is integrated with the Shuttle, the vertical tail is located below the Orbiter and extends in the -z (ET coordinates) direction. This orientation will not generate any severe impacts to ascent aerodynamic loads on the Orbiter.

Axial, bending, shear, and torsion loads on the booster are carried through the RP tank, intertank, and LO₂ tank structure. Structural hard points for the wing and canard attachment are located in the aft skirt and intertank areas, respectively. All structure is designed to accommodate thermal contraction due to cryogenic LO₂ loading and expansion due to aerodynamic heating.

The RP tank is located at the forward end of the booster, in front of the intertank. The tank is cylindrical, with an ogive forward dome and elliptical aft dome. The tank is of skin-and-stringer construction and is 16 ft in diameter and 46.5 ft long. The ogive dome extends into the booster nose cone, but leaves enough volume in the cone for the booster separation motors and forward avionics bay. RP propellant is fed to the main engines by a single feed line that starts at the aft dome of the tank, curves up and around the forward dome of the LO₂ tank, and runs along the side of the LO₂ tank. The feed line splits into branches in the aft compartment to carry the propellant to each engine.

The intertank structure provides the structural connection between the RP and LO₂ tanks. It is a cylindrical member of skin-and-stringer construction, is 16.8 ft long and 16 ft in diameter. The intertank has cut-outs for the nose landing gear, main avionics bays, and RP feed line.

The LO₂ tank is located aft of the intertank. This tank is cylindrical with elliptical end domes. The tank is of skin-and-stringer construction and is 16 ft in diameter and 66.6 ft long. LO₂ propellant is fed to the main engines through four feed lines extending from the tank's aft dome.

The aft skirt provides the base for the booster to sit on the launch pad, carries thrust and hold down loads, provides attach points for the wing and vertical tail, and forms the aft compartment which houses the majority of the LFBB systems. The primary structure of the aft skirt is a space truss, which supports the weight of the booster, holds the booster to the pad during engine startup, and provides for the attachment of the main engines. Concentrated loads from the main engines, vertical tail, and wings are distributed to the LO₂ tank, where they can be distributed to the rest of the vehicle structure. The space truss is designed to be self-supporting, so that the aft skirt skin can easily be removed. This allows open access to the subsystems in the aft compartment, enhancing servicing and maintenance operations.

Minor frames spaced along the top of the booster provide for the attachment of the expendable fairing that covers the wing and canards during ascent. These frames also provide support for a fairing that covers the top and sides of the booster intertank and LO₂ tank. The RP and JP fuel feed lines, data lines, and electrical cables are routed underneath this fairing.

All of the reaction control system (RCS) propulsion components are located in the aft compartment. The RCS components include the thrusters, 3 cylindrical gaseous oxygen (GO₂) tanks, 1 spherical RP fuel tank, and 1 spherical helium tank. The thrusters are arranged around the perimeter of the aft skirt, and provide attitude control until the booster's aerodynamic surfaces achieve sufficient effectiveness. The GO₂ tanks are located in the upper portion of the compartment, with the helium and RP tanks located just below the GO₂ tanks. By locating the thrusters around the aft portion of the booster, firing the jets will have less of an effect on the aerodynamics of the vehicle during reentry than if they were located further forward. Locating the tanks in the aft compartment provides a relatively short and direct propellant route from the tanks to the thrusters.

The air-breathing fuel (JP) tank is a 11.6-ft-diameter spherical tank located inside the main RP tank. This location allows the storage of a large volume of JP fuel without affecting the booster outer mold line to a large degree. It also provides the possibility of evolution to the use of RP from the same tank for the main engines and the turbofan engine. Due to the large volume of JP fuel required, there is not sufficient room to store it in the vertical tail. Storage inside the wings was considered, but the scissor-folding scheme would require a complex system to acquire the fuel and route it to the turbofan engine.

A single turbofan engine is located in the booster's vertical tail. During ascent, an aerodynamic fairing will protect the engine inlet. The cover will be jettisoned before the turbofan engine is started.

Booster separation motors (BSMs) provide the impulse required to move the LFBB away from the Orbiter/ET after separation. Forward and aft assemblies, each consisting of 4 solid motors, are used. The forward assembly is located in the nose cone, and the aft assembly is located in the aft skirt. Each assembly is similar in size to the BSM assemblies used on the current RSRM.

The main avionics bays are located in the intertank structure. The bays are located on the side of the booster to provide unobstructed access while the booster is on the ground and while it is integrated with the Shuttle on the launch pad. The main bays contain most of the components required for navigation, data management, communications, and power generation. Some data management components will be located in the aft compartment, and some navigation equipment will be located in the nose of the booster. Antennas can be located in the nose cone, intertank area, and aft compartment. The main path for routing data and electrical lines will be between the LO₂ tank and the aerodynamic fairing underneath the wing.

The main landing gear (MLG) is located 1485 inches aft of the nose of vehicle and folds up into the aft compartment. With this location, tail scrape occurs at 32°. External pods that would be mounted on the side of the LO₂ tank to contain the MLG were considered as an alternative to locating the gear in the aft compartment. However, the cg location limits how far forward the MLG can be located. Moving the MLG forward 10 ft reduces the tail scrape angle to 14°. Since this is close to the landing α , the MLG would have to be longer to enable a forward location. The MLG would still be in the aft skirt of the vehicle even if moved forward 10 ft. Therefore, external pods for the landing gear were not selected.

Locations considered for the nose landing gear (NLG) include the intertank and the nose cone. There is not enough room to locate the NLG in the nose cone because the RP tank uses most of the available volume. Booster separation motors and forward avionics (such as the air data system) also occupy space in the nose cone. Moving the RP tank aft to make room for the NLG in the cone is not practical since the minimum spacing between the RP and LO₂ tanks is defined by the allowable curvature of the RP feed line. Intertank spacing could be reduced by having the RP feed line run directly through the LO₂ tank, but this is an undesirable requirement on the propulsion system. Therefore the nose gear is stowed in the intertank structure.

The LFBB configuration described above was used as a reference for subsystem definition and integration, estimation of mass properties and vehicle performance, and identification of impacts to the Orbiter, ET, and existing ground facilities. The configuration meets the requirements and satisfies the constraints given for this phase of the LFBB study. In future work, variations of this configuration, as well as different configurations, can be investigated.

SECTION 4 AERODYNAMICS AND AEROTHERMODYNAMICS

4.1 Aerodynamic & Aerothermodynamic Assessments

In support of the LFBB Pre-Phase A study, aerodynamic and aerothermodynamic evaluations of the proposed vehicle were conducted in a variety of areas. Included were "aerodynamic" configuration trade studies and development (e.g., wing, canard, vertical tail type, size and shape). Proposed vehicle aerodynamic characteristics were also determined using the Aerodynamic Preliminary Analysis System II (APAS II). Introducing any new element to the Shuttle will impact the system. In the case of a new booster, aerodynamic impacts to the Orbiter wing loads are a major concern. A preliminary assessment of these impacts was performed using a high fidelity computational fluid dynamics (CFD) analysis tool. Aerodynamic deltas to the Orbiter and ET were calculated for a proposed ascent configuration at Mach 1.25. These results were forwarded to the loads group for more detailed evaluation. Additionally, an aerothermodynamic analysis of the LFBB configuration for a nominal ascent and entry trajectory was completed. The calculated heating rates were provided in support of TPS design trade studies. Finally, in support of ascent performance calculations, inputs concerning existing Shuttle constraints were provided by the Space Shuttle Program Ascent Performance technical manager.

4.2 Preliminary Aerodynamic Configuration Trade Study and Development

The objectives in the design of the entry and landing configuration are to provide a feasible and workable configuration that minimizes ascent aerodynamic impacts to the Shuttle, is trimmable throughout the entry flight regime, and does not interfere with current Shuttle vehicle elements or launch tower structure. The general ground rule, to minimize impacts to the Orbiter and ET, was a principle configuration driver. Additional constraints which drive the end design are vehicle mass properties (weight and cg) and a specified landing speed of 170 knots.

4.2.1 Design Philosophy of the Scissor Wing Concept

During supersonic and hypersonic entry flight, the main function of the vehicle is to turn the velocity vector back toward the landing site and slow to subsonic flight conditions for ABE ignition and cruise return to launch site. A configuration with a high drag-to-weight ratio would be desirable to quickly slow the vehicle and minimize the required flyback cruise distance. Since the cruise portion of the return flight will determine required air-breathing engine (ABE) fuel, there is a direct impact (reduction) on ascent performance. However, the relationships between wing size and shape, drag-to-weight, and entry g-load constraints were uncertain and the subsequent effects on flyback cruise distance undetermined. Additionally, the large base area (to incorporate two RD-170/four RD-180 engines) is a limiting factor to flyback cruise efficiency regardless of the wing type employed. Ultimately, packaging requirements along with the 170-knot landing speed constraint provided a clear boundary on wing size and appeared to be the most limiting factors. Therefore, the configuration was designed to optimize the landing configuration in order to minimize wing size and ease packaging constraints.

Once the configuration was developed to optimize landing, a review was made of the other flight regimes to ensure the best possible cruise performance, and to ensure that the vehicle is trimmable. During hypersonic/supersonic entry at high angles of attack, yaw stability is not provided by aerodynamic surfaces and must be augmented by RCS jets. Additional trade studies should be performed in follow on phases to better optimize the configuration for all flight regimes.

4.2.2 Design Study Baseline Configuration

To establish baseline aerodynamic coefficients, estimates were made of the Space Industries, Inc., LFBB concept shown in figure 4.2.2-1. Aerodynamic analysis of the configuration was provided through the use of potential panel computer codes. Specifically, APAS II and QUADPAN (Quadrilateral Element Panel Method) were the computer codes used. These estimates provided initial data for other disciplines to begin their studies.

The first plan to design an LFBB configuration included the development of six types of configurations ranging from fixed wing, folded wing, etc., to fully deployable configurations. Time constraints, however, permitted evaluation of only two concepts. Initially one of the six configurations was developed and aerodynamic characteristics provided to support ongoing trade studies. This configuration was a fixed wing/deployable canard configuration as shown in figure 4.2.2-2 and integrated with the Shuttle in figure 4.2.2-3.

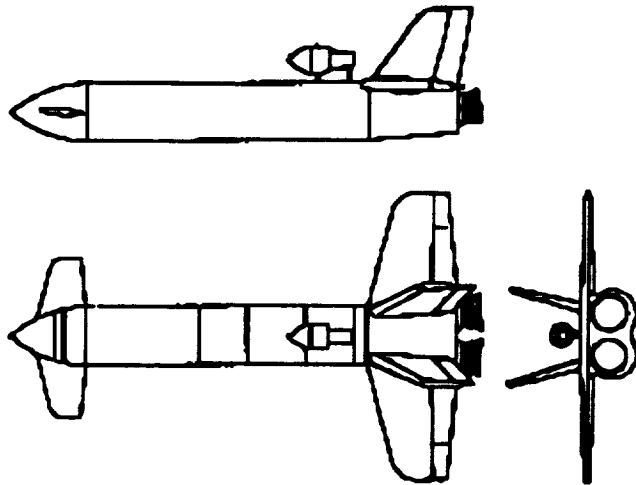


Figure 4.2.2-1 Space Industries, Inc., LFBB concept.

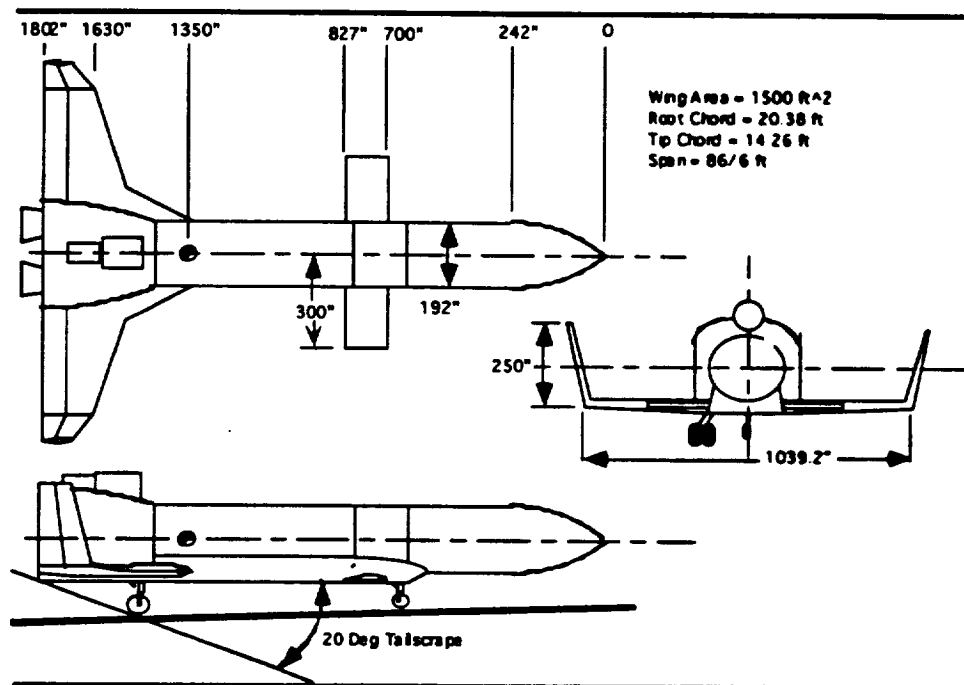


Figure 4.2.2.2 Fixed wing/deployable canard LFBB concept.

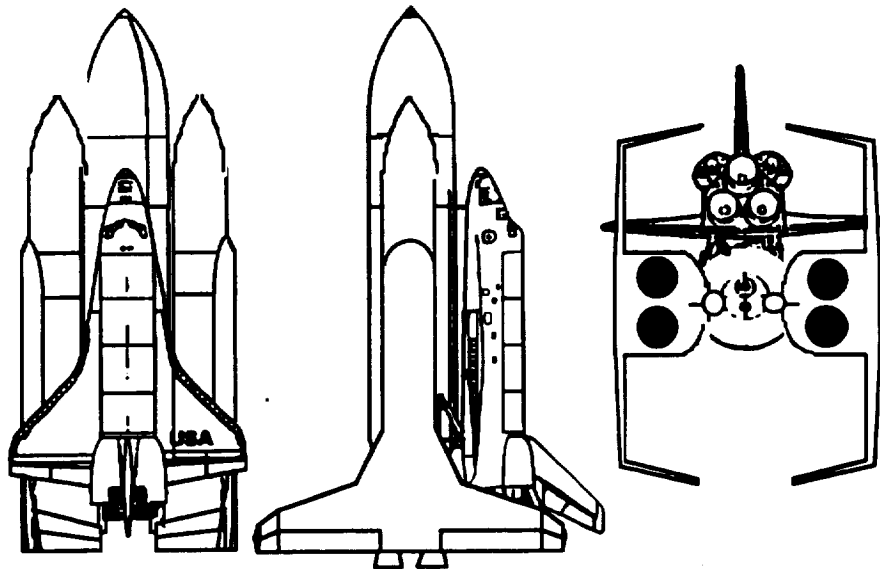


Figure 4.2.2-3 Fixed wing/deployable canard LFB launch configuration.

Eventually, one configuration was selected for detailed development and evaluation during this Pre-Phase A study. The configuration developed as the baseline in this study was a deployable scissor wing, deployable canard, fixed vertical tail configuration shown in figure 4.2.2-4. The principle design driver leading to the selection of this configuration was the ground rule to minimize impacts to the Shuttle ascent aerodynamic loads environment. By "packaging" the wing and canard during ascent (and subsequently locating the fairing away from the Orbiter), the aerodynamic loads impacts to the Orbiter wing are minimized.

It should be noted that other configuration concepts (such as the fixed wing configuration) were eliminated primarily due to perceived unacceptable impacts to the Orbiter. Detailed analysis evaluating ascent load impacts, geometric constraints, and design complexity in support of trade studies of fixed wing and folded wing concepts should be considered in any follow-on phases of this study.

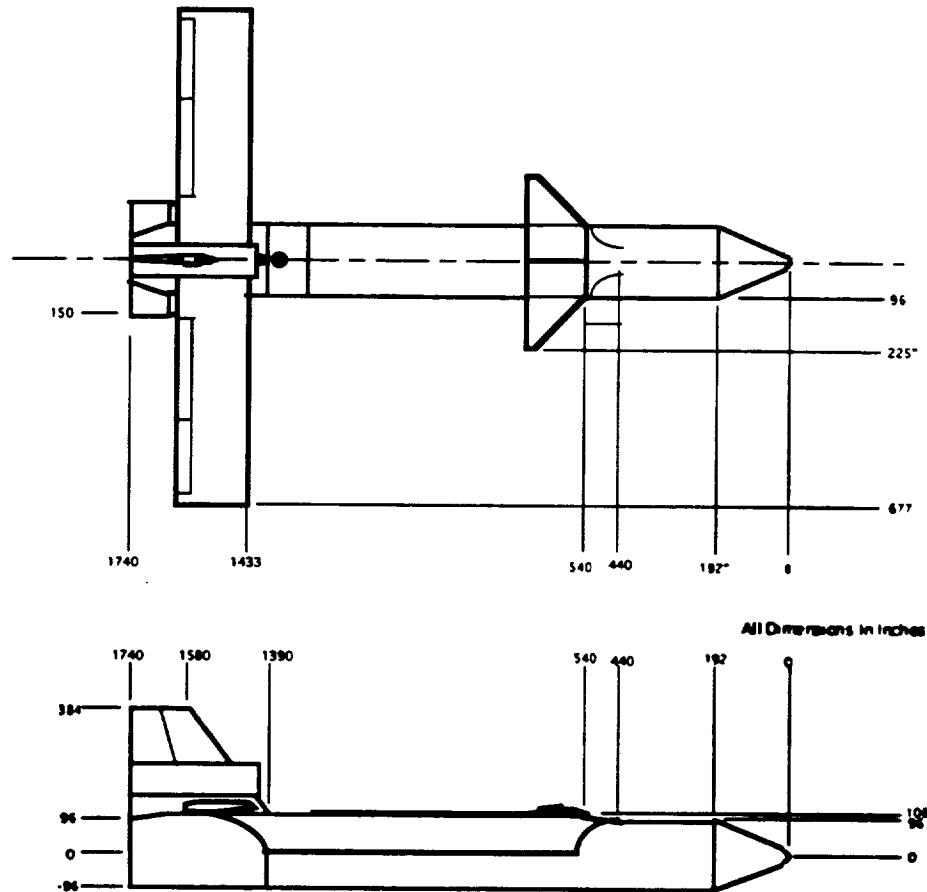


Figure 4.2.2-4 Pre-Phase A LFBB baseline configuration.

4.2.3 Baseline Configuration - Optimization for Landing (Minimum Wing Area)

Optimization of the landing configuration will provide the minimum wing area requirements. Wing packaging constraints will directly influence wing planform. To minimize wing area for a given landing speed, lift capability of the configuration was maximized at landing conditions. In general this means landing with a thick wing, near stall speed with a maximum flap deflection. Canard configurations (like figure 4.2.2-4) have additional limitations to consider when attempting to achieve maximum lift.

In longitudinally stable vehicles, canard deflections provide pitching moments necessary to offset trim requirements for attaining high angles of attack and flap deflections necessary to maximize lift coefficients. To minimize canard trim power requirements and allow more of the canard power to be used to offset lift generating moments (flaps), the vehicle was designed to be neutrally stable or slightly unstable in pitch. This design goal sizes the canards and provides the most available canard power for offsetting flap deflections while maintaining trim at angles of attack near stall. The canard must be capable of operation at high angles of attack near wing stall to provide trim at the landing condition. Therefore, an all-moving, low-aspect ratio planform with large leading edge sweep was selected for the canard to provide necessary landing aerodynamic performance characteristics.

Wing position was selected, coupled with canard position and size, to meet the design goal of neutral pitch stability. The aft cg position dictates the aft wing location. A straight wing with zero sweep was selected to maximize landing lift capability. Wing chord was limited (<16 ft) to allow packaging parallel to the booster fuselage for ascent. Using a 15.5-ft chord resulted in a wing span of 112.8 ft to provide the required wing area of 1750 ft². Figure 4.2.3-1 displays the relationship between wing area required for a given vehicle weight as a function of maximum lift coefficient in the ranges considered for the LFBB. This

wing configuration provided the necessary landing aerodynamic performance characteristics while minimizing packaging for ascent.

LFBB AERODYNAMIC CONFIGURATION DEVELOPMENT

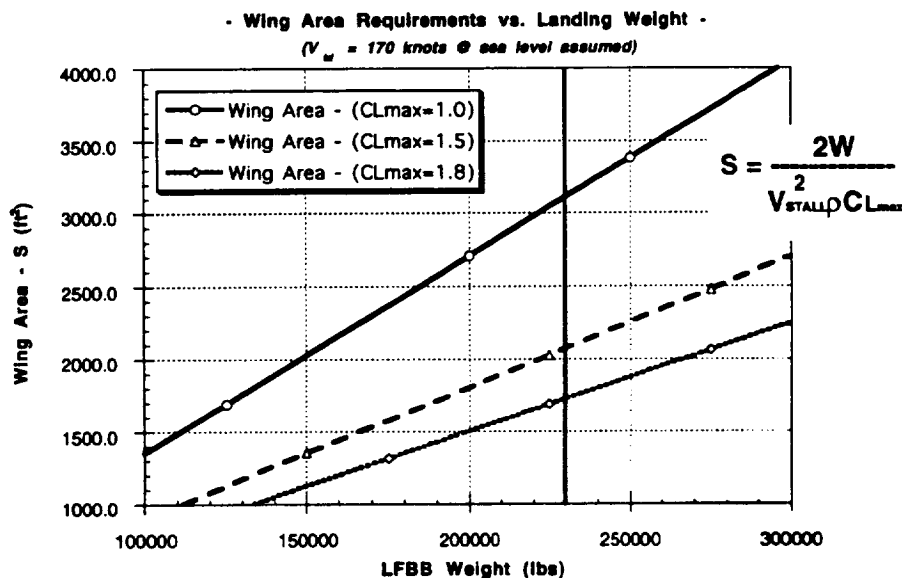


Figure 4.2.3-1 Wing area vs vehicle weight as function of C_{Lmax} .

Wing and canard airfoil sections were selected to minimize the zero α nose-down pitching moment. Minimizing nose-down pitching moment allows more wing flap deflection, thereby providing higher lift, for the equivalent available canard power. A canard airfoil section with high lift at zero α decreases nose-down pitching moment and was selected for this application. Considering the limited study time available, an exhaustive search of airfoil sections was not conducted, but the NLF(1)-0215F possessed the desired characteristics and was selected for the baseline configuration. A symmetric airfoil section, NASA series 65-012, was selected for the wing to provide zero lift and moment at zero α and to minimize nose-down pitching moment.

The vertical tail was sized to provide a minimum amount of directional stability ($C_{n\beta} = .001$). The relatively short moment arm available (vertical tail to cg) and the long flat sided fuselage (see figure 4.2.2.4) drive the vertical tail to large areas. A 10% thick symmetric NACA 65 series airfoil was selected for the vertical tail section. Further work is needed to define interactions between lateral-directional stability characteristics and vehicle flight qualities.

4.3 LFBB Entry Aerodynamic Characteristics

With detailed design objectives (cambered canard, symmetric wing, neutral pitch stability, etc.) defined, empirical and handbook methods (Reference 5) were used to provide preliminary size and location of the aerodynamic surfaces. Preliminary aerodynamic estimates were also determined. Once initial size and location of the aerodynamic surfaces had been defined, a more detailed aerodynamic analysis of the configuration was provided through the use of the potential panel computer codes APAS II and QUADPAN. These codes provided the accuracy needed to estimate vehicle stability and to refine surface sizes and locations throughout the anticipated flight Mach range. In addition, estimates were made of control surface sizes and associated trim capabilities.

4.3.1 Baseline Configuration Aerodynamics

Lift and drag coefficients were provided for performance and trajectory studies. Table 4.3.1-1 lists the basic lift and drag (L/D) aerodynamics of the baseline configuration. Figure 4.3.1-1 plots maximum L/D across the Mach range. These data form the basis of information for use in trajectory design and trade studies.

Table 4.3.1-1 LFBB Baseline Configuration Lift and Drag Aerodynamic Characteristics

MACH	C_{La}	$C_{La=0}$	Induced Drag K	C_{D0}	α of Max Lift
0.30	0.1054	0.1498	0.0876	0.0645	14.00
0.60	0.1161	0.1733	0.0903	0.0800	14.00
0.80	0.1348	0.2147	0.0916	0.1050	14.00
0.90	0.1600	0.2753	0.0872	0.1640	14.00
0.95	0.1766	0.3056	0.0850	0.1980	14.00
1.05	0.1400	0.2000	0.2000	0.2180	17.90
1.10	0.1260	0.1000	0.2500	0.2210	18.60
1.20	0.0950	0.0200	0.3300	0.2190	22.30
2.00	0.0430	0.0000	0.6010	0.1610	39.50
4.00	0.0363	0.0000	0.7580	0.1400	43.20
6.00	0.0357	0.0000	0.7750	0.1290	45.00

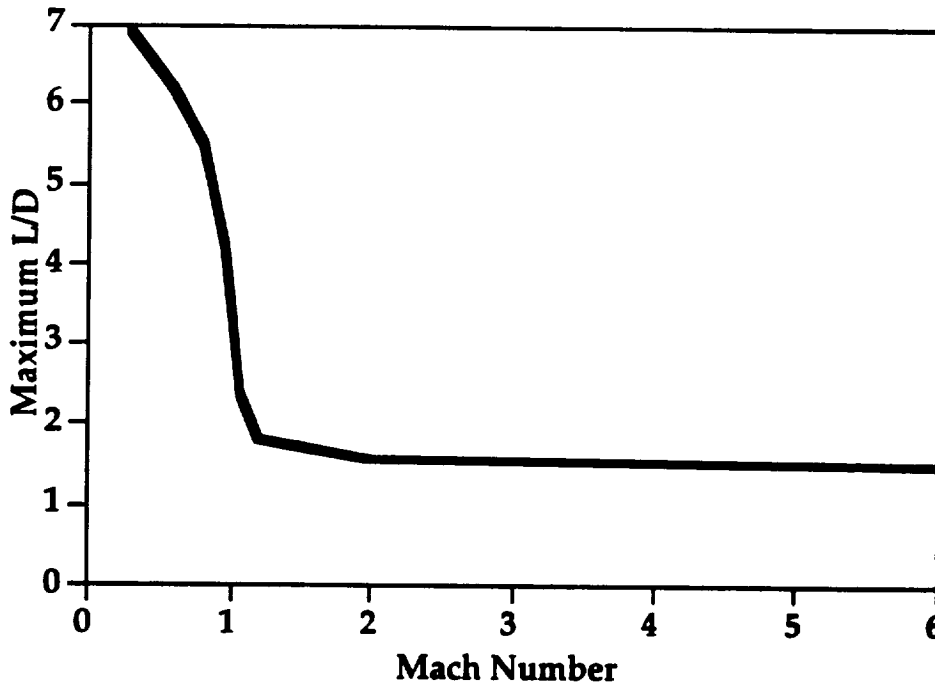


Figure 4.3.1-1 LFBB estimated maximum L/D.

4.3.2 Baseline Configuration Aerodynamic Stability Assessment

Aerodynamic characteristics were generated for all six components ($C_N, C_A, C_Y, C_m, C_i, C_n$) to facilitate longitudinal and lateral stability estimates, surface sizing, control surface sizing, and trim point estimates. There is a large rearward cg shift as flyback fuel is burned. In addition, the center of pressure moves aft as the vehicle passes through Mach 1 from higher Mach numbers. Aerodynamic trim capability was verified for each major portion of the flight envelope.

During hypersonic and supersonic entry flight, the cg is in its most forward location. Due to the long fuselage, the center of pressure is also forward, resulting in a configuration which is marginally stable with the canard stowed. At these conditions, the inboard elevators have the capability to trim the vehicle in pitch to angles of attack in excess of 50° . Yaw control, however, will need to be augmented by the RCS jets during this portion of the flight. Sufficient roll control is provided by the outboard ailerons, assuming reattachment of upper surface wing flow in transition from high to low angles of attack is symmetric. The α transition (high to low) is currently being made at supersonic Mach numbers where symmetric reattachment remains to be verified. Mechanical means of ensuring symmetric attachment of the flow are available, if required.

As the vehicle moves from higher Mach numbers through Mach 1, the center of pressure of the vehicle moves aft. This, along with a relatively forward cg, results in a very longitudinally stable configuration, requiring large elevator deflections to trim if the canard remains stowed. For this reason it is recommended that the canard be deployed before reaching Mach 1, or very shortly thereafter. With the canard deployed, vehicle trim can be achieved by a modest combination of canard and elevator deflections.

During cruise, the cg gradually moves aft until an aft cg point is reached. At this condition the vehicle is neutrally stable in pitch with the canard deployed. The aft movement of the cg eases trim control deflection requirements for the remainder of the flight and at some point prior to landing, the canard becomes the primary pitch control device. As mentioned previously this neutrally stable condition allows for trim at the high angles of attack (near stall) necessary for landing.

4.3.3 Crosswind Landing Capability

The low value of directional stability, along with a substantial rudder size, results in a high crosswind landing capability. This is based on the ability to offset sideslip with rudder deflection. An investigation into lateral-directional coupling and interaction is required to evaluate 6-degree of freedom vehicle motions during landing. However, using only the rudder to offset large sideslip angles (i.e., cross winds) indicated that 10° of rudder deflection is sufficient to handle 40-knot cross winds (13° sideslip). Further evaluation in follow-on phases is recommended.

4.3.4 Summary

Aerodynamic surface size, location, planform, and airfoil sections have been defined for this Pre-Phase A study baseline configuration. Estimates of the aerodynamic coefficients have been defined for the entire flight regime and provided to the other disciplines in support of other trade studies. Interactions between the disciplines has resulted in an iterative design process which is still ongoing. The current baseline vehicle produced by this study, from an aerodynamic standpoint, is feasible and workable in all flight regimes and meets the objectives and constraints defined. Further optimization in areas noted is required and should be pursued in follow-on phases.

4.4 LFBB Ascent Aerodynamic Impacts to Shuttle

The replacement of the RSRMs with LFBBs will have an impact on the Shuttle ascent aerodynamic environment. The differences in the geometry of the LFBB will produce changes to the external pressure distribution on the Shuttle. This effect will manifest itself in two ways. First, the launch vehicle force and moment (F&M) characteristics (i.e., the integrated external pressure distribution) will change. This is expected to result primarily in an increase in drag, as well as in changes to the launch vehicle's normal force and pitching moment. Lateral directional aerodynamic characteristics should be comparable to the current Shuttle. Second, these changes to the external pressure distribution will alter the aerodynamic loads on the various components of the launch vehicle elements. Of particular concern are the Orbiter wings, which are extremely sensitive to external load distribution changes. Impacts to the Orbiter and ET requiring re-design or modification could result in significant incurred costs.

4.4.1 LFBB-Induced Ascent Aerodynamic F&M Factors

The incorporation of LFBBs into the Shuttle will impact the vehicle's ascent aerodynamic F&M characteristics. For the purpose of the pre-Phase A study, a rough order of magnitude estimate was determined by geometric comparison of the two launch vehicle configurations, Shuttle with RSRMs vs Shuttle with LFBBs. This evaluation assumed that the lateral-directional (C_N , C_l , C_Y) aerodynamic characteristics of the Shuttle are unchanged. Changes in the longitudinal (C_N , C_A , C_m) aerodynamic characteristics were estimated based on area ratios of the two launch vehicle configurations. Geometric details were gathered from Reference 6 concerning the three main Shuttle elements, the Orbiter, ET, and RSRMs. LFBB geometric details were provided by the configuration team. The summation of the projected areas of the Shuttle elements in the Y-Z and X-Y planes (fig. 4.4.1-1) were completed for each configuration. In the Y-Z plane, area ratios for both the forebody and base were calculated. Based on these ratios, a preliminary set of factors was determined for the Shuttle longitudinal aerodynamic coefficients. Table 4.4.1-1 summarizes these results.

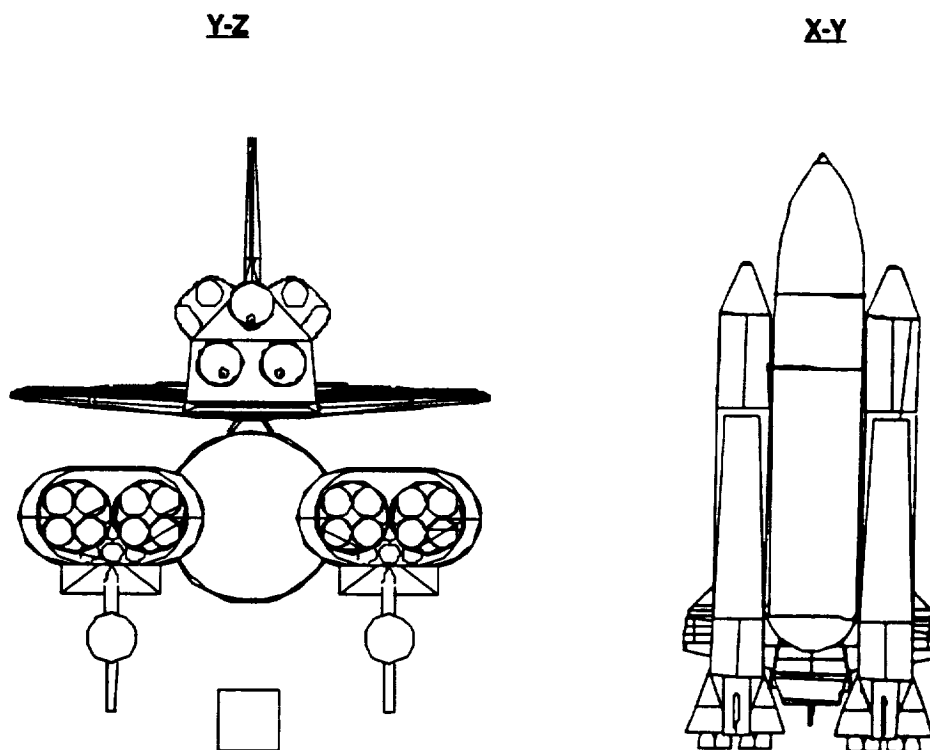


Figure 4.4.1-1 LFBB Y-Z and X-Y plane geometric area projections.

Table 4.4.1-1 Ascent Aerodynamic F&M Factors, LFBB-Induced

Axial Force:	$C_{A- Shuttlew/LFBBs} = 1.4 \cdot C_{A- Shuttlew/RSRMs}$	(forebody)
	$C_{A- Shuttlew/LFBBs} = 1.2 \cdot C_{A- Shuttlew/RSRMs}$	(base)
Normal Force:	$C_{N- Shuttlew/LFBBs} = C_{N- Shuttlew/RSRMs} - 0.1 \cdot C_{N- Shuttlew/RSRMs}$	(forebody)
Pitching Mom:	$C_{m- Shuttlew/LFBBs} = C_{m- Shuttlew/RSRMs}$	(forebody)
Side Force:	$C_{Y- Shuttlew/LFBBs} = C_{Y- Shuttlew/RSRMs}$	(forebody)
Rolling Mom:	$C_{l- Shuttlew/LFBBs} = C_{l- Shuttlew/RSRMs}$	(forebody)
Yawing Mom:	$C_{n- Shuttlew/LFBBs} = C_{n- Shuttlew/RSRMs}$	(forebody)

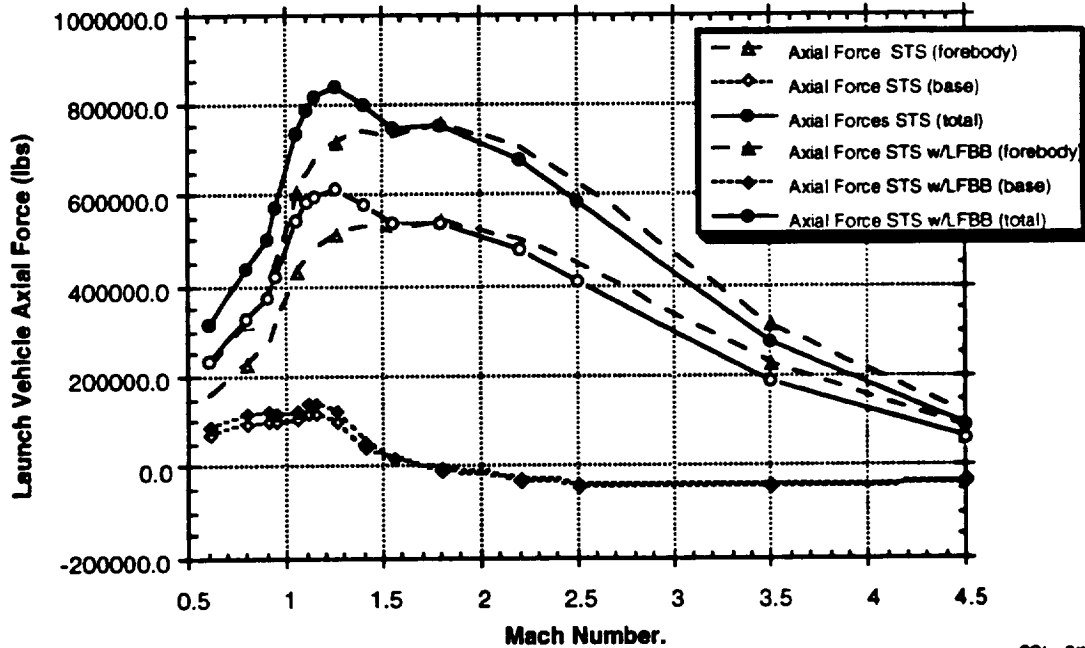
These factors are assumed constant across the Mach range (0.6 to 4.5)

Figure 4.4.1-2 shows the effect of applying these factors to the Shuttle axial force. Because the base axial force changes sign at approximately Mach 1.8, the increase in drag is more pronounced prior to this flight condition. The effect of this drag increase is a small reduction in excess vehicle performance.

LFBB ASCENT AERODYNAMIC EVALUATION

Axial Force ('Drag') vs. Mach Number

COMPARISON OF STS vs STS w/LFBB



SGL - 2/18/94

Figure 4.4.1-2 LFBB ascent aerodynamic evaluation - axial force vs Mach.

As mentioned previously, high-fidelity CFD analysis was applied to evaluate the launch vehicle configurations at Mach 1.25 (see section 4.3.2 for more details). Integration of the external pressure distribution results of these solutions was completed and the resulting aerodynamic coefficients extracted. For the particular condition evaluated (Mach 1.25, $\alpha = -3.30^\circ$, $\beta = 0.02^\circ$, $\Delta \text{Elev} = 10.5^\circ / 6.25^\circ$), significant changes to the longitudinal F&M aerodynamics were predicted (figures 4.4.1-3a, b & c). As can be seen, the increase in Shuttle axial force is approximately 40% and compares favorably with the simplified area ratio estimate. However, normal force and pitching moment changes are substantially larger than predicted. Follow-on analyses and wind tunnel tests are necessary to evaluate the full impact of the LFBB on the Shuttle ascent aerodynamics. Additionally, these effects should be evaluated for the impact on ascent performance in the next phase of this study.

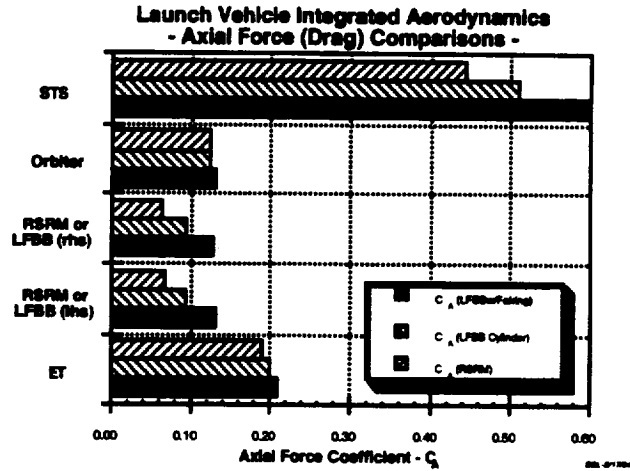


Figure 4.4.1-3a LFBB impacts to Shuttle aerodynamics @ Mach 1.25 - axial force.

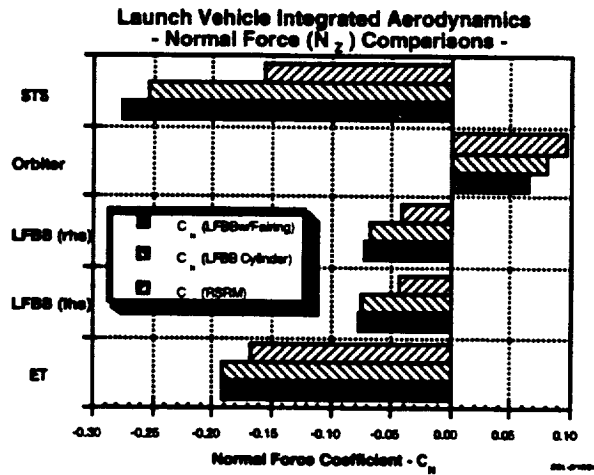


Figure 4.4.1-3b LFBB impacts to Shuttle aerodynamics @ Mach 1.25 - normal force.

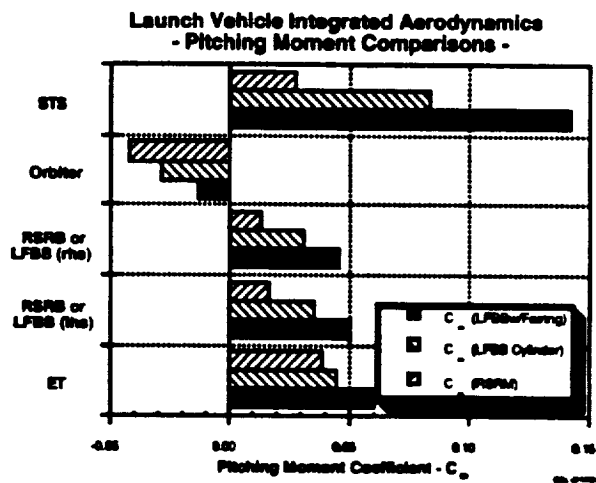


Figure 4.4.1-3c LFBB impacts to Shuttle aerodynamics @ Mach 1.25 - pitching moment.

4.4.2 CFD Analysis of a Preliminary Shuttle with LFBBs Ascent Configuration

As previously mentioned, changes to the external pressure distribution will alter the aerodynamic loads on the various components of the launch vehicle elements. Of particular concern are the Orbiter wings, which are extremely sensitive to external load distribution changes. In order to provide a preliminary evaluation of the impact of integrating an LFBB into the Shuttle ascent configuration, CFD analysis of a proposed configuration was utilized. This high fidelity analysis has demonstrated extremely good correlation with flight-measured data obtained on STS-50.

The LFBB configuration was exported from a CAD (computer-aided design) model in the IGES (initial graphics exchange standard) format. The NGP (National Grid Project), Gridgen, and HYPGEN grid generation programs were used to generate grids based on the IGES CAD model. The LFBB grids were incorporated into the current Shuttle CFD model. Flow field solutions were calculated using the OVERFLOW CFD code. By comparing solutions of the current Shuttle with those of an Shuttle with LFBBs, changes to the pressure distribution induced by the LFBB were determined.

Three CFD solutions were completed in order to assess the ascent aerodynamic impacts of the LFBB. All solutions were performed with the booster plumes off. This was primarily due to time constraints and the lack of information on the LFBB engine exit conditions. The three solutions consisted of an Shuttle solution with the current RSRM, a "clean" LFBB solution (150'L x 16'D with nose cone and aft skirt) without the wing fairing and tail, and an LFBB solution with the wing fairing and tail. Due to the evolving nature of the LFBB design, the CFD geometry and the "final" LFBB geometry are somewhat different. However, the overall dimensions (e.g., length, diameter, etc.) are consistent with later iterations of the LFBB design and the geometric differences should have a minimal effect on the wing loads. Figure 4.4.2.1 shows the surface geometry model of the Shuttle with LFBBs used in the CFD analysis solutions. Calculations were performed at a single critical flight condition corresponding to a previously validated STS-50 trajectory point (Mach 1.25, $\alpha = -3.30^\circ$, $\beta = 0.02^\circ$).

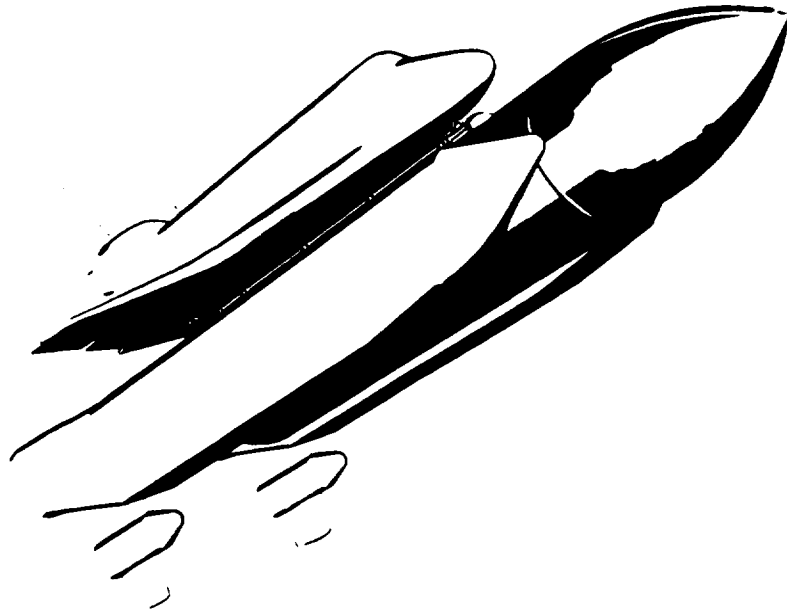


Figure 4.4.2-1 Shuttle with LFBBs "packaged" CFD model surface geometry.

The CFD solutions were post-processed to calculate the wing loads, element forces, and integrated aerodynamics. These results were forwarded to the loads team in a tabular form to be used in determining the structural impacts of the LFBB on the Shuttle. Figures 4.4.2-2a, b, & c show the integrated pressure results on the left wing in terms of wing shear, bending, and torsion, respectively, plotted vs wing span. As can be seen at this particular flight condition, the wing root loads are less for the LFBB-configured Shuttle than the current Shuttle. This effect is attributed primarily to the smooth outer

moldline on the LFBB as opposed to the RSRM protuberances (i.e., attach ring/IEA box) on the current vehicle. The removal of these protuberances more than offsets any increases in wing loads due to the larger booster diameter (16' vs 12') and thus results in lower wing loads.

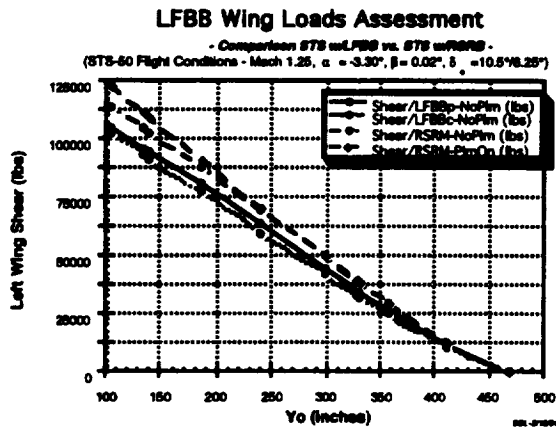


Figure 4.4.2-2a Shuttle with LFBBs ascent aero Orbiter wing load impacts—shear force.

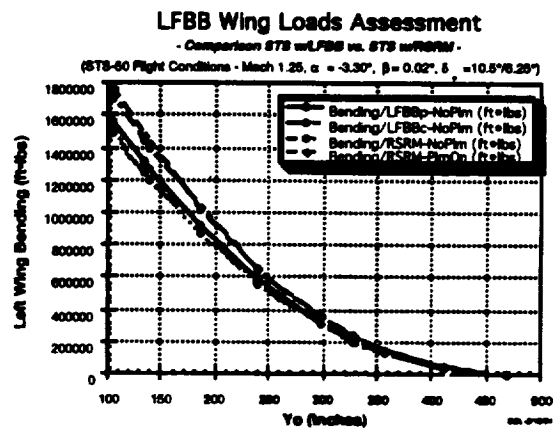


Figure 4.4.2-2b Shuttle with LFBBs ascent aero Orbiter wing load impacts—bending moment.

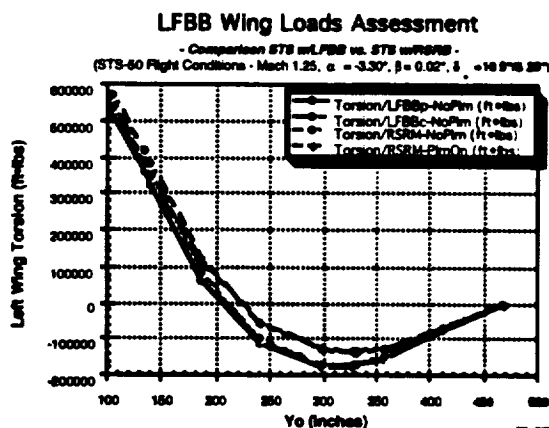


Figure 4.4.2-2c Shuttle with LFBBs ascent aero Orbiter wing load impacts—torsion moment.

As a point of comparison, MSFC wind tunnel test results from an LRB parametric study were reviewed. This evaluation corroborates the CFD analysis result trends of lower external wing root loads. While the LRB testing does not provide a direct geometrical comparison, the diameter effects are thought to be similar. At the CFD analysis condition (Mach 1.25, $\alpha = -3.3^\circ$), wind tunnel test results indicate a reduction in wing root bending moment of -325000 ft-lb vs the CFD-predicted -225000 ft-lb. This agreement is considered very good for trending purposes.

4.4.3 Conclusions

The introduction of the LFBBs will have an impact on the ascent aerodynamic environment of the Shuttle. Changes to the Shuttle's F&M characteristics must be accounted for in trajectory design and performance evaluations. The increased drag will result in a slight reduction in excess performance. Preliminary results indicate that the LFBBs will reduce the external Orbiter wing root loads. The effect of these new environments on the internal structure is being evaluated by the loads and structures teams. If further analysis and wind tunnel testing confirm these trends, the impacts to the Orbiter wing would appear to be manageable.

4.5 Aerothermodynamic Analysis of the LFBB

A preliminary engineering analysis was performed to evaluate the aerothermodynamic environment of the LFBB. Since the LFBB ascends as part of an integrated vehicle and descends as a winged vehicle, both ascent and entry aerothermodynamic heating analyses were required. These analyses were limited to aerodynamic and shock-induced convective heating. Also, because it launches as part of the Shuttle, interference heating to the ET was assessed. Time constraints allowed for only a limited number of points on the booster, the wing leading edge, and impacts to the ET to be evaluated during this study. Other issues such as plume convective and radiative heating, heating to the Orbiter, ET base and aft attach region, and radiative heating to the SSMEs were either closed by engineering assessment and experience or left open for analysis during the follow on phases of this project. The initial assessment of these issues along with those covered in more detail can be reviewed in Appendix B. Results of the detailed analyses presented herein were provided for thermal and TPS analysis.

In the following sections, a more detailed discussion on the analysis performed is presented. This will first begin with the reference heating analysis, then impacts to the ET, and finally, aerodynamic heating to the booster during ascent and entry. Atmospheric parameters needed for this study were modeled using the 1962 Standard Atmosphere.

4.5.1 Reference Heating to a 1-ft Sphere

Before specific geometric information on the LFBB was available, ascent and entry trajectory designers, using preliminary aerodynamic and engine performance data, were able to develop a complete trajectory for the booster. A quick look analysis of the resulting heating of this trajectory was done in order to allow TPS designers to complete an initial assessment. Trajectory heating analyses were performed using the LANMIN code (Reference 7) which uses the theory of Fay-Riddell (Reference 8) to calculate the stagnation point heating to a sphere at various free stream conditions.

Figures 4.5.1-1 and 4.5.1-2 show the altitude, velocity, Mach number, and heating to a 1-ft reference sphere with radiation equilibrium wall temperature boundary conditions during the ascent and entry phases of flight of the LFBB. This trajectory results in a double-peaked heating profile for the booster. During ascent, heating to the boosters increases until they separate at Mach 5.7 and an altitude of approximately 175 kft. Although the booster engines have stopped firing, the momentum of the LFBBs carries them to an altitude of over 250 kft and a Mach number of 6.2. Because of the high altitude, the heating decreases to a minimum. At this point, the main wings of the boosters are deployed and the heating increases again as the vehicle enters the denser atmosphere. The boosters fly at a $62^\circ \alpha$ during reentry. The heating to the LFBBs becomes negligible when the booster flies at conditions below Mach 2.5.

4.5.2 ET Impacts Assessment

As stated previously, a more detailed analysis was performed on the configuration and trajectory impacts to the ET as related to the convective heating environment. Geometric differences between the RSRM and LFBB would result in changes to the shock interference and protuberance heating environments on the ET. These changes could necessitate modifications to the TPS of the ET (Reference 9). Also, since the performance of the booster results in LFBB separation from the ET at Mach 5.7, compared to Mach 4 for the RSRM, higher heating rates at separation would be expected.

In order to assess these impacts to the ET, we needed to compare the LFBB ascent trajectory to the ET Generic Certification design trajectory (Reference 10). The ET Generic Certification trajectory (head wind case) represents the most severe heating rate and heat load flight conditions for which the ET is certified to fly. All current Shuttle ascent trajectories must fly within this envelope. The comparison of the trajectories was done using stagnation point heating to a 1-ft reference sphere with 650°F wall temperature. Figures 4.5.2-1 and 4.5.2-2 show the comparison of velocity vs altitude and reference heating rates as a function of time, respectively, for the two trajectories. Because of the increased performance of the RD-170/RD-180 engines, the reference heating rate to the ET is 200% higher than that of the ET generic certification values. However, since lofting of the Shuttle with the LFBB occurs at a

higher altitude, the heating rate rapidly decreases to levels well below the generic certification heating. This results in a 16% reduction of the reference total heat load to the ET.

Since the heating rate to a vehicle determines the type of TPS material and the heat load determines the thickness of that material, further analysis of the heating impacts to the ET was required. To do this, the design aerodynamic heating distribution for the ET as impacted by the advanced solid rocket motor (ASRM) was modified to assess the LFBB effects to the ET. Figures 4.5.2-3 and 4.5.2-4 show the ET maximum circumferential heating rates and total heat loads, respectively, between x/l of 0.0 and 0.95 resulting from the LFBB and ET generic certification trajectories. As can be seen, the peak convective heating rate distribution for the ET increases due to the LFBB. The heating spike at $x/l = 0.35$ is caused by the forward attach and occurs for both the LFBB and the RSRM. A similar spike can be seen for the RSRM only at a $x/l = 0.45$. This is due to the field joint of the solid fueled motor casing. The LFBB will not have similar design features. Finally, the heating rise at $x/l = 0.85$ is a result of the cross beam support and attach ring on the ET. The maximum heat load for the ET due to the LFBB increases only slightly from that due to the RSRM.

4.5.3 Aerodynamic Heating to LFBB

We completed preliminary aerodynamic heating evaluation for nine selected body points (BPs) on the LFBB. The nine BP locations selected were agreed upon by representatives from aerothermal, structures, and thermal protection disciplines. Hot wall (i.e., radiation equilibrium wall temperature with $e = 0.8$) and 350°F wall heating rates for each location during ascent were provided for TPS evaluation. Figure 4.5.3-1 shows the nine BP locations and surface wetted length of each location from the nose tip. Note that this was an early configuration of the LFBB. The final configuration located the fairing at BP3 further aft along the booster axis.

4.5.3.1 Ascent Heating Methodology

Ascent heating to the LFBB was obtained by adapting heating methodologies developed for the RSRM. The results of these methodologies have been compared to the heating rates listed in the RSRM aerodynamic heating data book (Reference 11). Since the LFBB is attached to the ET during ascent, the flow field just upstream of the LFBB has been affected by the presence of the forward ogive of the ET. In order to accurately calculate the upstream conditions to the LFBB, the local pressure coefficient as a function of Mach number was obtained from previous CFD analyses. This data was linearly extrapolated to Mach 6 so that the Mach 5.7 separation point could be included. After the flow is expanded to the proper pressure, heating to the various BPs was calculated using engineering algorithms for spheres, cones, wedges, and flat plates. BPs on the attachment line (5, 7, and 9) were modeled similarly to BPs 4, 6, and 8, except that heating multiplication factors of 2.0, 1.6, and 1.6, respectively, were used to model the interference heating effects due to the proximity to the ET.

For a majority of ascent, heating to the LFBB is caused by turbulent flow over the vehicle. The flow around the integrated vehicle does not begin to re-laminarize until just before separation. In order to model this effect, onset of transition and fully turbulent Reynolds Numbers were given as 3×10^5 and 1.3×10^6 , respectively. These Reynolds Numbers are used in RSRM heating models and have been shown to give accurate results.

4.5.3.2 Entry Heating Methodology

After first stage separation, the booster deploys its wings and reenters the atmosphere at Mach 6. BPs 2, 4, 6, and 8 lie along the windward centerline of the LFBB, the stagnation point being at BP1. Entry heating was modeled using swept cylinder correlations along with the engineering algorithms previously mentioned in the ascent heating section. Using Orbiter flight experience, transition onset and turbulent flow Reynolds Numbers were set to 8×10^6 and 15×10^6 , respectively.

In addition to the nine BPs, wing leading edge heating was calculated using the shock interaction model developed for the Orbiter (Reference 12). Since the LFBB uses a constant cross section straight wing to generate lift for the return, heating to the wing leading edge must be determined. Of most importance

here is the effect of the bow shock interacting with the wing shock. Since the flow behind the bow shock of the LFBB is still supersonic, a shock develops in front of the wing leading edge. Between Mach 6 and 4, the bow shock is inboard enough to intersect with the wing shock. As was seen for the straight winged Orbiter studies of the early 70's (Reference 13), the intersection results in a Type V shock interaction where localized heating can be increased between 1.5 and 3 times the undisturbed values, at these free stream Mach Numbers. For this study a factor of 2.0 was applied.

4.5.3.3 Integrated Ascent and Entry Heating Results

Figures 4.5.3.3-1, 4.5.3.3-2, and 4.5.3.3-3 show hot wall heating rates as a function of time from liftoff for all nine BPs. For BPs 1-3 and 5, 7, and 9, peak heating is observed during ascent. This is a result of the turbulent forebody heating and interference heating between the ET and the LFBB. The highest heating in seen on the nose cap, BP1. Here the heating rates exceed 3 BTU/ft² sec during ascent and 2 BTU/ft² sec during entry. The sharp rise in the heating for BPs 4, 6, and 8 at 140 seconds is generated when the vehicle transitions from booster orientation to flyback orientation at 62° α . Peak heating of just under 1 BTU/ft² sec for these BPs occurs at 310 seconds during the flight. All three BPs have similar heating because they lie on the windward centerline stagnation streamline. Turbulent heating effect can be seen as a small increase in the heating at about 340 seconds.

Heating to the wing leading edge at an α of 62° can be seen in figure 4.5.3.3-4. The curves in the figure show the heating to the wing root, the main wing up to the shock interaction, the shock interaction heating, and the heating to the wing outboard of the interaction. Figure 4.5.3.3-5 shows a schematic of these regions. Also shown for comparison is the heating to a sphere of the same radius as the wing leading edge at 62° α . Because of the shock interaction and the small leading edge radius of the wing, heating to this area is more than double than anywhere else on the vehicle. The wing root shows the lowest heating because the flow has to expand around the fuselage before encountering the wing. Moving outboard, the heating to the wing increases until the interaction region is reached, after which it decreases to a value less than half of the peak value.

Based on Orbiter/Shuttle experience, a heating uncertainty factor of 1.3 was developed to cover any dispersions that were not accounted for in the nominal trajectories developed for the LFBB. This factor was not applied to the heating rates presented herein, but was used in the thermal and TPS analyses, as will be noted later in this report. This factor covers both aerodynamic and plume heating uncertainties due to such parameters as guidance, winds, atmosphere, thrust vector misalignment, SSME thrust, and propellant load.

4.5.3.4 30° Angle of Attack Entry Results

Near the end of the Pre-Phase A effort, a 30° α entry trajectory for the LFBB was developed. The heating models described previously were rerun using this updated trajectory and the results are shown here for completeness, figures 4.5.3.4-1 through 4.5.3.4-5. Because of the lower α , the LFBB flies a higher entry velocity profile, and the heating to the vehicle during the entry increases. Of significance is the rapid increase in heating at the 320 second mark. This heating rise is due to transition from laminar to turbulent flow based upon the Reynolds Numbers listed previously. Referring to the altitude-velocity profile comparison plot, it can be seen that the magnitude of the increase is a result of the booster flying at a higher velocity lower in the atmosphere at this time than was flown for the 62° α trajectory. Finally, the heating to wing leading edge increases even more than the BPs because, as the α is decreased, the effective leading edge radius along the stagnation line decreases. The combination of all these effects results in heating in the shock interaction region of greater than 14 BTU/ft² sec. The overall increase in the heating to the LFBB for the 30° α entry may require different or additional TPS on the vehicle. This should be further evaluated in follow-on phases of this study.

4.5.4 Conclusions

We conducted a preliminary ascent and entry aerothermodynamic heating analysis in support of the Pre-Phase A study of the LFBB. This analysis included an initial assessment of the heating impacts to the Orbiter, ET, and SSMEs, of which the ET was evaluated in greater detail. We also made predictions of

the aerodynamic convective heating rates for the main wing and nine BP locations on the LFBB forebody. Reference heating analysis for the ET flying with the LFBB showed that, although the peak heating rate was 200% of the generic certification trajectory, the total reference heat load was reduced by 16% due to higher lofting of the trajectory after booster separation. As can be seen, for the booster forebody, the heating environments can be maximized on ascent or entry. This implies that the complete flight (ascent and entry) of the LFBB must be considered in establishing the aeroheating environments. Finally, between Mach 6 and 4, the main wing of the LFBB will be exposed to Type V shock interaction heating, resulting in local heating rates over twice as high as seen anywhere else on the vehicle.

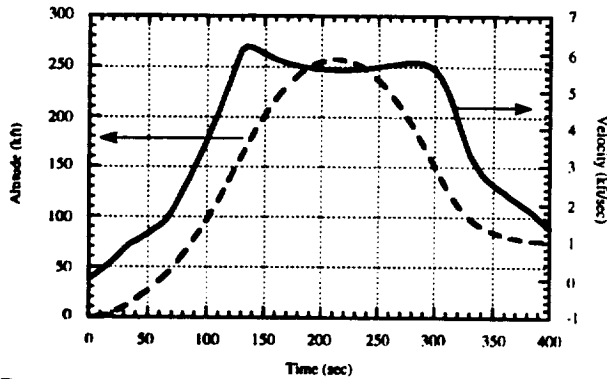


Figure 4.5.1-1 Altitude/velocity profile for LFBB ascent and 62° α entry.

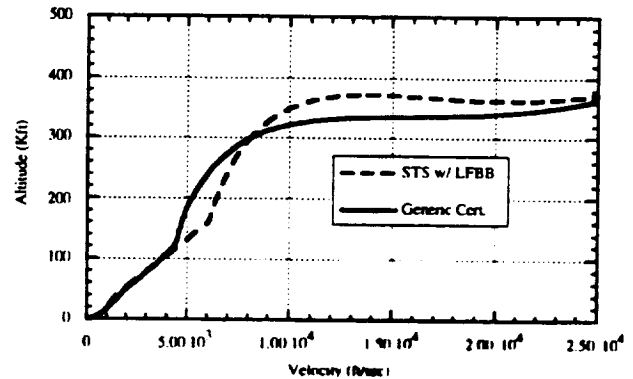


Figure 4.5.2-1 LFBB vs generic certification ascent trajectory.

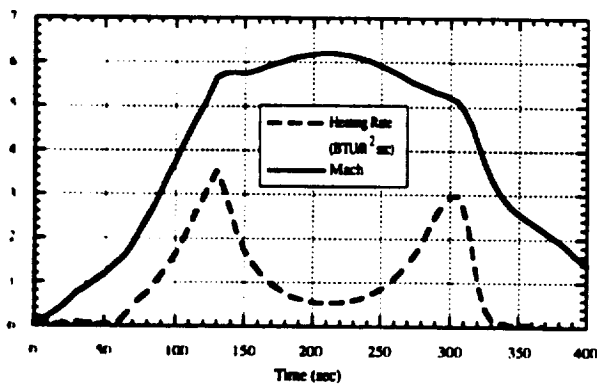


Figure 4.5.1-2 Mach number and 1-ft reference sphere heating profile for LFBB ascent and 62° α entry.

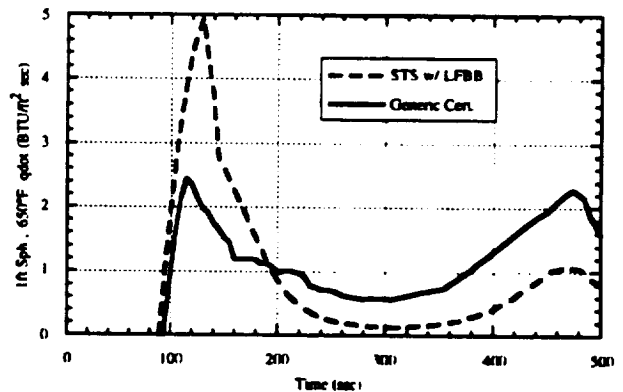


Figure 4.5.2-2 Reference heating comparison between LFBB and generic certification ascent trajectories.

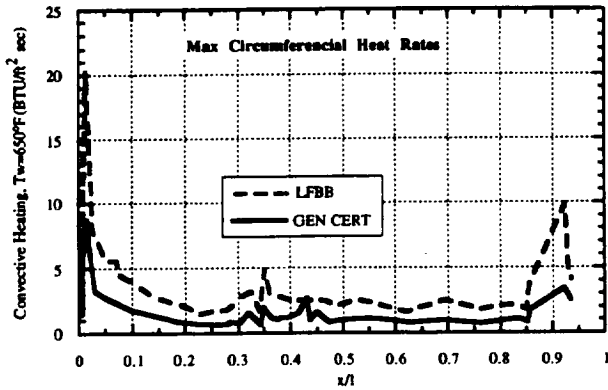


Figure 4.5.2-3 Maximum ET circumferential heating rate comparison.

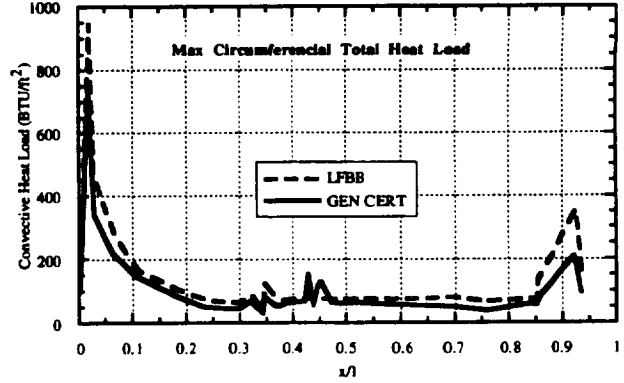


Figure 4.5.2-4 Maximum ET circumferential total heat load comparison.

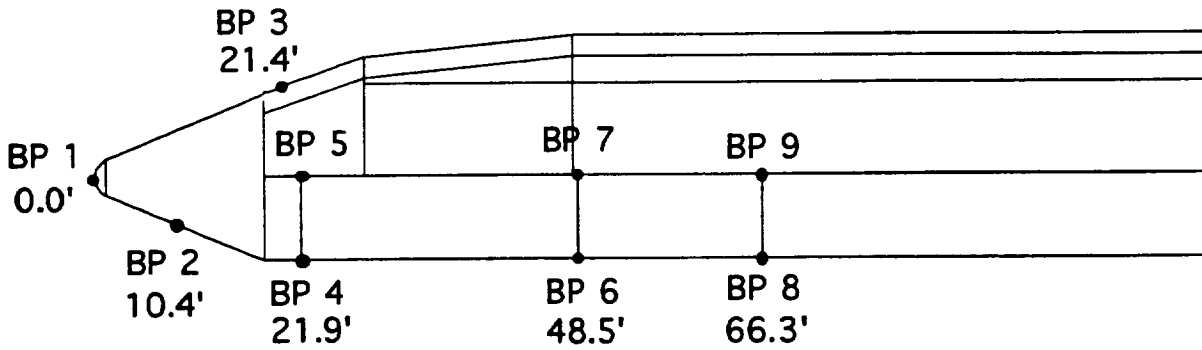


Figure 4.5.3-1 Body point locations on the LFBB forebody.

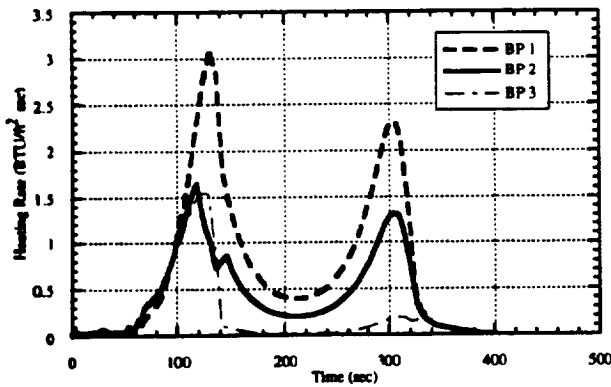


Figure 4.5.3.3-1 LFBB forebody heating to BPs 1-3, ascent and 62° α entry trajectory.

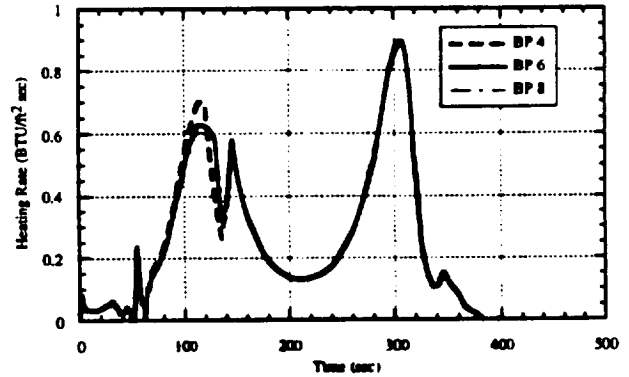


Figure 4.5.3.3-2 LFBB forebody heating to BPs 4, 6, and 8, ascent and 62° α entry trajectory.

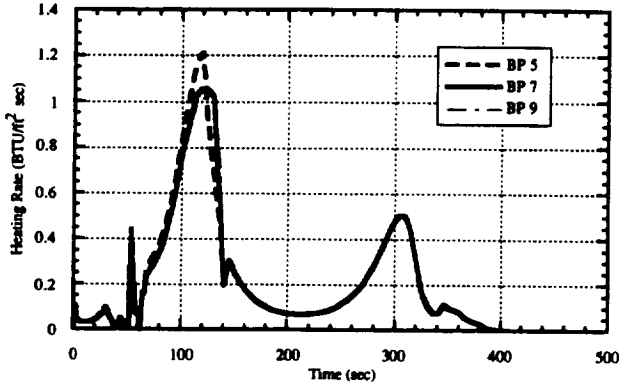


Figure 4.5.3.3-3 LFBB forebody heating to BPs 5, 7, and 9, ascent and 62° α entry trajectory.

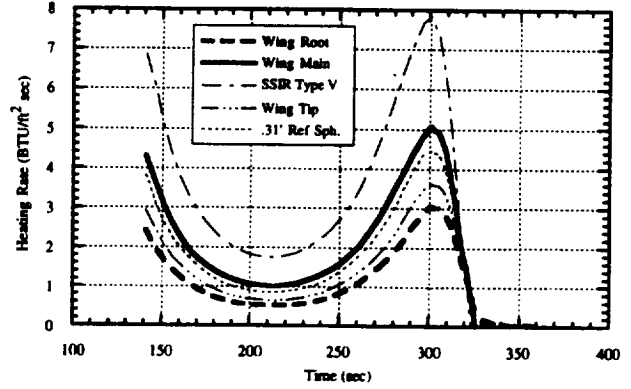


Figure 4.5.3.3-4 LFBB wing leading edge heating during 62° α entry.

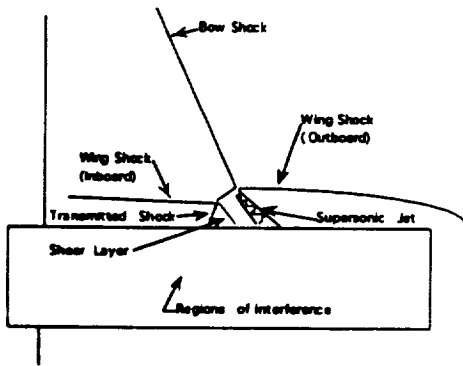


Figure 4.5.3.3-5 Schematic of bow shock/wing shock interaction on the LFBB.

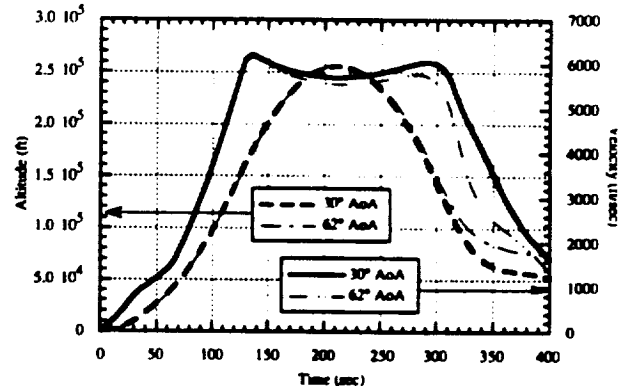


Figure 4.5.3.4-1 Entry trajectory comparison. (30° α vs 62° α)

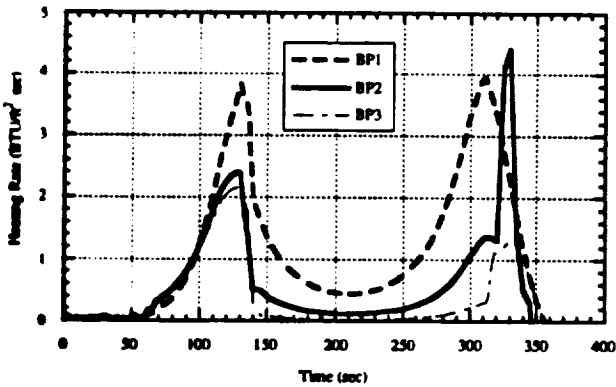


Figure 4.5.3.4-2 LFBB forebody heating to BPs 1-3, ascent and 30° α entry trajectory.

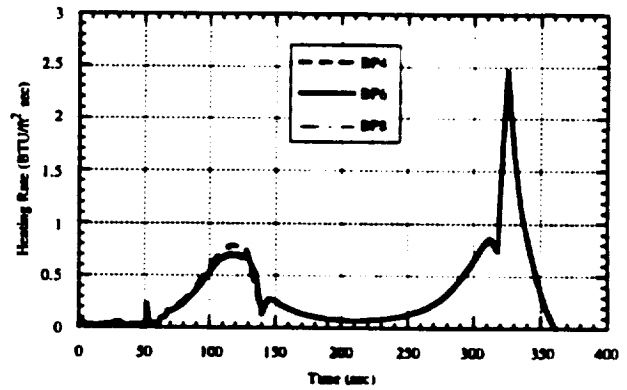


Figure 4.5.3.4-3 LFBB forebody heating to BPs 4, 6, and 8, ascent and 30° α entry trajectory.

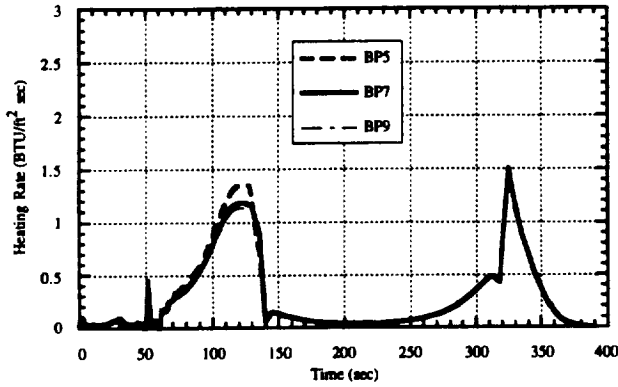


Figure 4.5.3.4-4 LFBB forebody heating to BPs 5, 7, and 9, ascent and 30° α entry trajectory.

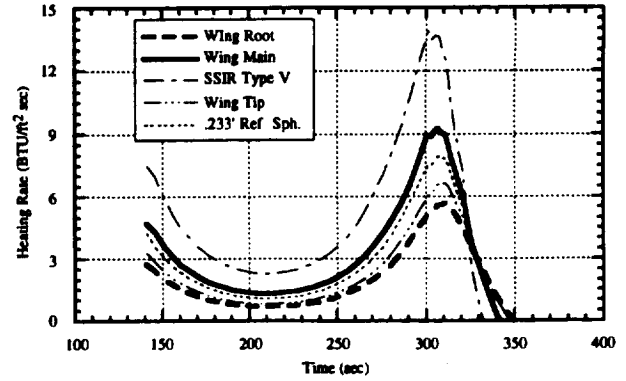


Figure 4.5.3.4-5 LFBB wing leading edge heating during 30° α entry.

4.6 Preliminary LFBB Study Ascent Performance Inputs

Consultation was provided in the definition of ascent trajectory ground rules to be used in the development of ascent trajectory simulations modeling the LFBB configured launch vehicle. These ground rules, reflecting current and/or projected Shuttle flight constraints, were incorporated into a final set of ascent trajectory design ground rules. This coordination was used to develop a baseline trajectory case. Table 4.6-1 identifies the LFBB ascent trajectory design ground rules.

Table 4.6-1 Additional Ascent Trajectory Design Ground Rules for LFBB

ITEM	VALUE	DOCUMENTATION	RATIONALE
Launch date	June 15	TDDP SPLAS028, 11/13/92	Worst season for SSME throttling; q target available for June
Launch pad	39A	TDDP SPLAS028, 11/13/92	Not a driver for performance
Inclination	51.6 deg	TDDP SPLAS028, 11/13/92	Space Station baseline
Insertion altitude	213 nm (rendezvous to 220 nm)	TDDP SPLAS028, 11/13/92	Consistent with OMS load and MECO targets in TDDP
No-fail MECO targets	$V_I = 25965$ fps $\text{Gam}_I = 0.917$ deg Alt = 57 nm	Obtained from RSOC/T. Huning, 1/27/94	Consistent with TDDP SPLAS028
MPS inventory	Rev EE	NSTS 08209, Volume I, Tables 4.38-4.43 (Change #22)	Current Shuttle flight-derived inventory
SSME tags	Average tags with 3 plugged posts	NSTS 08209, Volume I, Table 5.5.4 (Change #22)	Current Shuttle data
Orbiter weights (OV-103)	--	TDDP SPLAS028, 11/13/92	Close to currently projected Shuttle value for Space Station time frame without FY94 proposed enhancements
SSME dry weights	--	TDDP SPLAS028, 11/13/92	Close to currently projected Shuttle value for Space Station timeframe without FY94 proposed enhancements
Weights for other items in Orbiter (Crew comp., OMS load, Shuttle Oper., etc.)	--	TDDP SPLAS028, 11/13/92	Close to currently projected Shuttle value for Space Station time frame without FY94 proposed enhancements
Payload wt	25000 lbs (adjust as required to match 248K downweight for baseline nominal ascent trajectory)	TDDP SPLAS028, 11/13/92	Close to currently projected Shuttle value for Space Station timeframe without FY94 proposed enhancements
External Tank wt	--	TDDP SPLAS028, 11/13/92	Close to currently projected Shuttle value for Space Station timeframe without FY94 proposed enhancements
First stage dynamic pressure limit (nominal and dispersed)	Nom: Low q for June, 57-deg incl Disp: 819 max	NSTS 08209, Volume IV, figure 700-22 (Change #8)	Current Shuttle data for low q launch in June for high inclination

Table 4.6-1 Additional Ascent Trajectory Design Ground Rules for LFBB
(continued)

ITEM	VALUE	DOCUMENTATION	RATIONALE
First stage nominal q-alpha limit during high q region	-3250 minimum	TDDP L63AF060(005), dated 11/17/93, page 15	Typical current TDDP data for Shuttle
Dynamic pressure limit (dispersed) at SRB separation	75 psf	NSTS 07700, Volume X; NSTS 08209 Volume I, Section 7.8	Current Shuttle limit
Ascent vehicle rate and acceleration limits	See Table 4.6-2 below	Provided by EG2/K. Shireman, 1/94	Current Shuttle I-Loads

Table 4.6-2 Ascent Vehicle Rate and Acceleration Limits

NO-FAIL:

ITEM:	<u>MM 101</u>	<u>L/O</u>	<u>SRB SEP</u>	<u>MECO</u>
RATE: (deg/sec)	10	15	5	
ACCEL: (deg/sec ²)	5	5	1.25	

RTLS:

ITEM:	<u>SRB SEP</u>	<u>PPA INITIATION</u>	<u>PPD INITIATION</u>	<u>ET SEP</u>	<u>MM 602</u>
RATE: (deg/sec)	5	10	12.57	2.25	
ACCEL: (deg/sec ²)	1.25	2.5	2.39	0.5625	

References

⁵Chalk, C.R., et al., "Background Information and Users Guide for MIL-F-8785B(ASG) Military Specification - Flying Qualities of Piloted Airplanes"; AFFDL-TR-69-72, Wright-Patterson AFB, Ohio; Aug. 1969

⁶STS 85-0118, "Operational Aerodynamic Data Book, Volume 1 & 2, Launch Vehicle Aerodynamic Data"; September, 1985.

⁷Engel, Carl D. and Praharaj, Sarat C., "MINIVER Upgrade for the Avid System"; REMTECH, Inc.; Huntsville, AL; Aug. 1983.

⁸Fay, J. A., and Riddell, F. R., "Theory of Stagnation Point Heat Transfer in Dissociated Air"; *Journal of the Aeronautical Sciences*, Vol. 25, No. 2; Feb. 1958; pp. 73-85, 121.

⁹Space Shuttle Generic Certification ETR Aerodynamic Heating Data Book External Tank - Ascent, Books 1 - 13"; Report No. STS90D0336A, prepared by Integration Ascent & Plume Heating Unit, Vehicle and Systems Analysis, Rockwell International, Space Systems Division, Contract No. NAS9-18500; June 1992.

¹⁰Thermal Data Book (Lightweight Model) Space Shuttle External Tank, Revision C". Report No. 80900200102, prepared by Thermal Analysis Unit, Martin Marietta, Manned Space Systems; March 1988.

¹¹Space Shuttle Generic Certification ETR Aerodynamic Heating Data Book Solid Rocket Booster - Ascent, Books 1 - 2"; Report No. SSD90D0159, prepared by Integration Ascent & Plume Heating Unit, Vehicle and Systems Analysis, Rockwell International, Space Systems Division, Contract No. NAS9-18500; September 1993.

¹²DeVenezia, J., Wang, K. C., and Caram, J. M., "Space Shuttle Orbiter Wing Leading Edge Heating Predictions and Measurements"; presented at the Orbiter Experiments (OEX) Aerothermodynamics Symposium, Williamsburg, VA; April 27-30, 1993.

¹³Kessler, W. C., Reilly, J. F., and Sampatacos, E., "Hypersonic Shock Wave Interaction and Impingement," Report No. MDC E0476, McDonnell Douglas Astronautics Company - East, St. Louis, MO; October 1971.

SECTION 5 SYSTEMS DEFINITION

5.1 Structures

5.1.1 Structural Factors of Safety

We selected factors of 1.5 and 1.4 for pressurized and non-pressurized structure, respectively. A factor of 1.5 is currently used for the Orbiter and by the USAF for pressurized tanks. This factor is based on the current methods used for analysis, manufacturing, and inspection.

5.1.2 Design Load Factors

Table 5.1.2-1 below contains estimated load factors that are applicable to the LFBB vehicle as a whole, and to large components such as tanks. These values were derived from those for the Shuttle.

Table 5.1.2-1 Estimated Load Factors

Liftoff	Ascent	Descent	Landing
Nx +1.0 / -1.9 g	Nx -3.2	Nx +1.2	Nx +1.0
Ny +/- .5 g	Ny +/- .5	Ny +/- 1.0	Ny +/- .5
Nz +/- .8 g	Nz +/- .8	Nz * +4.0/+2.5/-1.0	Nz +3.0

* 4.0 g for hypersonic flight / 2.5 g for subsonic flight

5.1.3 Booster Sizing

Structural sizing was performed using shear and bending moment diagrams derived from current Shuttle values. Tank, intertank, and skirt structure loaded in compression were sized using optimization equations for compression panels¹⁴. Weights from this sizing were then compared to those weights predicted using historical weight equations. The larger of the weights was then selected for each vehicle component.

5.1.4 Booster Stiffness

The LFBB bending stiffness was estimated to be 30% of the RSRM stiffness. This reduction in stiffness should result in larger booster deflections as the SSME thrust builds on the launch pad. Larger deflections will cause higher base bending moments, require longer umbilicals, and increase the time for the vehicle stack to rock back to vertical. Loads on the external tank due to shrinkage during cryogenic tanking should be reduced by using a less stiff booster. During ascent, the booster's "rolling" modal frequency may affect vehicle control margins and should be assessed in the next phase of design. The filament-wound RSRM case considered by the USAF had less bending stiffness than the current D6AC steel RSRM.

5.1.5 Structure-TPS Configuration Options

Three structure-TPS configurations were evaluated for their potential use for the LFBB structure forward of the LO₂ tank. This task was initiated to determine the effects of eliminating the proposed TPS in the forward region of the booster for the possible cost savings associated with maintenance reductions. The three configurations were:

- 1) Aluminum 2219 structure with TPS tailored advanced blanket insulation (TABI) blanket) on regions forward of the RP-1 tank

- 2) Aluminum 2219 structure without TPS
- 3) Titanium Ti-6-4 structure without TPS

An approximation for structural details needed for this evaluation was accomplished by sizing the structural components for the design loads estimated for the LFBB. The cone and spherical cap were sized for ascent dynamic pressure using equations for monocoque shells. Design optimization equations for stiffened compression panels were used for cylindrical sections of the booster. Tank ellipsoidal domes were sized as membranes subjected to peak pressures from the combination of ullage and head pressures.

Aeroheating resulting from a mach 6 staging trajectory was used with average structural thicknesses (t-bar) to obtain peak structure temperatures. Skin thickness for booster configurations without TPS was then increased beyond what was sized for mechanical loads to add thermal mass needed to keep the structure temperatures at or below the designated allowable peak temperature for that material (see table 5.1.5-1 below).

Table 5.1.5-1 TPS-Structure Configuration Options

<i>configurations:</i>	2219 w/ TABI blanket	2219 w/o TPS	Ti-6-4 w/o TPS
<i>max allowable temp:</i>	350 F	350	800
<i>structure weight:</i>	11928 lb	13211	15320
<i>TPS weight:</i>	171	0	0
<i>total weight:</i>	12099	13211	15320
<i>delta from 2219 with TABI blanket:</i>	0	1112	3211

5.1.5.1 Configuration 1: Aluminum 2219 With TABI

Thermal gradients for this configuration were not evaluated since the aluminum configuration without TPS had more severe gradients.

5.1.5.2 Configuration 2: Aluminum 2219 Without TPS

Peak structural temperatures occurred ~350 seconds into flight during re-entry. A finite element model was constructed to obtain the internal forces caused by the thermal gradients. Results from the model indicate that peak compressive loads due to the thermal gradients would be about 13% of the prelaunch compressive loads that the structure would be subjected to when the SSMEs pitch over the integrated vehicle.

5.1.5.3 Configuration 3: Titanium Ti-6-4 Without TPS

The thermal gradients for the titanium structure were the largest of the three configurations. The effects of these thermal gradients on the titanium configuration were not evaluated since initial sizing for the mechanical loads indicated that this structure would weigh 2000 lbs, or more than either of the aluminum configurations.

5.1.5.4 Recommendations and Conclusions

Configuration 2, the aluminum configuration without TPS on the structure forward of the LO₂ tank, is recommended of the three configurations. Results indicate that the internal loads caused by the thermal gradients are not severe. Although the combined effects of mechanical and thermal loading were not

checked, it is anticipated that prelaunch and lift-off would envelope other load cases for structure aft of the ET forward attach fitting.

The aluminum configuration without TPS does weigh more than the aluminum TABI blanket option, but it also eliminates any maintenance or inspection associated with the TABI blankets on this region of the booster. The weight difference between the two aluminum options is expected to be smaller if the weight due to non-optimum structure (weld lands, secondary structure, access panels, etc.) is considered.

The results of this assessment also indicate that the use of titanium for all structure forward of the LO₂ tank will lead to a large weight penalty over the aluminum configurations. The results also show that titanium or other high-temperature materials would be a good candidate for the spherical nose cap. To keep the nose cap within temperature limits (for the aluminum configuration without TPS), the thickness had to be increased to .661". This is not a practical thickness and weight savings could be obtained by using a high-temperature material (titanium, inconel, etc.) for this portion of the booster.

The results from this assessment are not conclusive due to the many simplifying assumptions made to account for the immaturity of both the design loads and the structural definition. The next design phase should investigate these and other options to a greater extent.

5.1.6 Material Selection

Titanium Ti-6Al-4V was compared with aluminum 2219 for the booster structure. The evaluation of the TPS-structure configurations indicated that large weight increases would result if the structure forward of the LO₂ tank were titanium rather than aluminum. Aluminum alloys are preferred due to the projected weight increase for the use of titanium as well as the added material cost and manufacturing issues. Aluminum 2219 is a weldable alloy that has been used successfully for cryogenic tanks in past programs. Using 2219 aluminum for the LFBB tanks and other common aerospace aluminums (2024, 7075, 7050) for most other structure is recommended at this time. High-temperature materials may have applications in areas of extreme heating, such as the nose cap and leading edges, and should be part of a Phase A assessment. The benefits and issues associated with the use of aluminum lithium for reusable cryogenic tanks and other structural elements should also be considered in the next design phase.

5.1.7 Landing Gear Trade Between Skids & Wheels

A previous Orbiter trade study concluded that a wheel configuration weighed less than a skid design. Wheels also offer more ground mobility. This trade study should apply to the LFBB since its landing weight is approximately that of an Orbiter.

5.1.8 Ascent Aerodynamic Loads on Orbiter

CFD results indicate that shear, bending, and torsion on both of the Orbiter's wings have decreased for the particular flight condition that was checked (Mach 1.25, $\alpha = -3.3$, angle of sideslip (AoS) = .02). Considering only this flight condition, the ascent wing loads would be within the wing's current capability. More flight conditions must be checked to determine whether the wing loads are within limits for the current Shuttle flight envelope. Should other flight conditions result in unacceptable loading, the ascent trajectories would have to be adjusted.

Aerodynamic coefficients from the CFD analysis were used to address the loading on the Orbiter/ET attach struts. Strut loads when using the LFBB were found to be at approximately the same level as with the RSRMs for the one particular flight condition that was evaluated (Mach 1.25, $\alpha = -3.3$, AoS = .02). More flight conditions must be checked to determine whether the strut loads are within limits for the current Shuttle flight envelope.

5.1.9 LFBB / External Tank Attach Strut Loads

[from informal MSFC memo 2/15/94]

5.1.9.1 Buildup and Liftoff

Tables 5.1.9.1-1 and 5.1.9.1-2 show the liftoff loads for a single booster. Some important numbers for buildup are as follows:

My = 373 million in-lbs
ET tip deflection = 55.8 in.

The design value for My is 357 million in-lbs. This should not be a serious problem. The ET tip deflection is significantly higher than the current tip deflection of ~35 inches. Assumptions made for these calculations are a delayed liftoff to coincide with the minimum moment during buildup and a slow-release mechanism to alleviate the Fx loads.

Table 5.1.9.1-1 Aft Booster/ET Strut Loads

LFBB Calculated Load (Kips)

Struts	P8	P9	P10
P8	347* / -418*	30 / 80	9 / -220
P9	-201 / 83	380* / -113	-121 / -55
P10	150 / -199	26 / 178	127 / -347*

RSRM Max Design Load (Kips)

Struts	P8	P9	P10
P8	271 / -264		
P9		277 / -127	
P10			224 / -314

Table 5.1.9.1-2 Forward Attach Booster/ ET Attach Loads

LFBB Calculated Load (Kips)

Struts	P8	P9	P10
P8	170 / -96	-21 / -131	-1091 / -1139
P9	86 / 4	109 / 265	-899 / -1151
P10	58 / 21	-68 / -208	-283 / -1349

RSRM Max Design Load (Kips)

Struts	P8	P9	P10
P8	208 / -100		
P9		76 / 201	
P10			-322 / -1309

5.1.9.2 Ascent

For the ascent trajectory provided by JSC, the maximum Fx that the forward attach point experiences is 1200 klb. The present system is designed for 1750 klb, so this should not be a problem area. A potential problem area is when the booster's thrust is at 0%. The tension limit of 165 klb on the separation bolt is exceeded at this condition and, therefore, separation must occur before booster shutdown.

5.2 Thermal Protection System/Insulation

TPS requirements were minimized by performing a thermal/structural assessment of the area forward of the LO₂ tank to identify heat sink materials and thickness. A reusable TPS cryogenic insulation must be applied to the LO₂ tank to prevent or minimize ice formation during launch preparation and to provide reusability.

The TPS/insulation was designed using the Mach 6 flyback trajectory with ascent and entry heating (figures 4.5.3.3-1 through 4.5.3.3-3 in Section 4) defined at nine locations on the LFBB (figure 4.5.3-1). Peak ascent and entry surface temperatures for the lower pitch plane, upper pitch plane and attachment plane (figures 5.2-1 and 5.2-2) indicate that the ascent environment is more severe for the upper pitch and attachment planes than entry. This is the result of a zero α during ascent and protuberance heating along the attachment line.

A heat sink TPS was designed forward of the LO₂ tank using aluminum or titanium. Tables 5.2-1 and 5.2-2 identify the required thickness values to limit the aluminum to 350°F and the titanium to 600°F for nominal heating. The aluminum thickness was then resized with a heating uncertainty of 30% and these results are given in table 5.2-3. For comparison purposes, a TPS system using a TABI blanket, 0.25-in. thick, with an aluminum skin was also designed.

Rohacell foam, with maximum surface temperature of 400°F, was selected as the cryogenic insulation for the LO₂ tank. Temperature predictions (figures 5.2-1 and 5.2-2) indicate exceedance of the 400°F limit, requiring application of a TPS over the Rohacell insulation. A TABI blanket (.25 in.) bonded to the Rohacell foam (1 in.) was used in this study (figure 5.2-3). The TABI blanket was selected based on increased temperature capability and durability over the Orbiter AFRSI blanket.

TPS/insulation weight results are shown in table 5.2-4. These are LFBB cylinder body weights only; the TPS for the wings, control surfaces, and engine area are undefined.

The preliminary results of this study indicate several areas requiring further investigation. Figure 5.2-4 shows the temperature distribution through the TABI, Rohacell foam, and aluminum structure at engine ignition for a hot day, eight-hour hold. Note that the TABI surface is approximately 24°F but the TABI/Rohacell interface is at -20°F. Further studies and/or tests will be required to understand any potential ice formation on the surface and at the TPS/insulation interface for this and other environmental conditions. This study used a Rohacell density of 6.9 lb/ft³, but other grades of Rohacell at lower density (3.2 lb/ft³) are available. In addition, trade studies need to be performed using the current Orbiter external tank insulation (2.4 lb/ft³) for this TPS/insulation application.

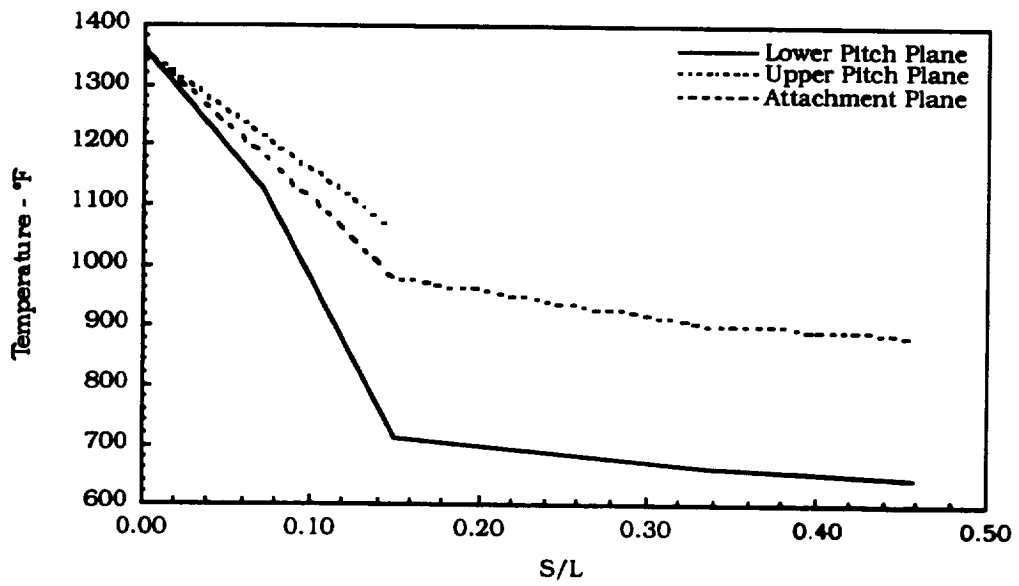


Figure 5.2-1 Flyback booster ascent surface temperatures: Mach 6 trajectory / 350°F wall.

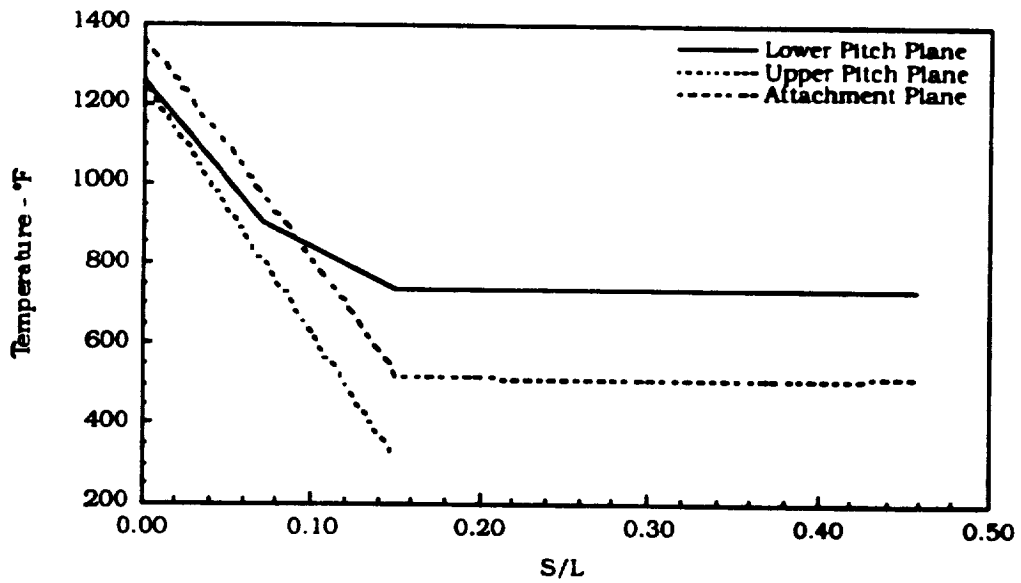


Figure 5.2-2 Flyback booster entry surface temperatures: Mach 6 trajectory / 350°F wall.

Table 5.2-1 Anodized Aluminum (Emissivity - 0.6)

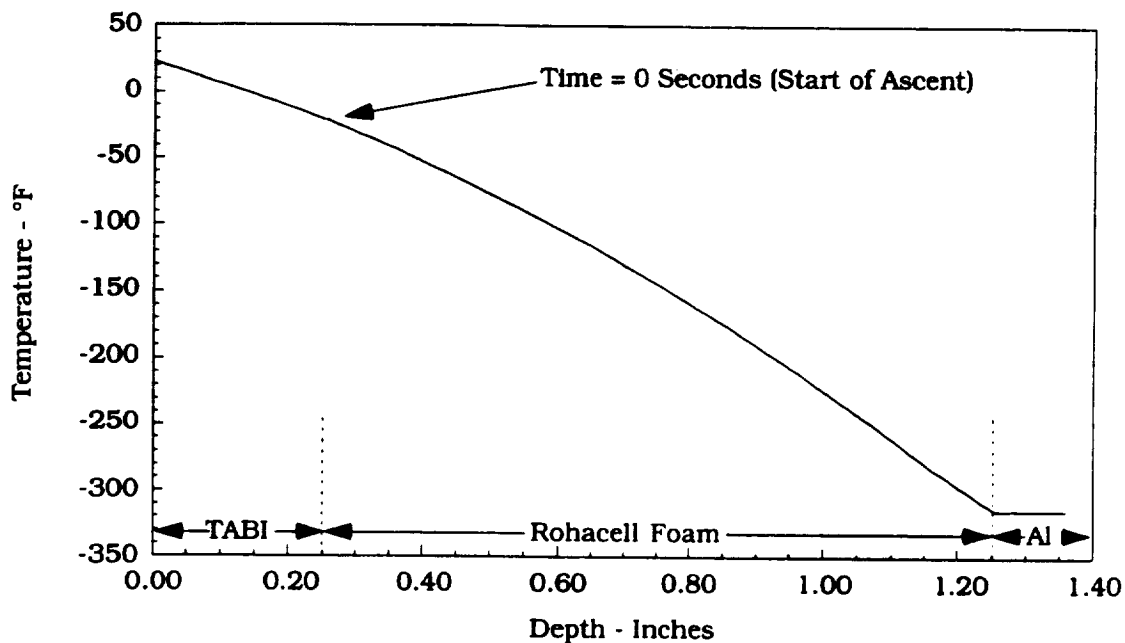
Body Point	Al Thickness (inch)	Ascent Time	Al Temperature (°F)	Entry Time	Al Temperature (°F)
1	0.503	212	226.42	355	349.55
2	0.256	212	250.01	340	349.98
3	0.125	144	344.83	338	344.10
4	0.125	212	220.26	336	344.14
5	0.125	184	292.43	328	355.97
6	0.236	212	150.85	350	225.28
7	0.236	212	186.26	334	218.11
8	0.311	212	130.70	355	189.09
9	0.311	212	157.09	345	182.89

Table 5.2-2 Titanium (Emissivity - 0.6)

Body Point	Ti Thickness (inch)	Ascent Time	Ti Temperature (°F)	Entry Time	Ti Temperature (°F)
1	0.152	212	-391.76	324	600.50
2	0.260	212	187.73	340	268.47
3	0.058	140	418.46	340	358.27
4	0.058	212	306.50	324	481.63
5	0.058	170	359.87	324	413.69
6	0.178	212	157.49	360	236.48
7	0.178	212	175.71	360	215.25
8	0.215	212	142.39	360	209.56
9	0.215	212	157.39	360	191.78

Table 5.2-3 Anodized Aluminum (Emissivity - 0.6), 30% Uncertainty

Body Point	Al Thickness (inch)	Ascent Time	Al Temperature (°F)	Entry Time	Al Temperature (°F)
1	0.661	212	225.89	355	349.24
2	0.340	212	249.12	345	350.21
3	0.163	148	348.10	350	349.03
4	0.165	212	222.12	350	349.18
5	0.161	196	299.29	330	349.33
6	0.236	212	176.25	350	272.11
7	0.236	212	221.41	334	262.59
8	0.311	212	149.97	355	225.54
9	0.311	212	183.81	350	217.44



**Fly-Back Booster (TABI/1.0 in Rohacell) (8 Hr on the Pad)
90°F Hot Day ($H_{env} = 2 \text{ Btu/ft}^2\text{-hr-}^\circ\text{F}$)**

Figure 5.2-3 NASA/Ames TABI elements.

Table 5.2-4 LFBB Thermal Protection System Weight

Structure/TPS Options	Fuel Tank	Lo ₂ Tank
2219 Aluminum/with TPS	143	2314
2219 Aluminum/no TPS	0	2314
Ti-6-4/no TPS	0	2314
TABI/Rohacell	0	2314

Note: LO₂ tank requires TPS/insulation for all options

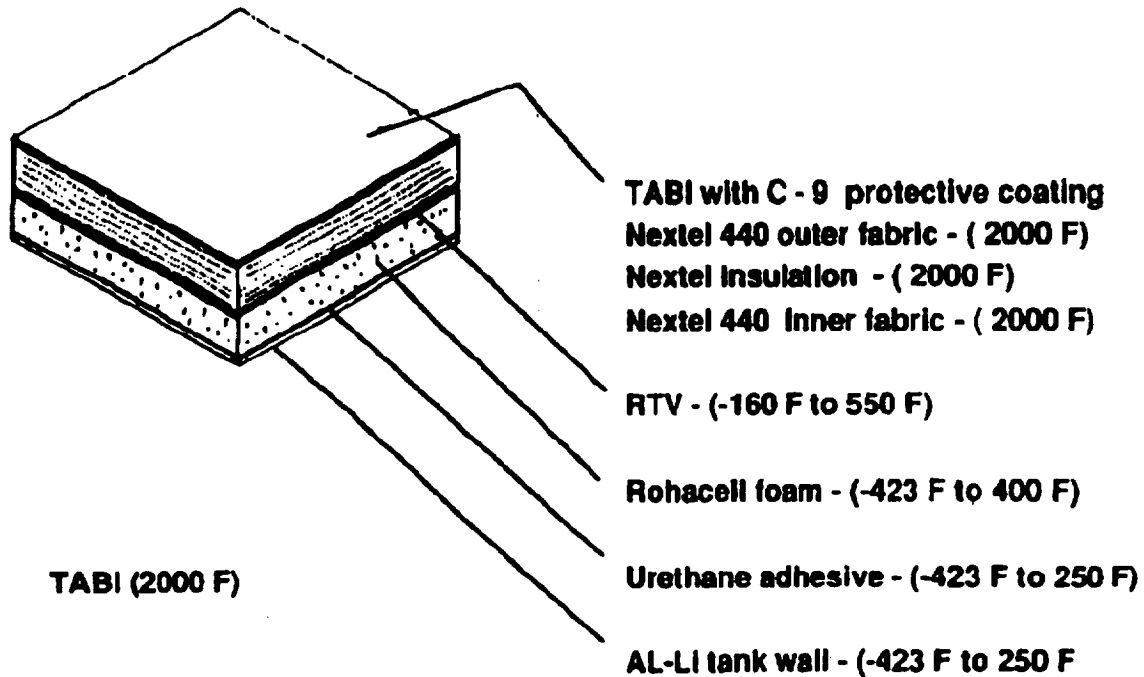


Figure 5.2-4 Flyback booster (TABI/1.0 in. Rohacell) (8 hr on the pad) 90°F hot day
($H_{env} = 2 \text{ Btu/ft}^2\text{-hr-}^\circ\text{F}$)

5.3 Ascent Propulsion

5.3.1 LFBB Main Propulsion System Description

The Russian RD-170 main engines were selected early in the Pre-Phase A study due to the near-term availability of the engines and excellent performance. A detailed main propulsion system design was developed based on the RD-170 engines. This section describes the details of the RD-170 engine-based propulsion system. Late in the study, the Russian RD-180 engine was selected as the baseline engine due to the engine-out abort capability that can be provided. The RD-180 engines deliver half of the thrust that an RD-170 engines provides. Therefore, each booster will require four RD-180 engines instead of two RD-170 engines. Feed lines and other main propulsion system components will be affected by this change. Due to time constraints, a detailed design of an RD-180-based main propulsion system was not developed. We envision no large impacts to the currently designed system due to the engine change.

The current configuration for the LFBB utilizes a LO₂ tank aft design. The schematic of the propulsion system is shown in figure 5.3.1-1. Feed line envelopes are shown in figures 5.3.1-2 and 5.3.1-3. Oxidizer line bends and slopes are minimized to ensure good quality propellant near the end of flight to minimize the residuals. The LO₂ line envelopes shown are worst-case and will be refined as the propulsion system and structural interfaces are identified. The LO₂ feed lines are sized to the RD-170 inlet diameter of 19.75 inches. A LO₂ sump configuration was eliminated when preliminary design indicated the sump volume was 72.43 ft³, which would result in approximately 5,150 lbm residual LO₂. The fuel feed line main trunk line from the tank is 20.5 in. diameter. The line branches to each RD-170 in the aft compartment. The fuel inlet diameter is 15.75 in.; propulsion system components other than the RD-170 engine are listed in table 5.3.1-1.

Functions supported by the propulsion system are:

- Rocket propulsion (2 RD-170 engines)
- Fuel (RP-1) fill, drain, and engine supply
- Oxidizer (LO₂) fill, drain, and engine supply
- Pressurization of the fuel tank with ambient helium
- Pressurization of the LO₂ tank with ambient helium passed through two engine heat exchangers (1 per RD-170)
- Ground supply of ambient helium to fill pressurization bottles (bottles are 30 ft³, 4000 psig)
- Pre-pressurization of the fuel and oxidizer tanks with ground-supplied ambient helium
- Ground supply of gaseous nitrogen to the engine
- Ground supply of missile grade air to the engine and to purge aft compartment
- Fuel and oxidizer tank vent and relief system
- Geysers avoidance during oxidizer tank fill
- Passive POGO system to suppress feed system and structural acoustics

It is assumed that the engine provides the LO₂ recirculation pump. The engine LO₂ recirculation line interface is 2.36 in. diameter.

In the absence of any stated system requirement, no purge has been provided to the forward compartment or intertank areas. Missile-grade air has been supplied to the aft compartment to provide environmental conditioning, but this requirement was not explicitly stated.

RD-170 operating data assumed in the design is shown in table 5.3.1-2. The net positive suction pressure (NPSP) requirements used to design the propulsion system are assumed to vary linearly with power level. Figure 5.3.1-4 shows the booster acceleration used to calculate the pump inlet NPSP and engine power levels as a function of time are shown in figure 5.3.1-5. JSC supplied engine power level and acceleration.

The fuel tank is pre-pressurized with ground supplied ambient helium to 10 psig to meet engine start conditions. The fuel tank is pressurized during mainstage operation with on-board ambient helium to 10 + 1 psig to maintain tank structural integrity. The mass of helium required is calculated to be 83 lbm. The Kevlar-wrapped titanium shell helium bottle is charged to 4000 psi. The volume of the storage bottle is 30 ft³. Mainstage fuel NPSP requirements are well surpassed due to fluid head pressure associated with the fuel tank forward configuration. Estimated fuel tank ullage pressure versus time is shown in figure 5.3.1-6. Resulting maximum tank bottom pressure is 43.0 psig for the fuel tank and is shown as a function of time in figure 5.3.1-7. The fuel pump inlet NPSP is plotted as a function of fuel mass remaining in figure 5.3.1-8. The propellant inventory is shown in table 5.3.1-3.

The LO₂ tank is pre-pressurized with ground supplied ambient helium to 34 psig to meet engine start conditions. The LO₂ tank is pressurized to 34 + 1 psig during mainstage operation to meet engine run conditions. The pressurant is ambient-stored helium passed through two engine heat exchangers. The mass of helium required is calculated to be 756 lbm. Six Kevlar-wrapped titanium shell helium bottles are charged to 4000 psi. The volume of each storage bottle is 45 ft³. Estimated LO₂ tank ullage pressure versus time is shown in figure 5.3.1-9. Resulting maximum tank bottom pressure is 92.6 psig for the LO₂ tank and is shown as a function of time in figure 5.3.1-10. The LO₂ pump inlet NPSP is plotted as a function of oxidizer mass remaining in figure 5.3.1-11.

The RD-170 servicing, pre-launch checkout, and launch commit criteria are available through Pratt & Whitney and NPO Energomash. The checkout procedures, loading procedures, and launch commit criteria for the rest of the propulsion system have not been examined.

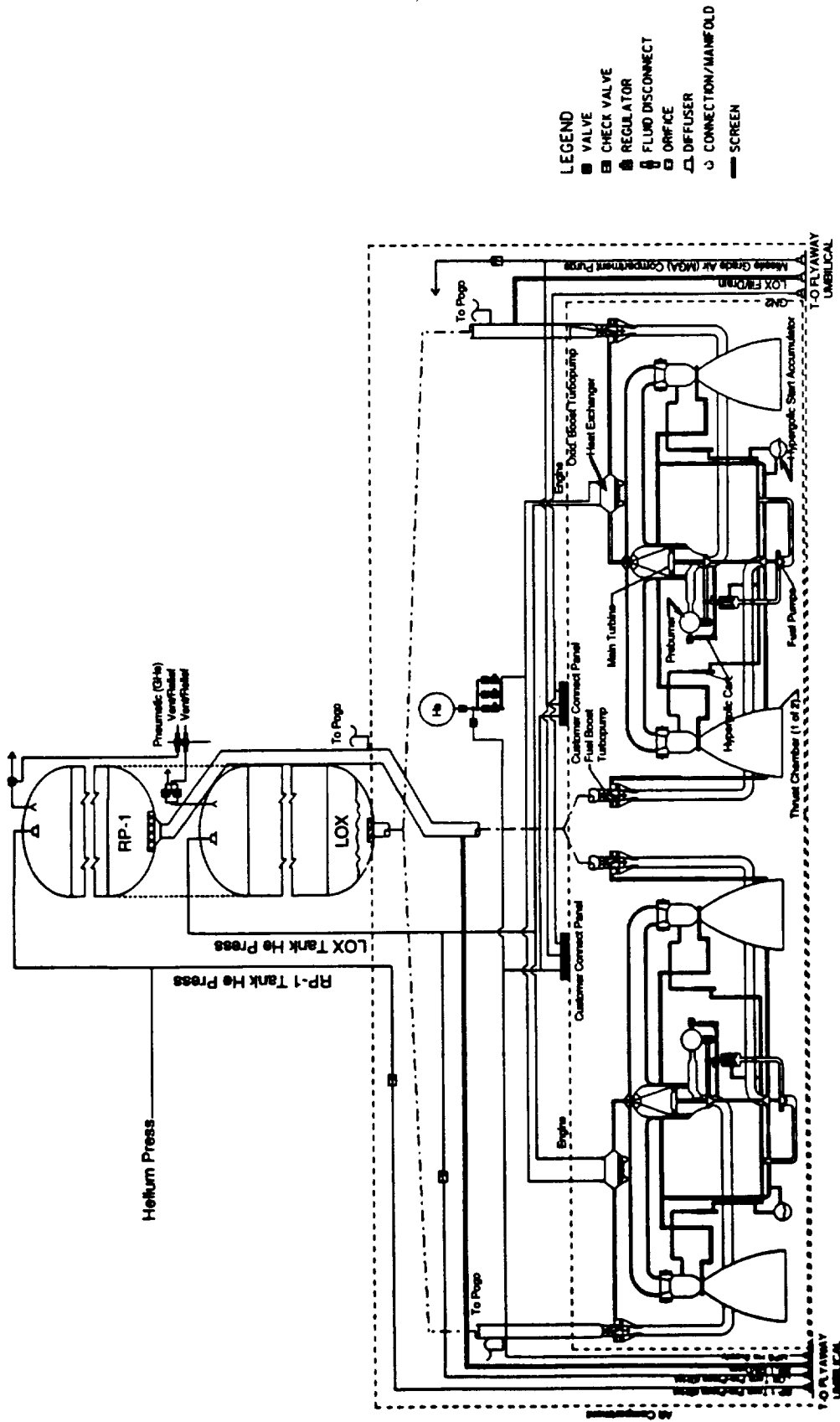
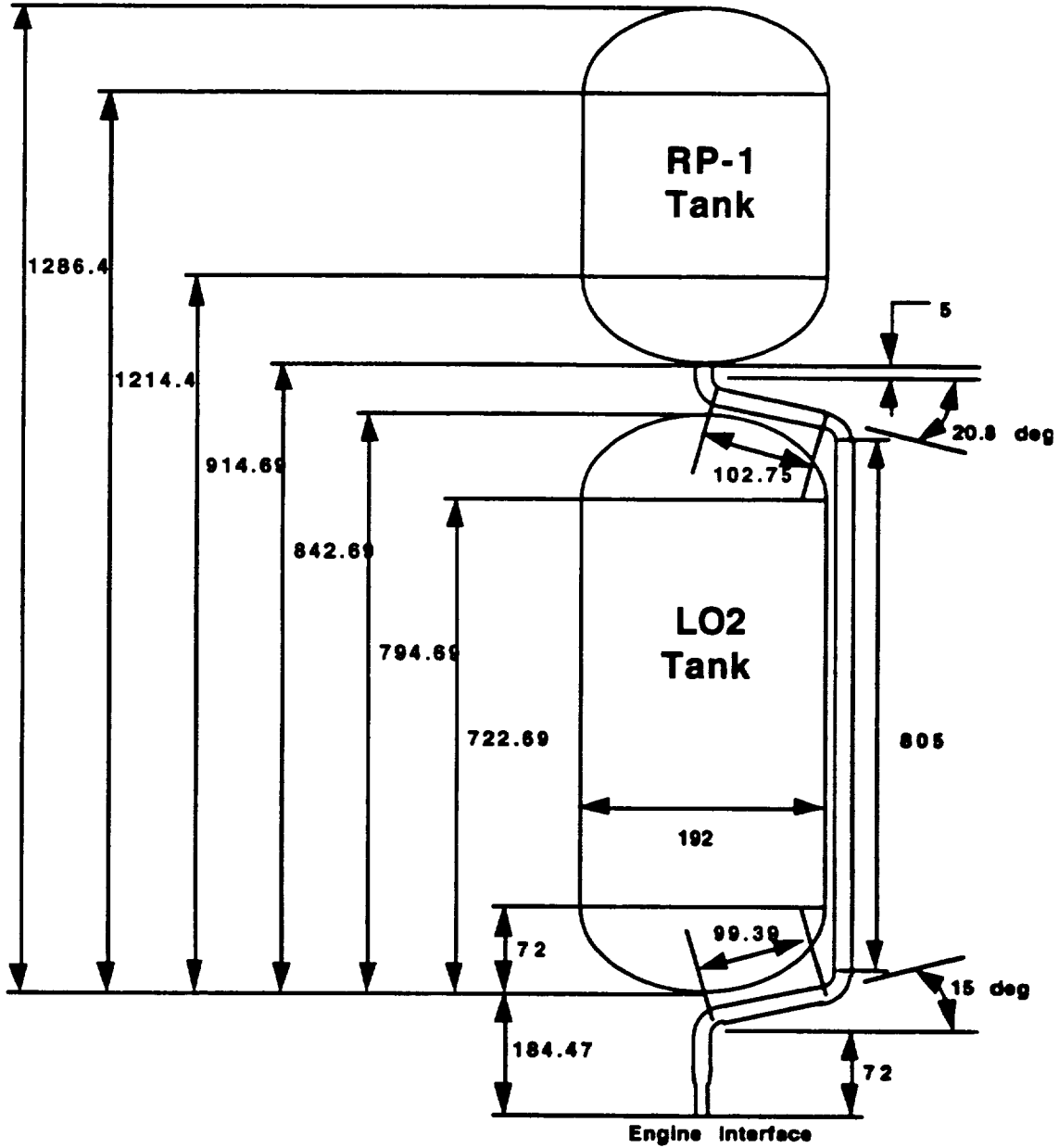


Figure 5.3.1-1 LFBB Main Propulsion System Schematic

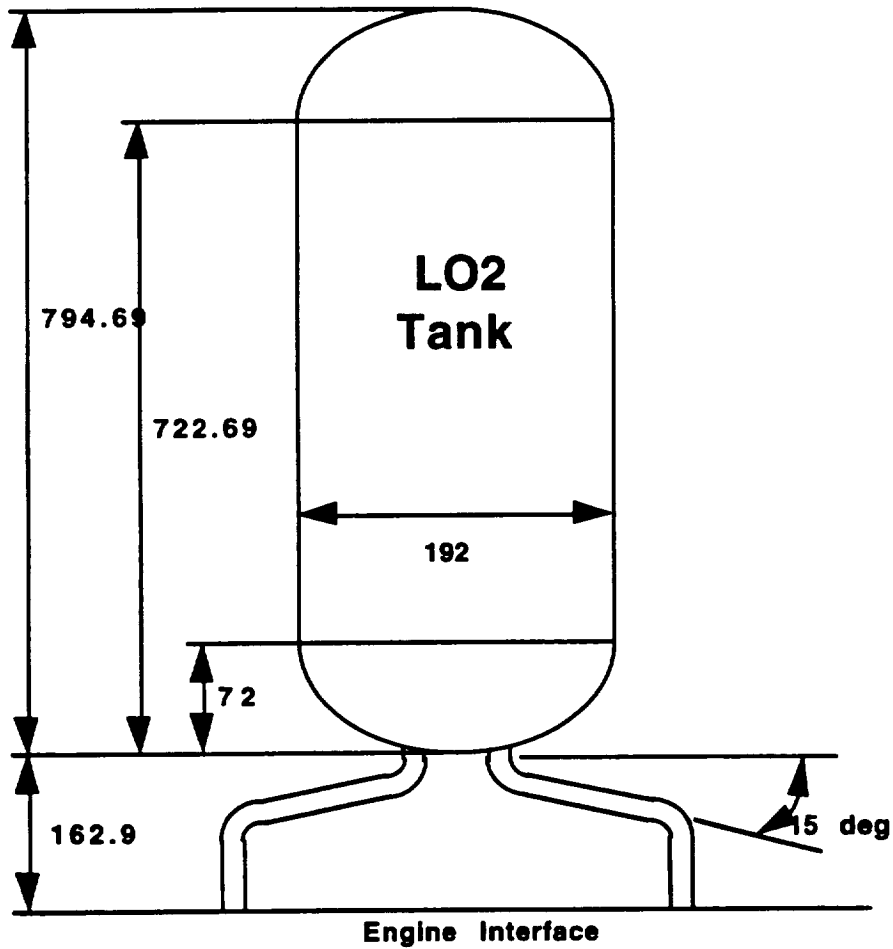
Shuttle Fly Back Booster Main Propulsion System (RP-1 Tank & Feedline)



NOTE: All units are inches unless otherwise stated

Figure 5.3.1-2 Shuttle flyback booster main propulsion system (RP-1 tank and feed line).

Shuttle Fly Back Booster Main Propulsion System (LO₂ Tank & Feedline)



NOTE: All units are inches unless otherwise stated

Figure 5.3.1-3 Shuttle flyback booster main propulsion system
(LO₂ tank and feed line).

Table 5.3.1-1 LFBB Preliminary Part List

ABS	Assembly Name	Usage	Qty	Unit Wt	Tot Wt
1	Engines				53200.0
1.1	RD-170	propulsion	2	26600.0	53200.0
2	Hazardous Gas Detection Sys				100.0
2.1	Aft compartment	Identify hazardous			
2.2	RP-1/LO ₂ intertank	gas concentrations			
3	RP-1 Feed System				2666.2
3.1	520 mm (20.5") feed line	Supplies 2 RD-170s			
3.1.1	RP-1 tank outlet assembly		1	0.0	0.0
3.1.2	RP-1 line assembly		1	660.1	660.1
3.1.3	Intertank elbow		2	32.5	65.1
3.1.4	Aft compartment elbow		2	30.2	60.4
3.1.5	Bellows		6	73.5	441.2
3.1.6	RP-1 POGO suppression		1	75.0	75.0
3.1.7	RP-1 engine 400 mm (15.75") line	Supplies 1 RD-170	2	42.0	84.1
3.1.8	RP-1 engine pre-valve		2	160.0	320.0
3.2	RP-1 feed system instrumentation		0	0.0	0.0
3.3	200 mm (8") fill and drain system				
3.3.1	RP-1 fill and drain Line assembly		1	55.0	55.0
3.3.2	RP-1 fill and drain inboard valve		1	50.0	50.0
3.3.3	RP-1 fill and drain disconnect		1	240.0	240.0
4	LO₂ Feed System				3327.4
4.1	500 mm (19.75") feed line	Supplies 1 RD-170			
4.1.1	LO ₂ tank outlet assembly		1	0.0	0.0
4.1.2	LO ₂ POGO suppression system		2	75.0	150.0
4.1.3	LO ₂ engine feed line		2	259.3	518.6
4.1.4	LO ₂ elbow		4	108.8	435.2
4.1.5	LO ₂ bellows		4	70.9	283.4
4.1.6	LO ₂ flex joint		2	136.7	273.4
4.1.7	1 in. foam insulation		2	48.4	96.7
4.1.8	LO ₂ engine pre-valve		2	194.0	388.0
4.1.9	LO ₂ 60 mm (2.36") circulation line		2	33.1	66.2
4.1.10	LO ₂ circulation valve		2	10.0	20.0
4.2	LO ₂ feed system instrumentation		0	0.0	0.0
4.3	200 mm (8") fill and drain system				
4.3.1	LO ₂ fill and drain line assembly		1	38.0	38.0
4.3.2	LO ₂ fill and drain inboard valve		1	50.0	50.0
4.3.3	LO ₂ fill and drain disconnect		1	240.0	240.0
5	LO₂ Tank Pressurization Sys				6416.7
5.1	Diffuser assembly		1	15.0	15.0
5.2	FWD He press line assembly		1	26.8	26.8
5.3	Main He press line assembly		1	274.7	274.7
5.4	He storage bottle assembly	45 ft ³ vol. storage	6	763.2	4579.2
5.5	He flow control valve		3	6.0	18.0
5.6	GHe Pre-pressurization line		1	20.2	20.2
5.7	GHe pre-press disconnect		1	2.0	2.0
5.8	LO ₂ tank press sys instru.		0	0.0	0.0

Table 5.3.1-1 LFBB Preliminary Part List
(continued)

ABS	Assembly Name	Usage	Qty	Unit Wt	Tot Wt
6	RP-1 Tank Pressurization Sys				767.7
6.1	Diffuser assembly		1	15.0	15.0
6.2	FWD He press line assembly		1	20.3	20.3
6.3	He storage bottle assembly	30 ft ³ vol. storage	1	515.1	515.1
6.4	He flow control valve		3	6.0	18.0
6.5	GHe pre-pressurization line		1	20.2	20.2
6.6	GHe pre-press disconnect		1	2.0	2.0
6.7	RP-1 tank press sys instrumentation		0	0.0	0.0
7	Pneumatic System				101.4
7.1	Ground supply/fill & distribution ass.		1	25.0	25.0
7.2	POGO pre-charge dist. & ctrl. ass.		1	0.0	0.0
7.3	Storage bottle assembly		1	40.0	40.0
7.4	Regulator and control assembly		1	8.0	8.0
7.5	GHe inject assembly		1	5.0	5.0
7.6	Pneumatic system instrumentation		0	0.0	0.0
8	LO₂ Tank Systems				55.9
8.1	Tank vent/relief valve		1	12.0	12.0
8.2	Vent line assembly		1	16.0	16.0
8.3	Vent valve actuation line & discon.		1	8.0	8.0
8.4	LO ₂ tank instrumentation		1	7.0	7.0
9	RP-1 Tank Systems				44.2
9.1	Tank vent/relief valve		1	10.0	10.0
9.2	Vent line assembly		1	12.0	12.0
9.3	Vent valve actuation line & discon.		1	7.0	7.0
9.4	RP-1 tank instrumentation		1	5.0	5.0
10	Compartment Purge Systems	Print Systems will, prevent ice buildup on valve and comp, Safe Engines			300.0
10.1	Aft comp purge manifold assembly		1		
10.2	Aft comp purge disconnect ass.		1		
10.3	Aft comp purge flow control ass.		1		
10.4	Aft comp purge instrumentation				

Table 5.3.1-2 RD-170 Operating Data

Power Level	Mass Flow (lbm/sec)		NPSP Req'd	
	LO ₂	RP-1	LO ₂	RP-1
50%	1894	741	22.0	12.32
102%	3856	1484	38.4	17.1

BOOSTER ACCELERATION VERSUS TIME FROM LIFTOFF

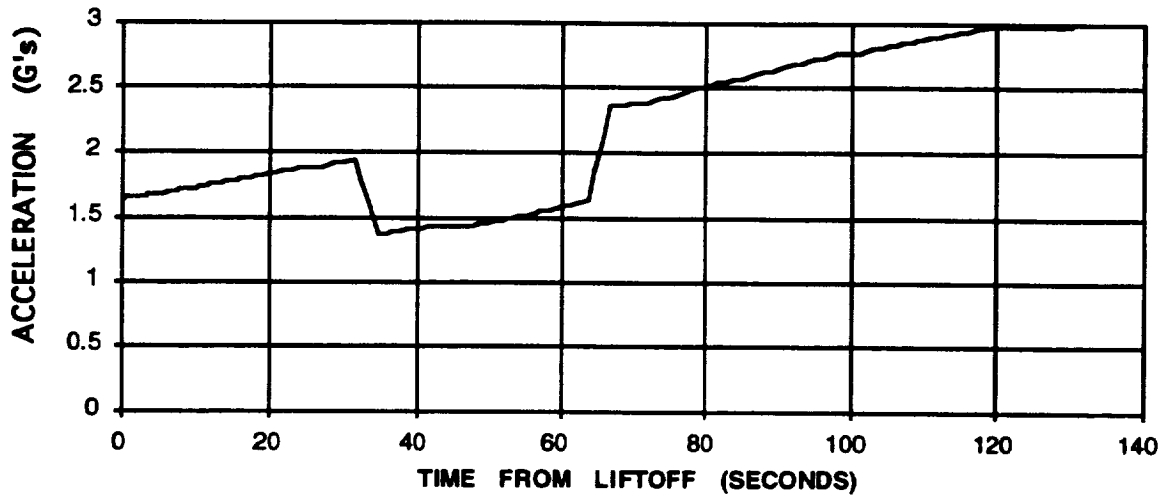


Figure 5.3.1-4 Booster acceleration vs time from liftoff.

ENGINE POWER LEVEL VERSUS TIME

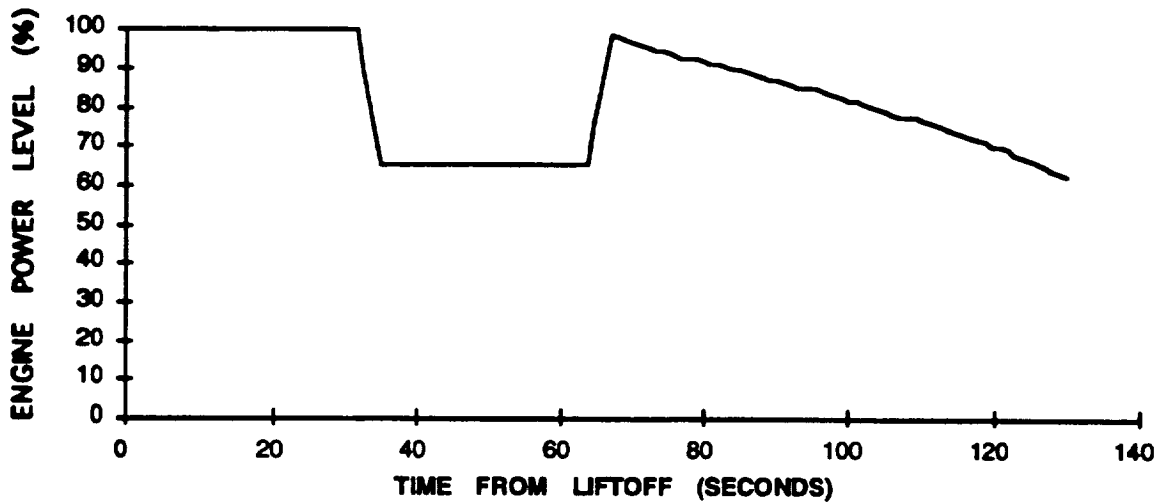


Figure 5.3.1-5 Engine power level vs time.

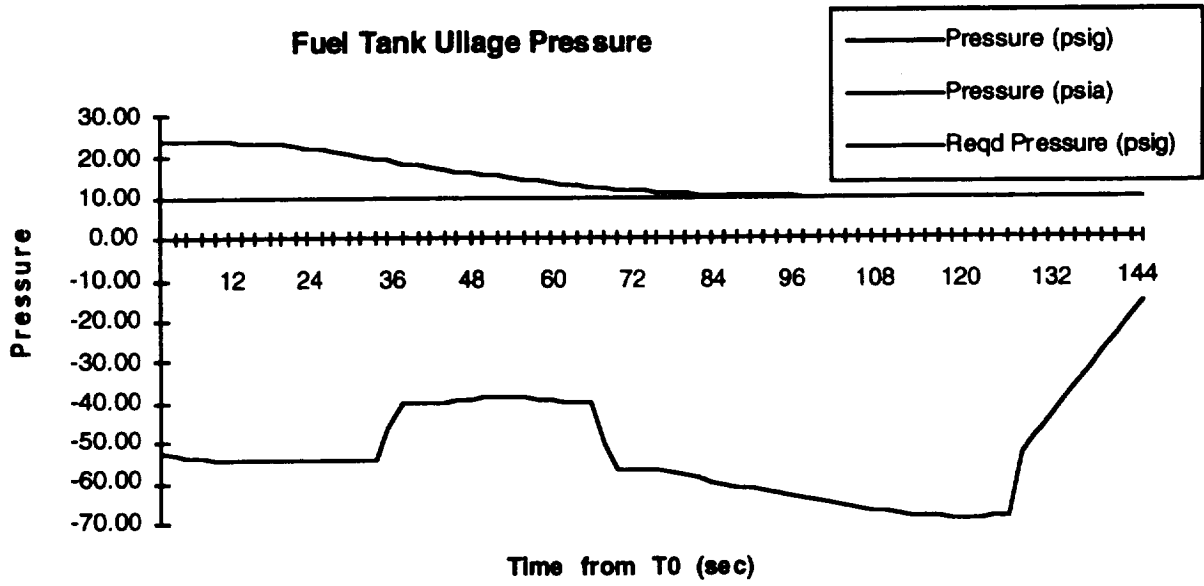


Figure 5.3.1-6 Fuel tank ullage pressure.

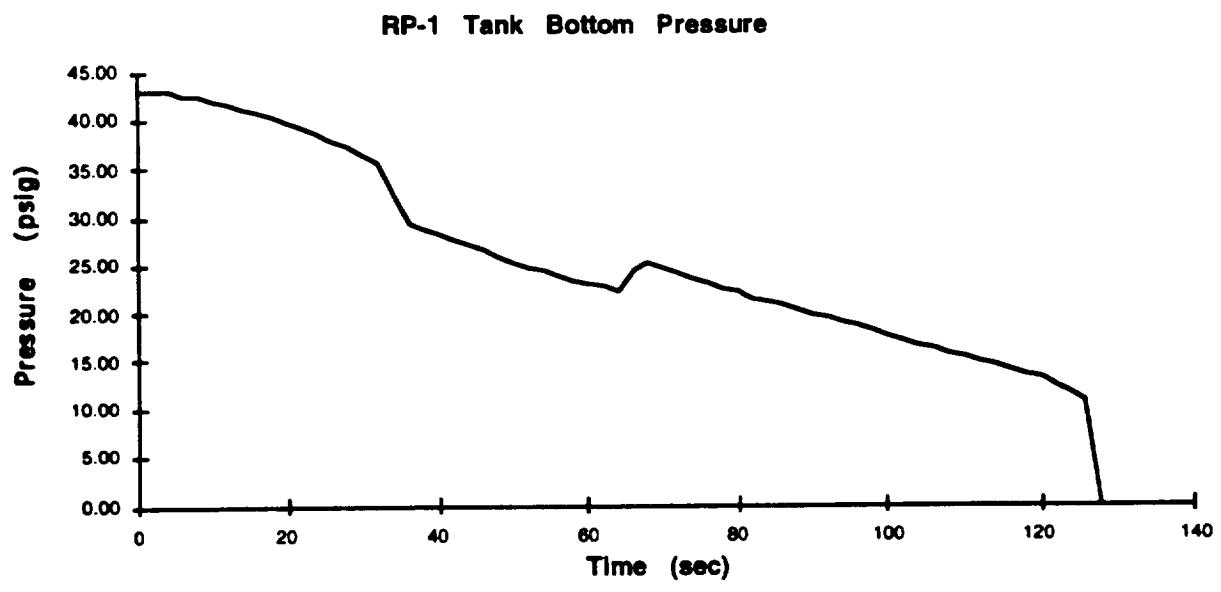


Figure 5.3.1-7 RP-1 tank bottom pressure.

Table 5.3.1-3 Booster (RD-170) Propellant Inventory Summary

Engine Thrust (lb)	3200000.00			
Required Propellant Load (lbm)	1138067.00			
Mixture Ratio	2.60			
Propellant Supply	LO₂	RP-1	Combined	M/R
Usable Propellant (lbm)	821937.28	316129.72	1138067.00	2.6
Unusable				
Tank residuals (lbm)	0.00	0.00		
Feed line and pump residuals (lbm)	8219.00	3161.00		
Engine shut-down consumption (lbm)	2260.20	713.92		
Gas residuals (lbm)	200.00	60.00		
Prestart boil-off (lbm)	0.00	0.00		
Start consumption	45699.00	17577.00		
Propellant Required at Full Thrust	878315.48	337641.64	1215957.12	2.6
Tank diameter (I.D. inches)	192.00	192.00		
Propellant density (lbm/ft ³)	71.13	51.00		
Feed system volume (ft ³)	78.27	229.00		
Mass in feed line (lbm)	5567.35	11679.00		
Dome volume (3/4 ellipse) ft ³	804.10	804.10		
Ullage height (inches)	35.00	35.00		
Liquid volume in dome (ft ³)	565.26	565.26		
Ullage volume (ft ³)	238.83	238.83		
% Ullage by volume (lbm, cryo-unpressurized)	0.02	0.04		
Equivalent ullage mass (lbm)	16988.22	12180.50		
Req'd tank capacity (lbm, cryo-unpressurized)	889736.35	338143.15	2.63	
Req'd tank volume (ft ³ , cryo-unpressurized)	12508.59	6630.26	0.53	

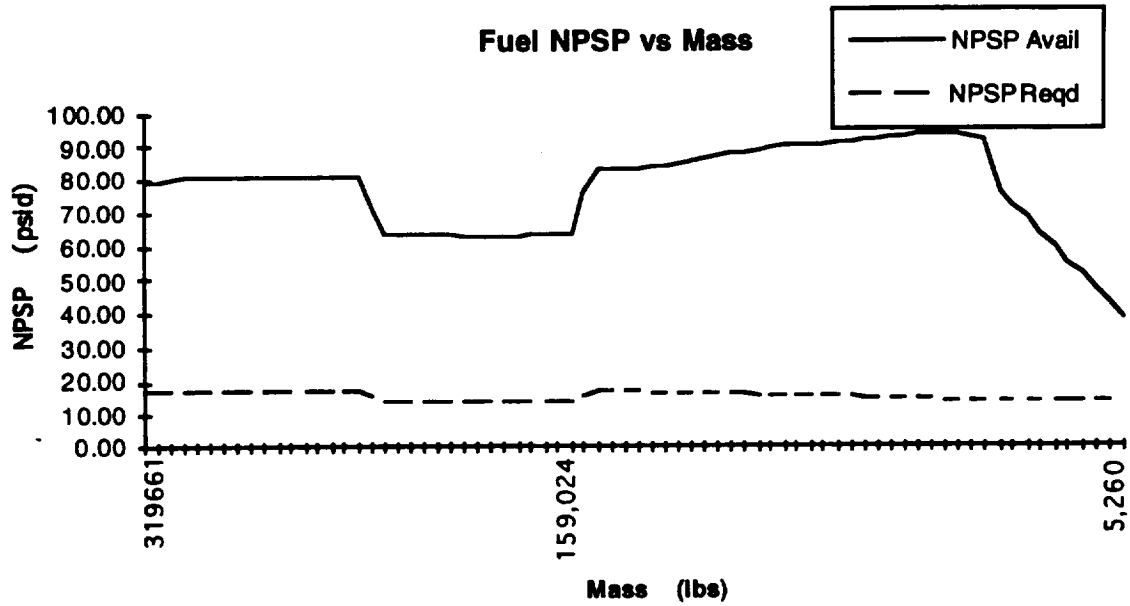


Figure 5.3.1-8 Fuel NPSP vs mass.

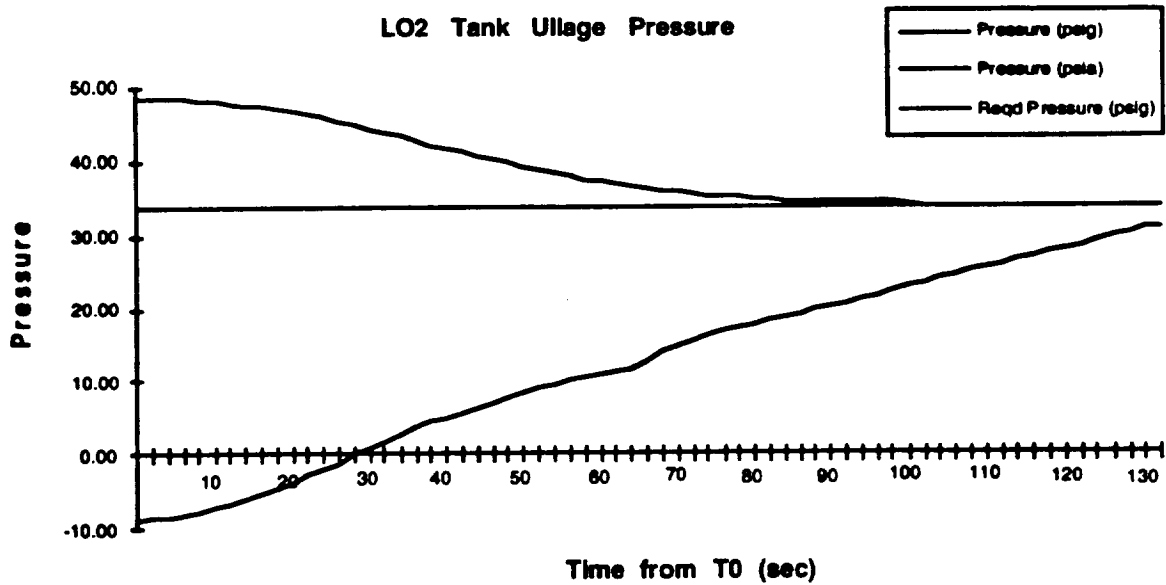


Figure 5.3.1-9 LO₂ tank ullage pressure.

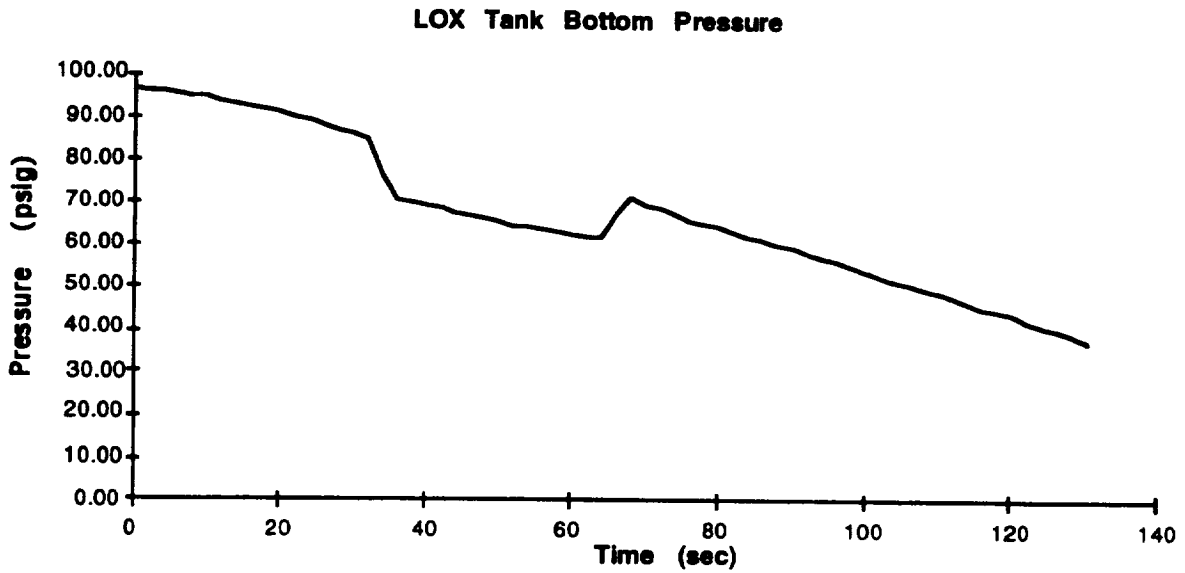


Figure 5.3.1-10 LO₂ tank bottom pressure.

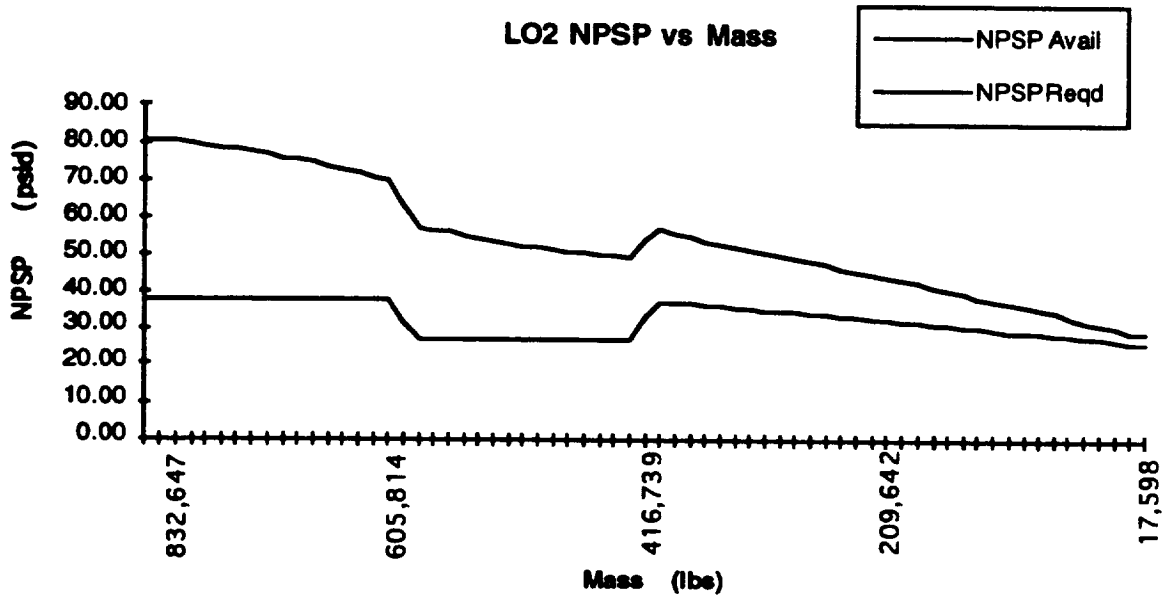


Figure 5.3.1-11 LO₂ NPSP vs mass.

5.3.2 Propellant Tank Pressurization Scenario Flyback Phase of Flight

The pressure inside the propellant tanks must be managed during the flyback portion of the mission to ensure that no structural damage is incurred. If the pressure gets too high in either tank, then that tank could experience structural failure resulting in yielding or explosion of the tank. If the pressure gets too low, the tank will implode during reentry. The following scenario shows how both the fuel tank and LO₂ tank pressures can be managed to prevent structural damage while making them ready for refurbishment as soon after landing as possible.

LO₂ Tank - The LO₂ tank will be pressurized to about 35 psi at booster engine cut-off (BECO). At the altitude that BECO occurs the external pressure will be near a hard vacuum. That means that the LO₂ tank pressure is 35 psia and it will decrease to about 20 psig upon landing provided no LO₂ is vaporized during flyback. LO₂ vaporization during flyback may require that the LO₂ vent and relief valve relieve the added pressure. This would be a routine venting with no adverse effects. After landing and roll out the LO₂ tank can be vented. The vented gases would be helium and GO₂ and the vent operation should take 10 to 15 minutes. Some residual LO₂ might remain in the bottom of the LO₂ tank and in the propellant lines. Any residual LO₂ would evaporate within a few hours with no adverse effects.

RP-1 Tank - The fuel tank will be pressurized to 10 psi at BECO. Without the addition of pressurant to the fuel tank the pressure would be approximately -4 psig on landing and roll out. That negative pressure would cause the fuel tank to collapse or implode. To prevent this damage, the pressurant control valves should be opened after BECO and the residual pressurant inside the helium bottles should be allowed to pressurize the fuel tank to at least 17 psia. Then, upon landing the fuel tank pressure would 2 psig. The pressurant gas would be helium and there would be some residual fuel in the bottom of the tank or in the feed lines. This scenario should pose no ground operations constraints following landing and roll out. The only flyback constraint would be that the pressure inside the fuel tank should be 17 psia before re-entering the atmosphere.

5.4 RCS Propulsion

5.4.1 Introduction

The RCS is designed to provide attitude control in the pitch, yaw, and roll axes for the LFBB from post-booster separation motor burnout to Mach 1. The control provided by the RCS has been assumed to be similar to that provided by the Space Shuttle Orbiter aft RCS during entry.

5.4.2 Requirements

5.4.2.1 General

The requirements and assumptions for the RCS during this Pre-Phase A activity can be found in table 5.4.2.1-1. The total impulse required by the RCS was derived from Orbiter propellants necessary to perform a 57° 3σ entry. Thruster size requirements are assumed to be similar to the Orbiter primary thrust class.

Table - 5.4.2.1-1 RCS Pre-Phase A Requirements and Assumptions

1	The RCS shall be enabled post-LFBB separation motor burnout to Mach 1
2	The RCS and aerosurfaces shall be compatible systems for combined flight control of the vehicle
3	The RCS shall provide a total impulse of 276000 lbf-s
4	Four thrusters capable of 500 to 1000 lbf shall be required for left and right yaw directions
5	Three jets capable of 500 to 1000 lbf shall be required for left-up, left-down, right-up and right-down directions,
6	The RCS shall be single-fault tolerant except at the thruster level which shall be two-fault tolerant
7	The RCS shall use dedicated tankage for propellant storage
8	The vehicle can be controlled using an aft RCS module

5.4.2.2 Thruster and Manifold

Discussions held with the LFBB vehicle dynamics group determined requirements for the number of thrusters, their placement, and thrust to control the vehicle. Due to similarities in mass with the Orbiter, aft-only RCS in combination with aerodynamic surfaces was assumed to be sufficient to control the vehicle after booster separation motor burnout. Definition of the thruster configuration is shown in figure 5.4.2.2-1. This figure shows the thruster plume directions looking forward. The system of 20 thrusters is similar to the Orbiter aft RCS without the +X and vernier thrusters.

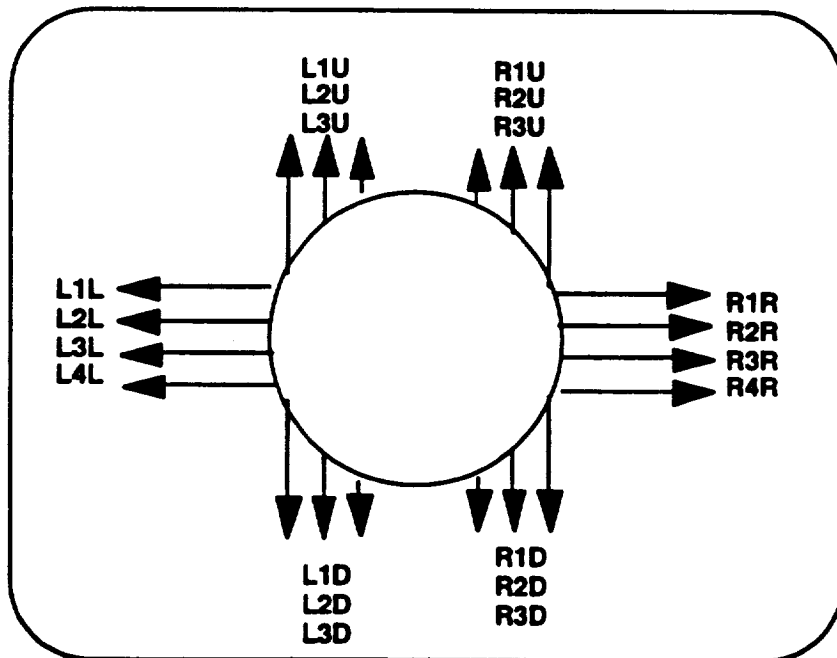


Figure 5.4.2.2-1 RCS thruster configuration.

The RCS manifold configuration must contain a minimum of four manifolds to achieve two-fault tolerance equivalent to the Orbiter. This assumes that a minimum of two yaw jets are required to provide adequate thrust during entry. However, the number of thrusters in this thrust range which can be operated on a single manifold without pneumatic or hydraulic transients becoming a concern will require more study. For this effort, a four-manifold system was assumed with thrusters assigned as shown in figure 5.4.2.2-2.

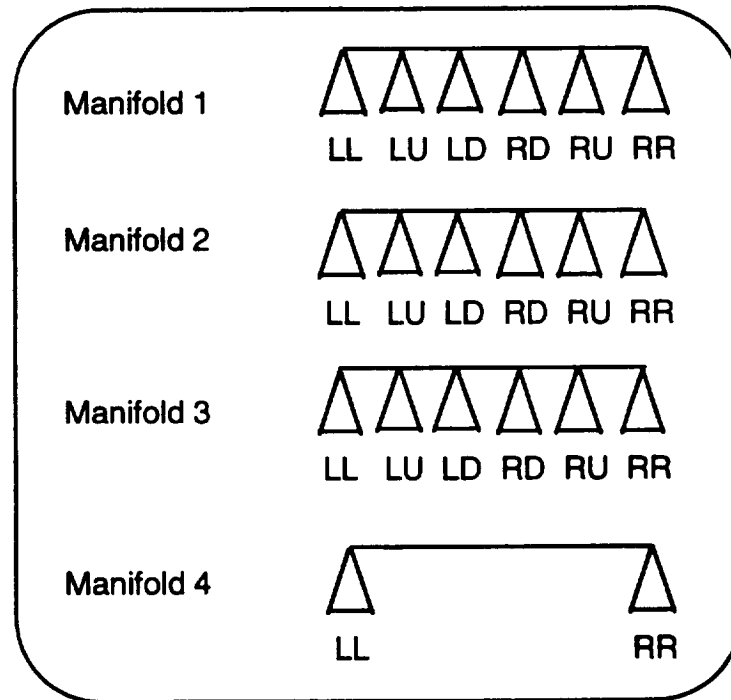


Figure 5.4.2.2-2 Manifold and thruster layout.

5.4.3 Propellant Selection

5.4.3.1 Combinations Considered

The propellant combinations listed in table 5.4.3.1-1 were considered for the LFBB RCS. Concepts were developed and sized for the four propellant options compared in table 5.4.3.1-2. In this table, the mass and volume of the systems are compared relative to an NTO/MMH system. Concepts for two RCSs were brought forward for programmatic consideration. The first system is a candidate non-toxic system using $GO_2/ RP-1$ propellants. The second is a reference system using NTO/MMH. The NTO/MMH system would have many components in common with the Orbiter OMS and RCS.

Table 5.4.3.1-1 RCS Propellant Combinations Considered

NTO/MMH
$LO_2/ RP-1$
$GO_2/ RP-1$
H_2O_2
GN_2
GO_2/ GH_2

Table 5.4.3.1-2 Comparison of Leading Propellant Combinations

System Type	Mass	Volume	Development Risk	Toxicity	Major Components
NTO/MMH	1.0	1.0	Low	High	48
GO ₂ /RP-1	1.4	2.2	Medium	Low	50
GO ₂ /GH ₂	2.5	12.0	Medium	Low	82
H ₂ O ₂	1.6	1.3	Medium	Medium	31

5.4.3.2 Combinations Not Selected

Of the original candidates, several were eliminated due to incompatibilities with the LFBB. Each propellant combination eliminated is discussed briefly below.

LO₂/RP-1 was eliminated due to the large tank volume required and the complexities of loading and maintaining liquid oxygen in a system which operates for approximately 10 minutes each mission.

GO₂/GH₂ and GN₂ systems were eliminated due to the excessive tank volumes required.

H₂O₂ was considered in a blowdown configuration only. The additional complexity of an active pressurization system did not seem to offset the minimal (3 to 5 second) specific impulse increase and propellant storage volume decrease.

N₂H₄ was eliminated due to the requirement for a primary RCS class engine development program and the high toxicity of the propellant.

5.4.3.3 Propellant Combination Selected

The selected GO₂/RP-1 system is shown in figure 5.4.3.3-1. The mass breakdown of the system is shown in table 5.4.3.3-1. The system uses three high-pressure carbon overwrapped bottles to store GO₂. The high-pressure oxygen is regulated to an intermediate pressure and distributed to the manifolds. Manifold-level oxygen mass flow control is used to maintain proper oxygen mass flow to the thrusters during operation. The fuel side uses gaseous helium to pressurize liquid RP-1. The propellant tank performs gas-free liquid delivery to the engines using a surface tension system.

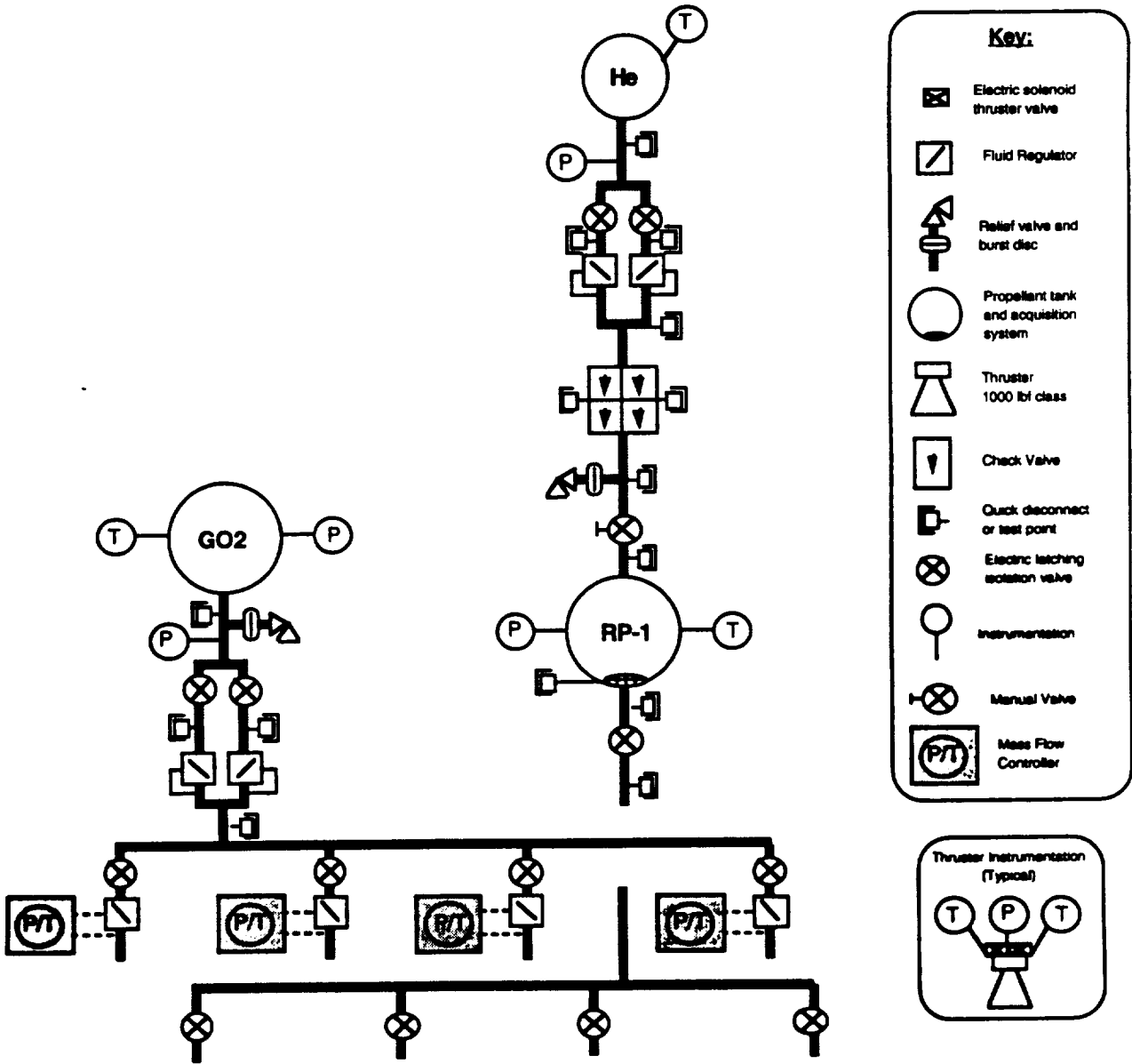


Figure 5.4.3.3-1 GO₂/RP-1 schematic.

Table 5.4.3.3-1 GO₂/RP-1 Mass Breakdown

Propellant System: GO ₂ /RP-1							
	Component	Req	Unit Mass (lbm)	Total Mass (lbm)	% Mass	Heritage	Vendor
1	Helium tank	1	26.50	26.50	1.75	RCS	Brunswick
2	GO ₂ Propellant Tank	3	171.00	513.00	33.94	New	SCI
3	QD - HP Gas	2	0.78	1.56	0.10	RCS/OMS	Fairchild
4	Burst Disk/Relief	2	4.60	9.20	0.61	RCS/OMS	Parker
5	Helium Iso Valve	2	2.26	4.52	0.30	RCS	Eaton
6	GO ₂ iso valves	2	2.26	4.52	0.30		Aerojet
7	TP - LP Gas	4	0.25	1.00	0.07	RCS/OMS	NSLD
8	Regulator	4	1.10	4.40	0.29	MX	Fairchild
9	Check valve	1	2.87	2.87	0.19	RCS/OMS	Rocketdyne
10	Manual Valve	1	2.32	2.32	0.15	RCS/OMS	Parker
11	Propellant tank - RP-1	1	30.00	30.00	1.98	APU	PSI/TRW
12	Manifold Iso Valves	9	4.10	36.90	2.44		Parker/Aerojet
13	Mass Flow Controller	4	15.00	60.00	3.97		Marotta
14	Engines	20	22.00	440.00	29.11	RCS	Marquardt
15	TP - HP Gas	4	0.25	1.00	0.07	RCS/OMS	NSLD
16	TP - LP Liquid	2	0.25	0.50	0.03	RCS/OMS	NSLD
17	QD - LP Liquid	2	1.00	2.00	0.13	RCS/OMS	Fairchild
18	QD - LP Gas	1	2.00	2.00	0.13		Aerojet
19	Pressure	4	0.60	2.40	0.16		Statham
20	Temperature	3	0.10	0.30	0.02		Rosemont
	Comp Sub Total			1144.99	75.76		
21	Lines (10%)			114.50	7.58		
22	20% Secondary Structure			251.90	16.67		
	DRY TOTALS	72		1511.39	100.00		
	Prop System Isp (sec)	295.00					
	WET						
	Propellant, usable			935.59			
	RP-1			267.31			
	GO ₂			668.28			
	Residuals			197.63			
	Total Propellant			1133.22			
	TOTAL WET			2644.61			

The NTO/MMH system is based on existing Orbiter hypergolic components and operation. A system schematic is shown in figure 5.4.3.3-2. The mass breakdown of the system is shown in table 5.4.3.3-2. The NTO/MMH propellant tanks use common part numbers and use a surface tension system to supply gas-free liquid propellant delivery to the thrusters.

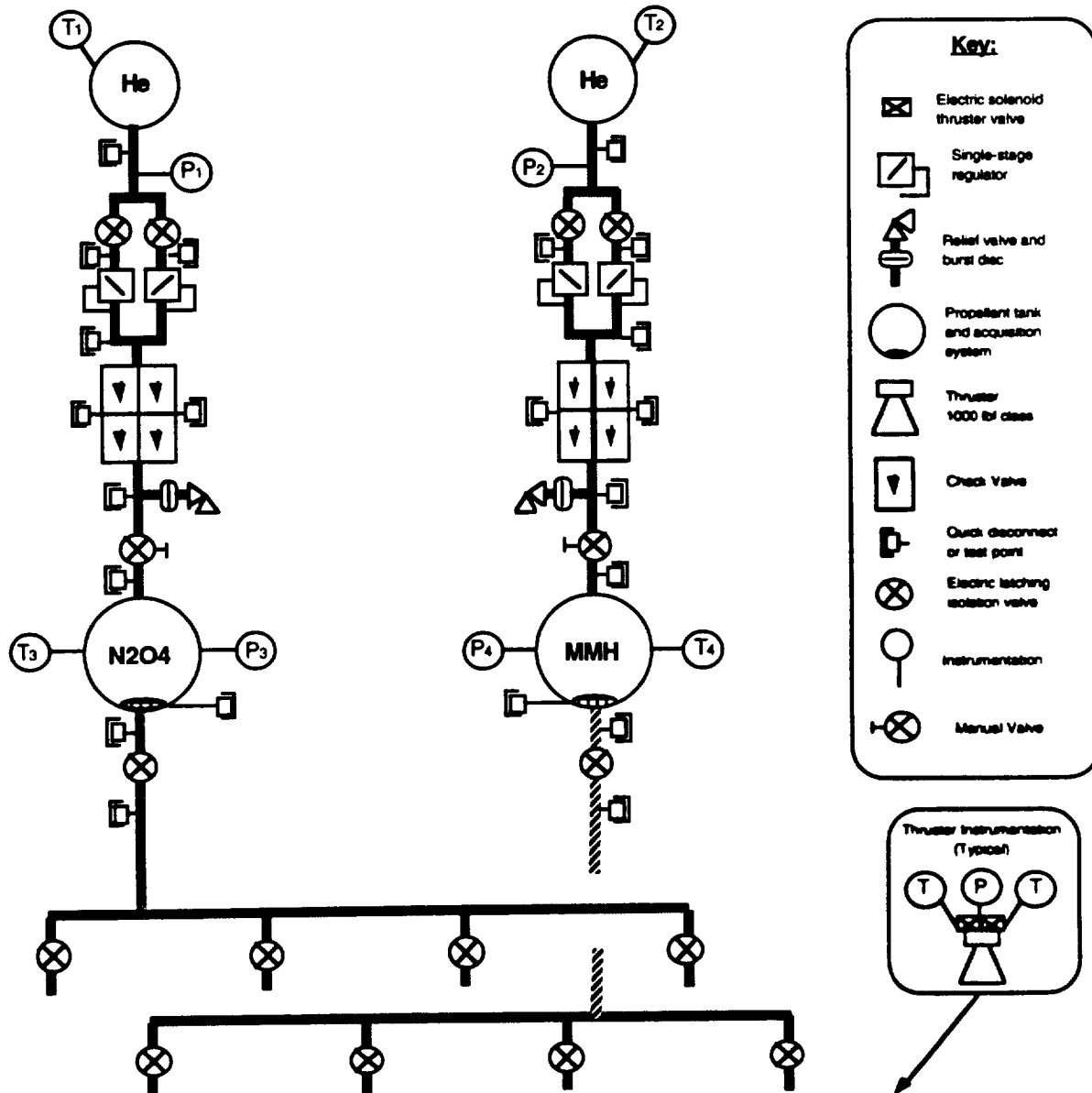


Figure 5.4.3.3-2 NTO/MMH schematic.

Table 5.4.3.3-2 NTO/MMH Mass Breakdown

Propellant System: MMH/N2O4							
	Component	Req	Unit Mass (lbm)	Total Mass (lbm)	% Mass	Heritage	Vendor
1	Helium tank	2	26.50	53.00	6.45	RCS	Brunswick
2	Helium Iso Valve	4	2.26	9.04	1.10	RCS	Eaton
3	Regulator	4	1.10	4.40	0.54	MX	Fairchild
4	Check valve	2	2.87	5.74	0.70	RCS/OMS	Rocketdyne
5	Burst Disk/Relief	2	4.60	9.20	1.12	RCS/OMS	Parker
6	Manual Valve	2	2.32	4.64	0.56	RCS/OMS	Parker
7	Propellant tanks	2	30.00	60.00	7.30	APU	PSI/TRW
8	Motor Valves	6	4.10	24.60	2.99	RCS/OMS	Parker
9	Engines	20	22.00	440.00	53.51	RCS	Marquardt
10	QD - HP Gas	2	0.78	1.56	0.19	RCS/OMS	Fairchild
11	TP - HP Gas	4	0.25	1.00	0.12	RCS/OMS	NSLD
12	TP - LP Gas	8	0.25	2.00	0.24	RCS/OMS	NSLD
13	TP - LP Liquid	4	0.25	1.00	0.12	RCS/OMS	NSLD
14	QD - LP Liquid	4	1.00	4.00	0.49	RCS/OMS	Fairchild
15	Pressure	4	0.60	2.40	0.29		Statham
16	Temperature	4	0.10	0.40	0.05		Rosemont
	Comp Sub Total			622.98	75.76		
17	Lines (10%)	1		62.30	7.58		
18	20% Secondary Structure			137.06	16.67		
	DRY TOTALS	75		822.33	100.00		
	Prop System Isp (sec)	276					
	WET						
19	Prop			1000.00			
20	Residuals (5%)			50.00			
21	Total Propellant			1050.00			
	TOTAL WET			1872.33			

5.4.4 Technology Development Identified

Several areas of concern were identified for the GO₂/RP-1 system. These areas would require technology development before entering Phase C/D of the program. The areas of concern are oxygen mass flow control, thruster development and preliminary system breadboard operation.

No technology development issues have been identified for the NTO/MMH system.

5.5 Separation Propulsion

A detailed analysis of the separation dynamics of the LFBBs from the Shuttle was not performed in this study. Therefore, a detailed design of the separation propulsion system was not pursued. Instead, the separation system from the RSRMs was used for initial sizing. The mass of the booster separation motors used on the RSRMs is 1343 lb, which includes 623.6 lb of solid propellant. This is the mass being reported in the mass properties statement and being used for costing purposes. Like the RSRMs, the LFBB booster separation motors are integrated into the forward nosecone. The aft motors are mounted externally on the aft skirt.

Further analysis was done in sizing the LFBB separation system subsequent to costing. A mass comparison at staging was done between the RSRMs and the LFBBs. The staging mass of the LFBBs is 44% higher than the RSRMs. Assuming the same motor characteristics (e.g., Isp, nozzle geometry, cosine loss), the LFBB motors would grow to 1907 lb. Strictly from a mass standpoint, 3.5 additional motors per booster would be required. If the RSRM motors are used as currently designed, two additional motors would be required at the forward and aft locations. The resulting system mass would be 2004 lb per booster.

5.6 Air-Breathing Propulsion

5.6.1 Air-Breathing Engine Mounting Options

A typical air-breathing propulsion system consists of one or more ABEs, a control system, a nacelle, structural attachments and fairings, engine accessories, and a fuel storage and distribution system. The design and arrangement of these components is related to the airframe configuration and the operational flight regime of the vehicle. Subsonic cruise was selected for the LFBB because supersonic flight offers no significant operational advantages and several major disadvantages, including higher thrust requirements and greater design and integration complexity.

Aircraft engines are typically mounted in either a buried or a podded configuration. Buried engines can be mounted internally to the fuselage or integrated with the fuselage and/or wing. An internal engine configuration is commonly used for military fighters to reduce the aircraft wetted area. Podded engines can be mounted on pylons attached to the fuselage or wing, integrated into the vertical tail, or mounted at the wingtips. The engine/inlet location will affect the quality of the inlet airflow, the likelihood of foreign object ingestion during takeoff and landing, and the ease of engine maintenance. For rocket vehicle applications, a deployed ABE configuration should also be considered. Like an internal engine, a deployed engine is protected from the launch and reentry environments by the vehicle structure. However, rather than ducting the inlet and exhaust flow, a deployed engine is pivoted into the freestream after reentry, providing a podded engine configuration for cruise flight. The deployed engine concept avoids the need for an ascent engine inlet fairing, but adds a deployment mechanism and requires significant internal volume.

The mounting options for the LFBB ABE(s) are limited by Shuttle integration factors and by the LFBB operations concept. Midbody and forebody LFBB protuberances, particularly on the side of the booster fuselage closest to the Orbiter, should be avoided because of Shuttle aerodynamic concerns. Multi-engine podded options, such as symmetric side-mounted engines, are constrained by the relative orientation and proximity of the ET and LFBBs. Wing-mounted configurations were eliminated because the LFBB wings are stowed during ascent. Potentially favorable mounting options include several buried engine configurations (aft skirt, intertank, or nose) and a podded vertical tail configuration. The aft skirt ABE location was not pursued because the main landing gear and ascent propulsion system fill most of the available useful volume. The nose and intertank engine locations were not pursued because both options require a stretch in the length of the LFBB, which alters the axial location of the nosecone relative to the RSRM position. The selected LFBB configuration has a single turbofan engine integrated into the vertical tail. This configuration has several drawbacks including a requirement for an expendable engine inlet fairing for ascent and reentry and the potential for inlet airflow distortion from the LFBB fuselage at higher angles of attack. None of the configurations briefly described above are clearly superior, and all of these configuration options should be re-evaluated in future design phases of the LFBB.

Regardless of its mounting location, an LFBB ABE will experience atypical vibration and acoustic loading relative to the flight environment of a conventional aircraft. The LFBB flight profile will also expose an ABE to pressure and thermal conditions that are beyond the design envelope for an aircraft engine. Turbine engines routinely operate at altitudes in excess of 35,000 ft. At those altitudes the ambient pressure is less than 24% of sea level static pressure. During a nominal Shuttle/LFBB mission, however, the LFBB coasts to an apogee of approximately 260,000 ft, essentially reaching a vacuum environment. Based upon aerospace design experience with vacuum enclosures, the decision was made not to provide a pressurized environment for the LFBB ABE. It is believed that a pressurized ABE compartment would increase the ground processing resources required for the air-breathing propulsion system. Also, the

additional failure modes contributed by the pressurized engine compartment (seals, pressure sensors, etc.) would adversely affect the Shuttle launch probability, resulting in higher launch costs. Finally, an in-flight failure of the pressurized compartment could result in the loss of an LFBB. Modifications to adapt an existing turbofan engine to the LFBB flight environment are projected to cost in the range of \$200 to \$600 million.

5.6.2 Types of Air-Breathing Engines

Several classes of subsonic aircraft engines were considered for the LFBB: turboprops, turbojets, and turbofans. Key engine parameters include maximum sea level static thrust, TSFC, engine dry weight, and maximum engine envelope dimensions.

The high drag resulting from the LFBB flared aft skirt translates to a cruise thrust requirement in excess of 40,000 lbf, exceeding the capability of individual turboprop or turbojet engines. Despite the favorable fuel consumption characteristics of turboprops at low Mach numbers, a multiple-engine turboprop installation was not considered to be practical because of the difficulty of packaging several large-diameter propellers. Consideration was given to a multiple-engine turbojet propulsion system similar to the Orbiter ABE configurations proposed during the Shuttle Phase B studies in the early 1970s. Turbojets suffer from a relatively high TSFC and fuel consumption is a key consideration for the LFBB despite its short cruise range. Of the aircraft engines that are currently in production, turbofans appear to offer the best combination of thrust per engine and cruise fuel efficiency.

Turbofans were derived from turbojets by adding a multi-bladed fan at the front of the engine. The fan is powered by a turbine that extracts energy from the hot core flow, thus reducing the engine jet thrust. In general, turbofans are more fuel efficient than turbojets, but at the expense of larger engine diameters. Turbofans are classified by bypass ratio, the ratio of fan (cold) airflow to core (hot) airflow. A turbofan with a zero bypass ratio is, by definition, a turbojet. It is not surprising, therefore, that low to medium bypass turbofans, which are commonly used in military aircraft, exhibit high to moderate TSFCs and provide insufficient thrust for a single engine LFBB air-breathing propulsion system. As the bypass ratio increases, a turbofan more closely resembles a turboprop, delivering improved TSFC at the expense of a larger cross-sectional area. The large-diameter, high-bypass turbofans that are currently used for commercial transport aircraft provide up to 87,000 lbf of thrust with a TSFC in the range of 0.30 to 0.34 lbf/(h-lbf). Larger turbofan engines are currently under development that will provide thrust levels exceeding 100,000 lbf at TSFCs under 0.29 lbf/(h-lbf).

A relatively new engine class is the propfan or unducted fan (UDF). A propfan is functionally similar to a turboprop, but is designed to operate efficiently at high subsonic Mach numbers. General Electric developed and tested a revolutionary 25,000 lbf-class UDF engine in the mid-1980s, obtaining excellent TSFC at cruise conditions (0.488 lbf/(h-lbf) at Mach 0.8 and 35,000 ft). The GE UDF engine uses counter-rotating propeller blades that are directly linked to the core turbines to eliminate the complexity of a gear box. General Electric analyses indicate that a propfan with a blade diameter in the range of 15 ft to 16 ft could produce a sea level static thrust of 45,000 lbf. One of the proposed LFBB concepts uses a nose-mounted propfan that is stored under the booster nosecone during ascent and reentry. The merits of propfan engines are sufficient to warrant further investigation.

5.6.3 Selection of the LFBB Air-Breathing Engine

The thrust delivered by an ABE is a function of the vehicle flight altitude and Mach number. In general, the available thrust is reduced at higher altitudes because of reductions in air density, and is reduced at higher subsonic Mach numbers because of increased engine inlet losses and sonic losses near the tips of propeller or fan blades. Table 5.6.3-1 provides estimates of the available thrust for a CF6-80E1A3 engine as a function of altitude and Mach number based upon normalized performance data for a "typical" high bypass turbofan.

Table 5.6.3-1 Estimated ABE Thrust vs Altitude and Mach Number

	Mach Number								
	0	0.1	0.2	0.3	0.4	0.5	0.6	0.7	0.8
Sea Level	72000	63648	57600	52416	48816	45504	42048	39744	37728
5K	60480	53568	49392	46080	44640	41760	38880	36720	35136
10K	48960	44640	40896	38304	36720	36144	36000	34560	32832
20K	33120	29952	27360	25776	24768	24336	24192	24480	25632
30K	21600	19440	18000	17136	16128	15696	15696	15840	16560
36K	16128	14688	13680	12960	12672	12096	12096	12384	12672
45K	10944	9936	9072	8640	8064	7776	7632	8064	8640

The fuel consumption of a turbofan engine, typically measured in terms of TSFC (lbm/(h-lbf)), also varies with Mach number. Table 5.6.3-2 provides estimates of the TSFC for a CF6-80E1A3 engine as a function of altitude and Mach number based upon normalized performance data for a "typical" high bypass turbofan. The TSFC of a turbofan engine appears to be relatively insensitive to variations in altitude at a given Mach number, decreasing gradually with altitude up to the tropopause (approximately 36,000 ft).

Table 5.6.3-2 Estimated ABE TSFC vs Altitude and Mach Number

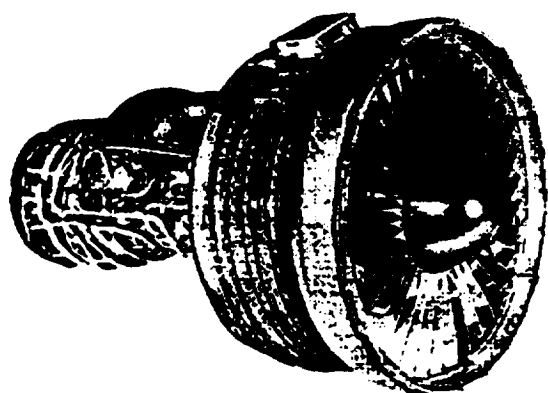
	Mach Number								
	0	0.1	0.2	0.3	0.4	0.5	0.6	0.7	0.8
Sea Level	0.339	0.380	0.425	0.474	0.523	0.575	0.627	0.681	0.735
5K	0.336	0.372	0.419	0.465	0.510	0.557	0.609	0.657	0.709
10K	0.328	0.368	0.412	0.457	0.500	0.547	0.592	0.640	0.688
20K	0.319	0.356	0.399	0.441	0.484	0.529	0.571	0.615	0.653
30K	0.311	0.345	0.387	0.427	0.473	0.512	0.554	0.595	0.631
36K	0.306	0.341	0.380	0.422	0.462	0.502	0.543	0.584	0.621
45K	0.318	0.353	0.394	0.433	0.473	0.512	0.554	0.595	0.631

The weight and aerodynamic characteristics of an aircraft determine the equilibrium flight conditions required to sustain straight-and-level cruise flight. The minimum flight dynamic pressure, which occurs at the aircraft maximum L/D ratio, defines the minimum drag (minimum thrust) cruise state. The absolute ceiling, which is defined as the maximum altitude at which an aircraft can sustain level flight, also occurs at the maximum L/D condition and is dependent upon the thrust characteristics of the aircraft engine. If an aircraft is flying at or near its absolute ceiling, it may not be able to maintain altitude during a turn. Maximum endurance (minimum fuel consumption rate) for a jet-powered aircraft occurs at a maximum L/D flight condition. Maximum range occurs at an L/D below the maximum possible value, since range is a product of cruise time and ground speed.

Special performance considerations, such as takeoff distance and climb rates for an engine-out condition, inflate the installed thrust requirements for conventional aircraft. A high installed thrust capability provides a high absolute ceiling, typically in excess of 35,000 ft for commercial transport aircraft. The LFBB air-breathing propulsion system, on the other hand, is designed primarily by cruise thrust and range requirements. Subsystem packaging efficiency and total subsystem mass are the critical integration factors for a rocket vehicle. For a given range, a minimum mass LFBB air-breathing propulsion system is achieved by compromising between the cruise fuel mass and the subsystem inert mass. All other factors being equal, a higher maximum thrust capability would reduce total fuel consumption and flight time for the LFBB by increasing its absolute ceiling. But a higher thrust capability is accompanied by an increase in the installed mass of the air-breathing propulsion system, as well as an increase in the ABE dimensions.

Evolution of the performance and trajectory estimates during the development of the LFBB concept resulted in substantial increases in the LFBB installed thrust requirement. Early in the study, it was felt that 20,000 to 25,000 lbf of available thrust would be adequate. Several factors combined to double the available thrust requirement to approximately 42,500 lbf by the end of the Pre-Phase A study. First, the estimated drag coefficient for the LFBB jumped sharply with the addition of a flared aft skirt to house multiple rocket engines. Second, the flyback cruise range more than doubled from approximately 115 nmi to over 250 nmi, due to increases in the booster staging velocity and downrange distance. Along with the increase in range, a thirty -minute loiter capability was included for booster phasing, adding approximately 10,000 lbm of jet fuel. Finally, the inert mass of the LFBB increased in response to higher fidelity estimates from the subsystem designers.

A representative high bypass commercial turbofan, the General Electric CF6-80E1A3, was selected for the LFBB feasibility study. The CF6-80E1A3, which is used on the Airbus A330, produces 72,000 lbf of sea level static thrust (uninstalled) at a corresponding TSFC of 0.339 lbm/(h-lbf). The dry weight of the engine (less tailpipe) is 10,726 lbf and the maximum envelope dimensions are 110 in. in diameter and 171 in. long. Both Pratt & Whitney (PW4168) and Rolls-Royce (RB211-Trent 768) produce similar engines for the Airbus A330, and the selection of the GE engine for the LFBB feasibility study is not intended to reflect vendor preference. The data in table 5.6.3-1 show that a 72,000 lbf-class high-bypass turbofan engine will produce sufficient thrust for LFBB cruise in the range of 7,000 to 8,000 ft above sea level (standard atmosphere) at Mach 0.4. Based upon the estimated cruise TSFC of 0.51 lbm/(h-lbf), the LFBB consumes approximately 22,000 lbm of fuel per hour of cruise flight. Figure 5.6.3-1 depicts both the GE CF6-80E1A3 turbofan and a GE UDF.



General Electric CF6-80E1A3 Turbofan	
Max Sea Level Thrust:	72,000 lbf
SL Static TSFC:	0.339 lbm/(h-lbf)
Cruise TSFC (est.):	0.51 lbm/(h-lbf)
Bypass Ratio:	unknown, high
Dry Weight (less tailpipe):	10,726 lbf
Max Envelope Diameter:	110 inches
Max Envelope Length:	171 inches

General Electric Unducted Fan (UDF)	
Max Sea Level Thrust:	25,000 lbf
SL Static TSFC:	unknown
Cruise TSFC:	0.488 lbm/(h-lbf)
Bypass Ratio:	36.0, ultra-high
Dry Weight:	unknown
Max Envelope Diameter:	140 inches
Max Envelope Length:	unknown

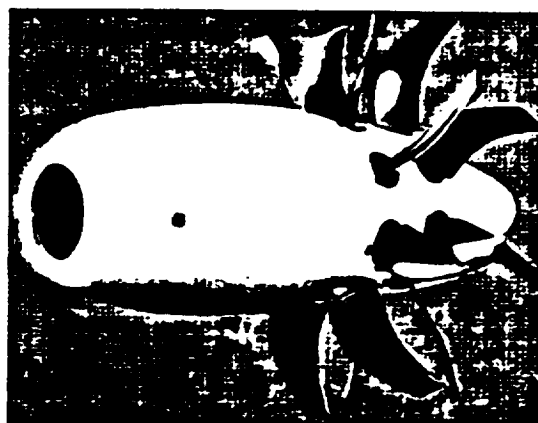


Figure 5.6.3-1 High and ultra-high bypass air-breathing engines.

5.6.4 Air-Breathing Engine Airstart

As noted previously, the LFBB ABE is protected from the ascent and reentry aerothermal environments by an inlet fairing. The inlet fairing is discarded as the LFBB reaches subsonic conditions, exposing the ABE to the free stream flow. In order to recover the LFBB, the ABE must be successfully airstarted and ramped up to cruise thrust levels. Aircraft engines are subjected to an extensive test program that includes airstart functionality. However, an aircraft engine that "flames out" is already at operating temperatures with spinning turbomachinery. Because the LFBB ABE must airstart from a dormant condition, an aircraft engine test program may not accurately predict the airstart reliability of an ABE on a LFBB mission. Because of the criticality of the LFBB airstart procedure, an airstart test program tailored to the LFBB flight environment is recommended.

After reviewing the LFBB mission sequence, U.S. aircraft engine manufactureres have indicated that a high bypass turbofan may be difficult to airstart using a windmill approach. One alternative is to include a starter to augment the ABE spin-up torque provided by the free stream flow. This strategy, known as an "assisted airstart," has been selected for the LFBB.

5.6.5 Air-Breathing Engine Accessory Power

Mechanical power from an aircraft engine can be used to drive hydraulic pumps and electrical generators through an accessory gearbox. Low-pressure and high-pressure bleed air from the engine compressor section is also available for cabin air conditioning, avionics cooling, and aircraft anti-icing systems. Depending upon the specific model, a large, commercial transport engine should be capable of supplying a continuous mechanical output of several hundred horsepower to drive auxiliary LFBB systems. The LFBB battery packs can be recharged during flyback to serve as a redundant power source in the event of an ABE failure during final approach and landing.

5.6.6 Alternate Fuel Capability

One of the issues that surfaced during the LFBB study was the possibility of using a common hydrocarbon fuel for the main engines, the RCS thrusters and the air-breathing engine. To simplify the LFBB feasibility assessment, the decision was made to defer the propellant commonality issue and to use separate tankage for the three propulsion systems.

Aircraft turbine engines have been operated on a variety of fuels, from crude oil to coal-derived liquid and gaseous fuels, according to U.S. manufacturers. The specifications for the RD-180 hydrocarbon fuel (kerosene) are expected to be similar to the specifications for existing grades of jet fuel, and should involve only minor engine adjustments.

5.7 Power System

The power system provides power to the Space Flight Data System, Guidance & Navigation, Communication & Tracking, Propulsion, and Aerosurface Actuation systems. The power and energy requirements for the LFBB are provided in table 5.7-1.

5.7.1 Assumptions

1. The power system redundancy is fail-operational/fail-safe.
2. The LFBB power system provides the primary power and energy to the Avionics during the entire mission and provides a portion of the Aerosurface Actuation system power. When the air-breathing engine starts, it serves as the main source of power for the 270 VDC electromechanical actuators (EMAs) for the remainder of the mission. The EMA's servo controller, however, continues to receive the 28 VDC supply.
3. The power source is located generally close to the user's loads. Cable routing is assumed to be simple point-to-point attachment.
4. The system is fully independent from the Orbiter's power system, control and distribution.
5. The method of cooling is passive. All cooling will be via conduction through the secondary attachment to the vehicle structure.
6. The general design philosophy is to use current technology, to maximize reusability, and to reduce the operational costs of the system.

5.7.2 System Description

The power source of choice is a rechargeable Silver-Zinc (Ag-Zn) battery. A fuel cell-based system was not recommended for the following reasons:

- An advanced fuel cell system capable of generating short pulse and high power will be required. Technology development of a high power density fuel cell will be significant
- Integration and operation costs with a fuel cell system will be high because it requires more interfaces, servicing procedures, and resources.
- Fuel cells require logistic supply, storage, and control of fuel (hydrogen) and oxidizer (oxygen). The associated services for these fluids will increase the system weight, complexity and cost.

The Ag-Zn battery was selected for the chemistry because it is a well-developed technology and has been used in other space applications, including the Surveyor and Apollo missions. Many batteries of various sizes have been built and tested, and are currently available. The battery charge/discharge behavior, as well as its control requirements, are well established. Ground servicing will be simpler than for a fuel cell system.

The rechargeable chemistry will allow 100-250 charge/discharge cycles at moderate depth of discharge (50%). The battery will be trickle-charged on the pad prior to launch. When the LFBB is on internal power, the battery will operate in discharge mode until the mission is completed.

Because of large differences in the line voltages, two separate batteries will be used. All the batteries will be packaged in modular boxes of 24 cells (32.4 VDC) per box. Boxes are electrically tied in series into a string to provide the required power and energy requirement. There will be (3) strings each for the 28 VDC and the 270 VDC system.

Table 5.7-1 LFBB Power Requirements

Mission Phase>>>>>	Prelaunch			Ascent			Coast			Landing			
Duration, Hr >>>>>	0.15			0.04			0.09			0.75			
(see note below)	Power	DC	Energy	Power	DC	Energy	Power	DC	Energy	Power	DC	Energy	
	(watts)	%	(W-hr)	(watts)	%	(W-hr)	(watts)	%	(W-hr)	watts	%	(W-hr)	
Space Data System													
(4) SDS Computer unit	300	1	45	300		12	300	1	27	300	1	225	
- Processor board													
- Single Ch. 1553													
- Dual Ch. 1553													
- Mass storage													
- Mass storage device													
(2) PDMMU	58	1	8.7	58	1	2.32	58	1	5.22	58	1	43.5	
(11) MDM's	715	1	107	715		28.6	715	1	64.35	715	1	536.3	
GN & C													
• Ascent Systems													
(4)Boostr Actuator box	180	1	27	480		19.2	180	0	1.62	0	0	0	
(2)Thrust Controller	240	1	36	800		32	240	0	2.16	0	0	0	
(4)Sep Controller	80	1	12	80	1	3.2	560	0	5.04	0	0	0	
(2)Ascent Rate Gyro	50	1	7.5	50	1	2	50	0	0.45	0	0	0	
• Flyback Systems													
(4)Integ Flt Mgt Unit	300	1	45	300		12	300	1	27	300	1	225	
(4) Air Data System	0	0	0	0	0	0	260	1	23.4	260	1	195	
(4) Cruise Engine Cntrl	0	0	0	0	0	0	400	1	18	400	1	300	
(4) Reaction Jet Drivr	80	1	12	80	1	3.2	530	1	27.67	80	0	0.6	
C&T													
(2) S-bd trnsponder	60	1	9	60	1	2.4	60	1	5.4	60	1	45	
(2) Diplexer	0	1	0	0	1	0	0	1	0	0	1	0	
(2) Signal Processor	10	1	1.5	10	1	0.4	10	1	0.09	10	1	7.5	
(2) RF Switch	12	1	1.8	12	1	0.48	12	1	1.08	12	1	9	
Propulsion													
() thruster valves	0	0	0	0	0	0		1	3.71	0	1	0	
(12) thruster heaters	240	1	18	240		4.8	120	1	1.08	120	1	9	
() motor valves	0	0	0	0	0	0	30	1	2.7	90	1	6.75	
() area heaters	1000	0	37.5	5000		6	500	0	13.5	500	0	112.5	
Subtotal (28VDC)	3325		368	3685		129	4325		229	2905		1715	
Aerosurf. Actuation													Peak Load
(2) Inboard Elevons	0	0	0	0	0	0	735	1	36.38	735	1	551.3	25890
(2) Outboard Elevons	0	0	0	0	0	0	439	1	21.73	439	1	329.3	15358
(2) Canard	0	0	0	0	0	0	230	1	11.39	460	1	345	8034
(1) Rudder	0	0	0	0	0	0	57	1	2.822	57	1	42.75	1607
(2) Tip Fin	0	0	0	0	0	0	114	1	5.643	114	1	85.5	3214
(1) Nose Whl Steering	0	0	0	0	0	0	0	0	0	8034	0	132.6	8034
(4) Brakes	0	0	0	0	0	0	0	0	0	19420	0	320.4	19420
(2) Main Gear Uplock	0	0	0	0	0	0	0	0	0	16068	0	24.1	16068
(1) Nose Gear Uplock	0	0	0	0	0	0	0	0	0	4017	0	6.026	4017
(4) Servo/FDI box	200	1	30	200		8	200	1	18	200	1	150	200
(15) Controllers	400	1	60	400		16	400	1	36	375	1	281.3	400
SUBTOTAL(270VDC)	600		90	600		24	2175		132	49919		2268	102242
Total (28v+270v)	3925		458	4285		152.6	4995		361.5	52619		3829	102242
Total (plus line loss)	4005		467	4372		156	5096		369	53692		3907	104329
Note:													
1. Power= total peak power required by the subsystem components													
2. Energy= Power * Duty cycle (DC) * mission duration													
3. Prelaunch = 9 min hold													
4. Ascent = launch until booster separation, 2 min 16 sec													
5. Coast = separation until air engine breathing ignition													
6. Flyback = powered return to stop													
7. Power for avionics only, power for the actuation system will be provided by the air breathing engine													

The architecture concepts of the battery management and distribution (BMAD) subsystem are depicted in figures 5.7.2-1 and 5.7.2-2 for the 28 VDC and 270 VDC, respectively. In general, the BMAD subsystem contains the main bus switching and isolation, the battery charge/discharge controller, instrumentation, and distribution. A secondary function of the BMAD subsystem is to regulate and monitor the battery, and communicate its health to the flight data system. Conceptually, the BMAD subsystem will be a microprocessor based box using state-of-the-art electronics and electrical components.

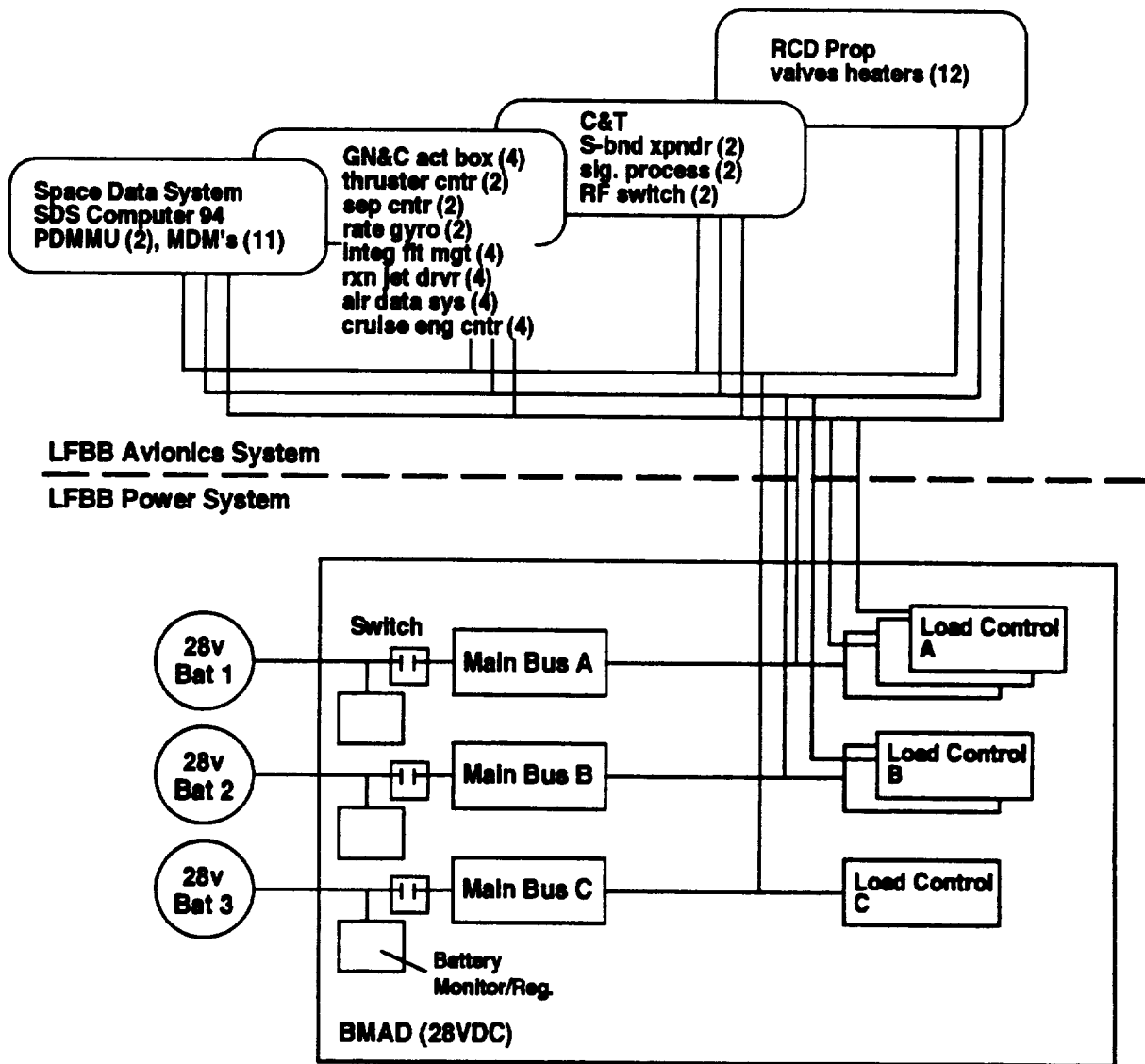


Figure 5.7.2-1 28 VDC battery management and distribution system.

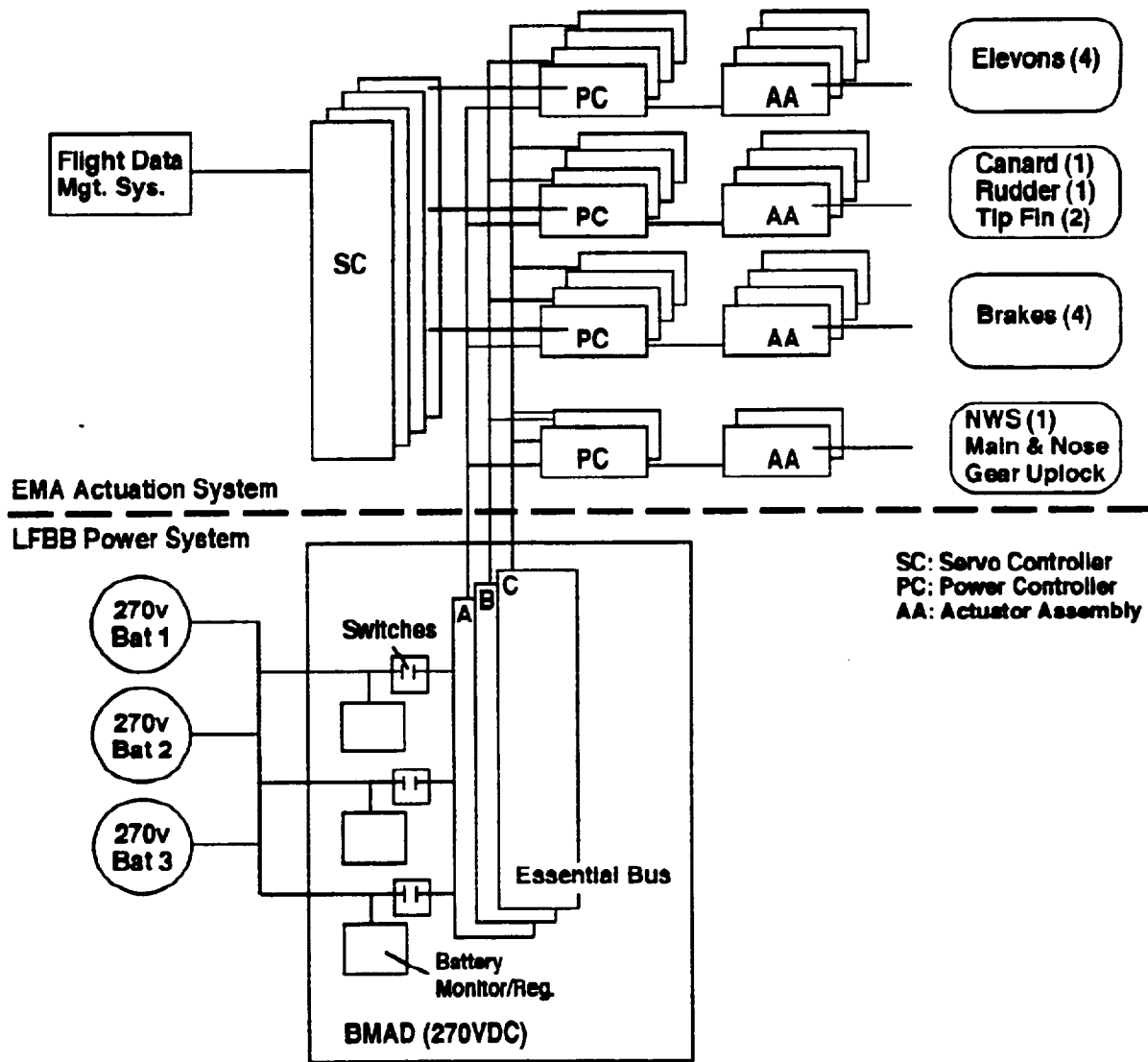


Figure 5.7.2-2 270 VDC battery management and distribution system.

5.8 Control Actuation

The control actuation function encompasses the systems responsible for effecting ascent booster engine gimbal, aerosurface deflection, landing gear deployment, braking and steering, and wing and canard deployment. Position commanding for actuator systems is provided by the Guidance, Navigation & Control (GN&C) software as it controls vehicle steering and stability maintenance functions. Similarly, event sequence commanding for wing, canard, and landing gear deployment is also a GN&C function. The power supply system (as described in Section 5.7) provides energy for actuator deflection, while the aerosurface, wing, canard, and landing gear mechanisms and their attachments are considered structural elements.

5.8.1 Assumptions

All actuators are assumed to be of the EMA type except those used for booster engine gimbaling. The EMA design is an all-electrical system using electrical motors or induction coils to drive a shaft that in turn moves the desired piece of structure. We chose this technology because it offers a significant weight savings and a reduction in system complexity over the current industrial standard of hydraulic actuation. An example of the expected savings is found in a Rockwell International study, during 1992 and 1993, that defined an EMA system capable of replacing the current Shuttle hydraulic system. Preliminary estimates showed a potential weight savings of 50% (including power supply). The concept would eliminate hydraulic and auxiliary power unit (APU) systems and their component liquids and consumables, which in turn would significantly simplify vehicle processing. Reducing complexity, especially in vehicle ground processing, is consistent with the goals of the LFBB program, and is a compelling reason to use EMA technology. This technology is not yet at a technology readiness level of 6, but with a continuation of funded NASA work (coordinated with industry, such as the NASA ELA Bridging Task), this level could be reached.

Additional assumptions involved in actuation system design include:

- Actuators for LFBB functions are defined and sized corresponding to those for similar Orbiter functions, as identified in the Rockwell study mentioned previously. Except for the LFBB pullout maneuver, this assumption appears reasonable as both vehicles are similar in size, weight, and flyback trajectory. The LFBB may encounter greater hinge moments during its pullout which may require larger actuators, though this has not been defined.
- The wings are deployed at zero q -bar, at an angular acceleration of 1 degree per second squared, to a maximum rate of 3 degrees per second.
- One controller box is required per actuator to interface with the power distribution and GN&C systems, receiving commands from the integrated flight management unit.
- 270 volt DC power is required from the power distribution system.

5.8.2 System Descriptions

5.8.2.1 *Booster Engine Actuation*

No additional LFBB hardware is required for booster engine gimbaling. The RD-180 booster engines consist of 2 engine bells, each with 2 gimbal actuators, for a total of 4 per engine. These actuators are hydraulic, driven by kerosene (the working fluid) bled off from the engine fuel pump, and are included with the ready-built RD-180 engine. These actuators only require pitch and yaw commands from the LFBB, which are generated by the GN&C and provided to the actuators via an engine controller box (part of the GN&C avionics system). The engine controller box (one per engine) receives 4 input signals (quad redundant) from GN&C and processes them through an internal voter function (probably a voter chip), to output a single signal to the booster engine actuators.

5.8.2.2 *Aerosurface Actuation*

A total of seven actuators, with accompanying controller boxes, are required for aerosurface actuation, and are itemized in table 5.8.2.2-1. Power and weight estimates, based on the Rockwell International work mentioned above, were used to size an EMA system for the LFBB aerosurface actuators. The preliminary dimensions are reasonably similar to those from NASA work, and prototype EMAs developed by Honeywell International. All pertinent information is included in table 5.8.2.2-1.

Table 5.8.2.2-1 LFBB Aerosurface Actuator Definition

Component	No. per LFBB	Peak Power (kW)	Avg Power (kW)	Mass (lbs)	Size (in)
Inb Elevon	2	12.9	0.37	250	40x10 dia
Outb Elevon	2	8.0	0.23	250	40x10 dia
Canard	2	8.0	0.23	250	40x10 dia
Rudder	1	1.6	0.06	125	25x6 dia

(NOTE: Values for power and mass are for a single component)

5.8.2.3 Landing Gear Actuation

A total of eight actuators, with accompanying controller boxes, are required for landing gear actuation, and are itemized in table 5.8.2.3-1. Similarly to the aerosurface actuators above, the power and weight estimates are based on Rockwell International work. Again, the preliminary dimensions are reasonably similar to those from NASA work and prototype EMAs developed by Honeywell International.

Table 5.8.2.3-1 LFBB Landing Gear Actuation Definition

Component	No. per LFBB	Peak Power (kW)	Avg Power (kW)	Mass (lbs)	Size (in)
NsWheel Steer	1	8.0	8.0	190	32x8 dia
NsWheel Deploy	1	4.0	4.0	125	25x6 dia
MainGear Deploy	2	4.0	4.0	190	32x8 dia
Brakes	4	4.9	4.9	190	32x8 dia

(NOTE: Values for power and mass are for a single component)

5.8.2.4 Wing and Canard Deployment Actuation

Two actuators with accompanying controller boxes, one actuator for the wing and one for the canard, are required for their deployment and are listed in table 5.8.2.4-1. The first power estimate is based on simple calculations to accelerate the wing mass by 1.0 degree per second squared. It is assumed, with negligible q-bar and with mechanical friction, that the motor can accelerate the wing to a maximum deployment rate of 3 degrees per second, resulting in a 35-second deployment time for 100 degrees of sweep. The mass and size of the wing deployment actuator was selected to be the same as that for the inboard elevon, as their power requirements were similar. Only the actuation system is sized below. Additional mechanical components, such as locking structure, pivot mechanisms, etc., which will most likely be required for wing deployment are not sized here (though an additional mass, equal to 20% of the wing as based on "historical data" was included in the vehicle mass properties for deployment mechanisms). Similar assumptions were made with the canard wing, only here the power requirement was found to be smaller even than that required to move the rudder, so an actuator size smaller than the rest was assumed. Again, only the mass of the actuator system is listed below. Further definition of the deployment mechanism would be beneficial early on, should LFBB design work continue.

Table 5.8.2.4-1 Wing and Canard Deployment Actuation Definition

Component	No. per LFBB	Peak Power (kW)	Avg Power (kW)	Mass (lbs)	Size (in)
Wing Deploy Actuator	1	13.3	13.3	250	40x10 dia
Canard Deploy Actuator	1	1.2	1.2	75	24x5 dia

(NOTE: Values for power and mass are for a single component)

5.9 Integrated Avionics

5.9.1 General Issues

5.9.1.1 Assumptions

A requirement for two-fault tolerance in boost control compatible with the Shuttle resulted in the same fault tolerance in the LFBB GN&C system, data management system (DMS), and Communication and Tracking (C&T) system. Two-fault tolerance was carried for the LFBB in order to increase the launch probability for component failure in the non-boost phase equipment.

No range safety is required; however, the impact to avionics is insignificant.

Two-way continuous communications from the Orbiter and each LFBB is required (prelaunch through shutdown). The Orbiter downlink is currently saturated. The magnitude of monitoring the status of the flyback systems and the booster data could not be routed through the Orbiter.

Data rates on the LFBBs will be the equivalent of the current Orbiter. No significant resource savings are made in the selection of a lesser capability, and the Orbiter data rates safely contain the system requirements.

The LFBB shall not reduce the Shuttle's launch probability.

A differential global positioning system (GPS) will be utilized as a landing aid (elimination of MSBLS).

5.9.1.2 Summary Description

From a feasibility standpoint, the avionics was never considered a technical risk factor; therefore, the optimization and refinement of an architectural model was not a concern. A somewhat conservative model was assembled for estimation of power utilization, weight, volume, and cost. The integrated avionics components will be described in more detail in individual sections, including GN&C, DMS, and C&T.

The architectural model is described here in terms of two operational groupings:

- 1) Boost - prelaunch through separation
- 2) Flyback- separation through shutdown including booster ground tests

Figure 5.9.1.2-1 depicts the LFBB integrated avionics architecture.

For the boost phase, the Orbiter computer systems are the prime control elements for the LFBB engines. A new development area referred to as the engine controller may, in a finalized design, share some of that responsibility with the Orbiter systems. To avoid an overload of the Orbiter computer systems and the Orbiter's downlink, the design architecture routes LFBB engine status data directly from the engine controller to the booster's active downlink.

For the flyback phase, active vehicle control is assumed by the booster's self-contained GN&C subsystem. During the boost phase, this subsystem is in a passive configuration, performing fault detection, isolation, and recovery (FDIR) and vehicle health monitoring (VHM) for the GN&C elements. Refer to the guidelines and groundrules for a vehicle health management system later in this section.

The data systems element provides the computational, control, and monitor functionality for all the non-GN&C systems, including power and C&T. It provides FDIR, VHM, uplink/downlink gathering and routing during both operational phases.

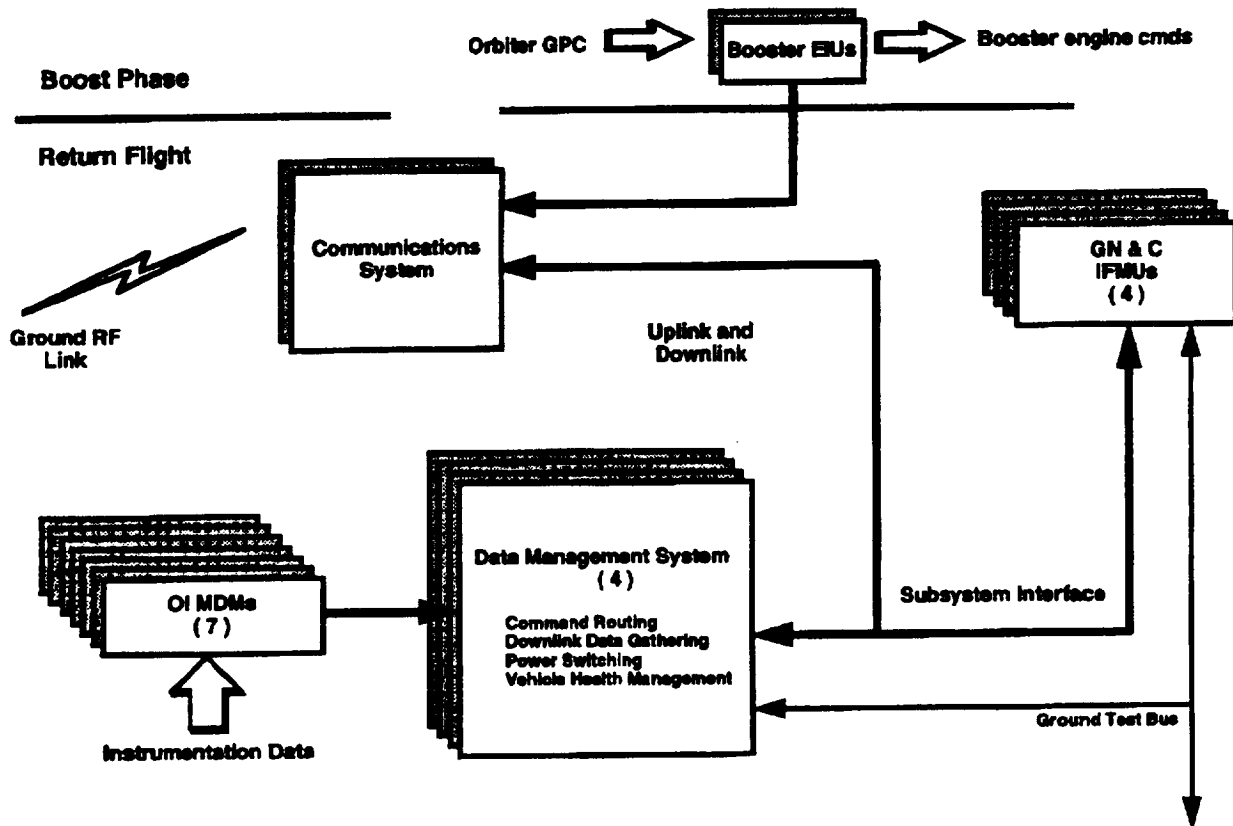


Figure 5.9.1.2-1 LFBB integrated avionics architecture.

5.9.1.3 Avionics Issues

5.9.1.3.1 Active/Passive Thermal Control

The integrated avionics team provided a list of all avionics boxes including power consumption at various mission phases, and operating range to support the analysis to answer the question of which type system would be needed. The conclusion was that passive thermal techniques can provide adequate cooling for all avionics in a 1-to-2-hr mission duration. The assessment results are included in section 5.10.

5.9.1.3.2 GPC I/O Margins

A potential problem exists in the Orbiter general purpose computer (GPC) input/output capacity and the data volume required to command/control and status the boosters. The current design profile was examined to determine if the additional four engine controller interfaces could be accommodated with the design, assuming the equivalent data exchange required on the engine interface units (EIU) for the SSMEs. That hypothetical fitting was marginal. The actual engine data volume is not known; however, the data interface to the GPC can be minimized since the engine controller will be a new development. Data acquisition for ground use only can be routed through other paths to the booster's independent telemetry system. Further examination of this item should be addressed when more is known about the engine data and a GPC/engine controller interface control document (ICD) can be established.

5.9.1.3.3 Thrust Balancing for Engine Shutdown

For thrust balancing on a booster engine shutdown, the transport delay associated with GPC noise filtering and its I/O profile make the new design engine controllers the best candidate to coordinate unplanned shutdowns. An Orbiter shutdown command transport lag analysis is included in section 8.1, Orbiter Impacts. Minimizing shutdown detection and corresponding opposing shutdown initiation intervals is best accomplished by cross-strapping engine controllers designed with a sample frequency to effect the required timing.

5.9.1.3.4 Avionics Integrated Testing

For cost estimates, the avionics team assumed that a systems verification facility would be required. An LFBB test station (LTS) to support integrated avionics system verification for the LFBB hardware and software, including both open-loop system testing and closed-loop testing with simulated dynamics, was sized and costed. The LTS would leverage off of existing Shuttle facilities by augmenting the GN&C test station (GTS) and its interface with the Shuttle Avionics Integration Laboratory (SAIL) for full, integrated verification.

5.9.1.3.5 Guidelines and Groundrules for Vehicle Health Management System (VHMS) Functionality

The basic concept behind VHMS is that auxiliary information captured during operational use can be used to determine/predict the health and readiness of a subsystem for its next recycle. Teardown inspections and special ground testing are targets for elimination. For an operational go/no-go to support FDIR, the instrumentation information and boundary conditions may be quite different from that needed to answer the question of whether the system is showing weakness. Auxiliary information refers to instrumentation information captured to answer the weakening question.

For specifications and requirements, subsystems should separate FDIR from VHMS actions:

Consider FDIR to be an operational category based on required fault tolerance.

Consider VHMS to be a ground support category intended to facilitate maintenance and turnaround activities in subsystem reuse.

Actual design implementation may overlap and utilize common elements or functionality in meeting requirements from each category. It is probably a safe assumption that FDIR is a subset of VHMS.

This concept is to be considered for all the elements of the subsystem: instrumentation, actuation, controls, and monitors. Sound system engineering should be applied to each augmentation beyond the fault-tolerance scope. Complexity/reliability, power, weight, and cost have to be traded against the value of the information for recycle maintenance.

The design of a subsystem should accommodate the capture and retention of both FDIR and VHMS instrumentation and state data. That data should be captured by a logical element that is by design a local monitor to the subsystem element of interest; for fault tolerant subsystems this should be the local monitor fault containment region (FCR) (1). This will require logic to capture, a time stamp, retention, and dispersion of the information. Retention must be non-volatile to power loss with capacity sized to support an operational interval.

It is assumed that VHMS data reduction and analysis is a ground-based function. In cases where the magnitude of data drives the retention capacity to an extreme, data compression/reduction logic should be considered.

The data capture element design should also have a dedicated ground support port to be used to extract the data and reset the retention area for the next operational usage. The ground support port should be common across systems, facilitating a common ground communication bus for VHMS data. The

subsystem elements shall act as a remote terminal on this port, acting only in response to ground commands.

The data capture element should support data dispersion to the ground port during ground operational intervals as well as for ground turnaround testing. Reset of the data area will be a unique ground command.

For ground turnaround testing, all that is required for the retention element to support downloading of the VHM data is that local power is available, and the ground bus is in communication.

All electrical logical elements shall incorporate built-in test logic and fault detection mechanisms that provide 95% failure detection within the element. That status data will be used in both FDIR and VHMS.

Fault-tolerant designs require partitioning or grouping for failure independence in hardware. A grouping can be referred to as an FCR. An FCR is a collection of components that will operate correctly regardless of arbitrary or electrical failures outside of the region. A failure in an FCR cannot cause a failure outside of its own domain. An FCR is electrically isolated from other design-related FCR domains. Its power source must be independent of other related domains, and, for logical units, the clocking sources are also independent.

Some fault-tolerant systems design may also require physical separation of FCRs for environmental effects or physical damage control. By definition, fault-tolerant designs will contain multiple FCRs driven by the fault tolerance required in the system and the specifics of the design implementation.

There are two types of FCRs, monitor and control. For a single functional path, control and monitor FCRs will be independent, although it is possible for a monitor or control FCR for one functional path to also serve as the same or opposite type for an independent function.

Monitor FCRs appear to be the logical choice for the unit to focus VHMS specific guidelines on.

5.9.2 GN&C System

5.9.2.1 Assumptions

Systems will be dual fault tolerant with FDIR where applicable.

Component selection was based in part on work from Access to Space, Option 1 Study.

Impact to Orbiter & ET will be minimized by keeping the booster interface similar to the current RSRM interface.

The vehicle will be able to operate autonomously after separation.

Vehicle control is provided with aerosurfaces and reaction control thrusters.

GPS with an inertial navigation system will be the primary means of navigation during the flyback phase. TACAN is not required.

The vehicle will use differential GPS with landing radar for landing.

EMAs will be used for aerosurface control to eliminate hydraulics and APUs.

Software development and maintenance will be minimized by starting with Shuttle algorithms (GRTLS GN&C and Autoland), and by maintaining with a graphical format.

Throttle controllers are included with the air-breathing engine.

Booster engines will use single port actuators.

5.9.2.2 Summary Description

A graphical chart of the GN&C avionics system is shown in figure 5.9.2.2-1.

The boost phase GN&C avionics system will support the same functions that are currently supported on the boost phase of the RSRMs and are quad-redundant to support a man-rated vehicle. This includes a booster separation system to activate pyrotechnic bolts and small solid rockets; rate gyros used by the Orbiter GPCs for attitude control during ascent (the gyros on the Orbiter experience too much vibration during this phase); and booster engine controllers (one per RD-180 engine) for throttle and actuation control. The Booster engine controllers will take throttle, pitch and yaw commands from the Orbiter GPCs, but will also be cross-strapped directly (through a connection across the Orbiter, but bypassing its GPCs) to enable a rapid compensating throttle-down of one booster should an engine fail on the other. The cross-strap connection may require a fiber optic line depending on path length.

The flyback phase GN&C avionics systems will support the function of returning the booster from separation to a landing strip and is also quad-redundant to protect against a launch scrub due to an on-the-pad failure in the flyback system. The core of the flyback GN&C system is the integrated flight management unit (IFMU) including an inertial navigation system, a central processor and several interface and sensor driver cards. The flyback GN&C system also includes two RCS electronics boxes (each internally dual-redundant) to open valves and activate RCS jets, as well as eight landing gear and eight aerosurface electromechanical actuators. The landing gear actuators control steering, braking, and gear deploy (uplock) while the aerosurface actuators move the aerosurfaces for control and steering. Each EMA requires a dedicated actuator controller box to interface with the power system and the IFMU. The IFMU also sends throttle commands to the air-breathing engine, through its controller. The air data transducer assembly (ADTA) is a velocity sensor of the airstream relative to the vehicle and is a part of the GN&C system. Radar and GPS antennas are also included to show their connectivity to the GN&C system.

5.9.3 Data Management System

5.9.3.1 System Description

The LFBB is controlled during the boost phase by the Shuttle Orbiter, and is controlled after separation and during return to base by onboard stored commands with the capability to accommodate ground-initiated commands.

The primary function of the LFBB DMS is to provide telemetry data gathering and downlink service. It also provides system initialization, configuration control, command processing, timing control, FDIR, data processing, and computation for all onboard subsystems other than GN&C system. The DMS monitors, records, and downlinks the health and status of the various vehicle systems as developed by a distributed VHMS. The DMS also interfaces with the communication system for receipt of ground-initiated commands and for telemetry formatting.

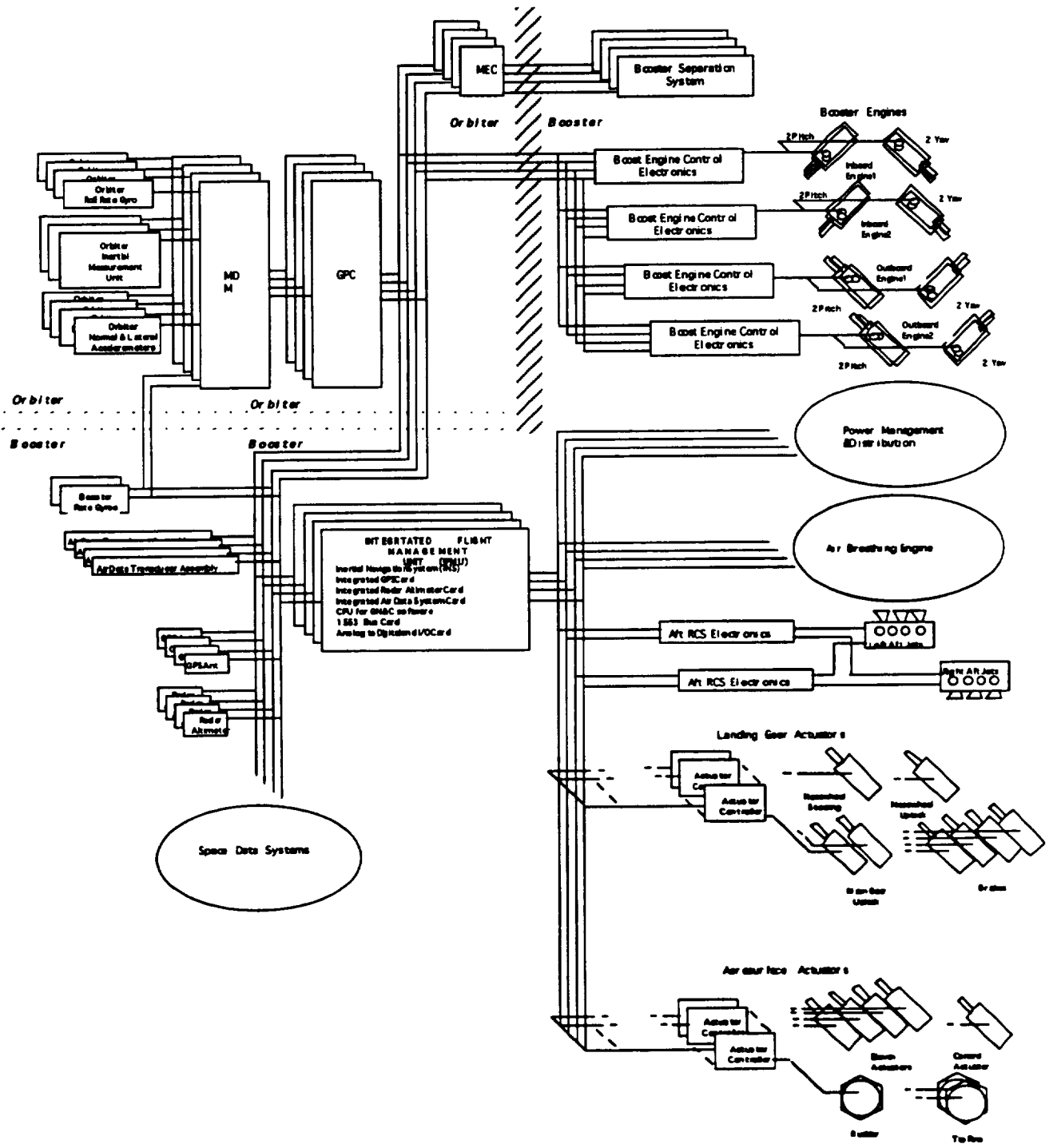


Figure 5.9.2.2-1 LFBB GN&C schematic.

The DMS is a fail-operational/fail-safe system. It consists of four general avionics processors (GAPs), two pulse code modulation master units (PCMMUs), and seven operational instrumentation (OI) multiplexer/demultiplexer (MDM) units. There are twelve 1553B buses which provide internal communications within the LFBB throughout the mission. External communication with the Orbiter are similar to the analog/discrete signal connections that currently exist. The downlink telemetry functions are performed via OI MDM and PCMMU. A Phase A trade study may be prudent to determine the economical benefits of moving PCMMU downlink functions into the GAP and reducing the DMS fault tolerance to be single-fault tolerant. For this study phase, two-fault tolerance of the DMS was assumed to be achieved by a voting process in a four computer set. A preliminary avionics functional architecture is shown in figure 5.9.3.1-1.

Each of the four GAPs consists of a processor board, an internal mass storage device and an interface to three 1553B data busses. One of the 1553B data busses is used for interface to vehicle command and control flight critical busses and the other two 1553B data busses for interface to the PCMMUs and the OI MDMs. The OFI and DFI sensors interface with the OI MDs. A functional block diagram of the GAP is provided in figure 5.9.3.1-1.

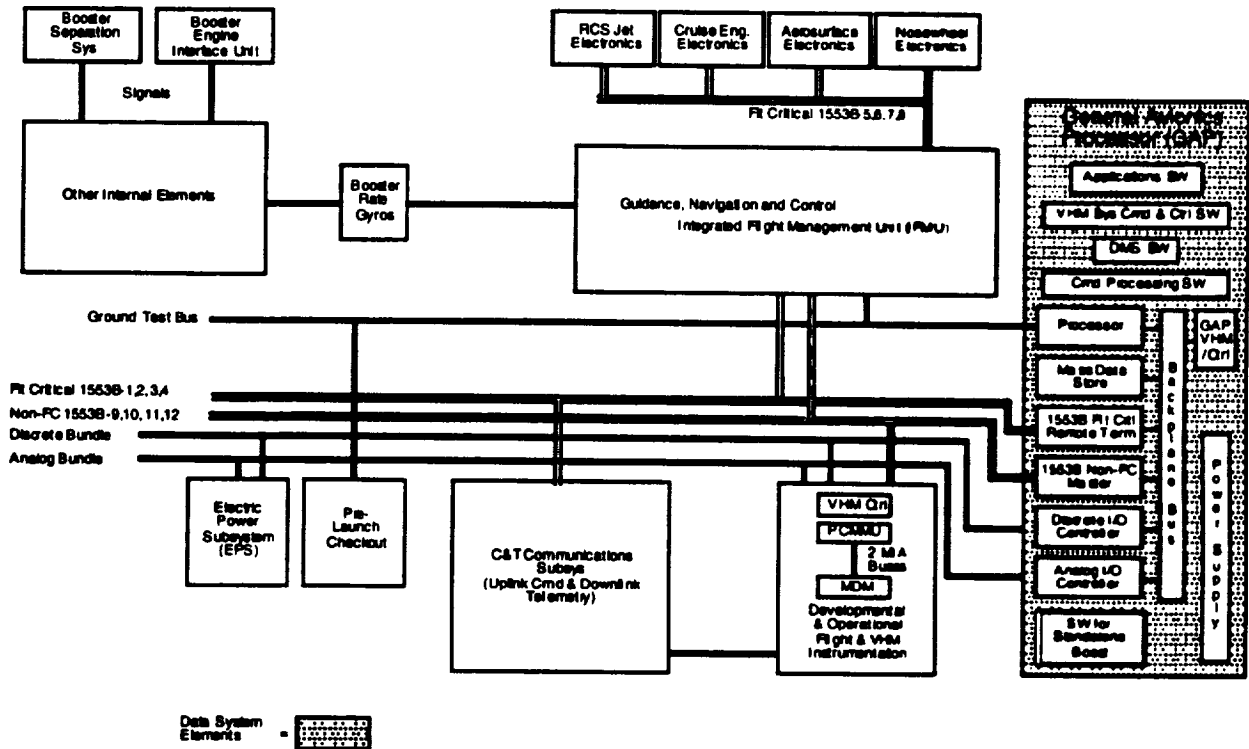


Figure 5.9.3.1-1 LFBB avionics functional architecture.

5.9.3.2 Major Hardware Components

GAPs (4)
PCMMU (2)
MDM (7)
1553B data cables (12)

5.9.4 Communication System

5.9.4.1 Assumptions

Two-way continuous communication is required.

A separate communication system will be provided for each LFBB, independent of Shuttle Orbiter communication system.

Loss of communication will impact the safe landing of the LFBB (ground command is required to direct the LFBB landing at KSC).

No range safety system is required.

Current Shuttle data rates will satisfy LFBB requirements.

Communications range is up to 260 nmi.

A separate, off-the-shelf FAA-certified transmitter will be included onboard to satisfy the FAA requirements for flying over populated areas.

5.9.4.2 Summary Description

Two-way RF communications will be provided during pre-launch, ascent, post separation, flyback, and landing phases. The proposed LFBB communication system depicted in figure 5.9.4.2-1 will consist of a pair of switchable omni antennas, an RF switch, and three strings of RF electronics. Each string of RF electronics includes an S-band transponder and a signal processor module. A standard 1553B interface will be provided to interface with the LFBB DMS and GN&C subsystems. A triple-string system is planned for the booster to provide a dual-fault tolerant system.

To provide command and telemetry capabilities for the booster, a standard S-band tracking and data relay satellite system (TDRSS)/spaceflight tracking and data network (STDN) transponder which communicates with TDRSS and GSTDN ground stations of MILA and BDA is proposed. All necessary power conditioning and telemetry interface circuitry for TDRSS operations are incorporated. This transponder will perform simultaneous TDRSS/STDN searches to provide an optimum communications link between the booster and ground via either TDRSS relay link or direct ground link. Uplink and downlink data rates of 10 kbps and 192 kbps, respectively, are planned.

The uplink will incorporate encryption and coding to ensure secure command transmission from the ground to the booster. Uplink commands will be received by the S-band receiver through one of two omni antennas flush mounted on the booster. The demodulated commands will be processed by the baseband signal processor to properly authenticate and verify the received commands to ensure security. The downlink telemetry will consist of booster engine data and other system parameters for health monitoring and fault recovery purposes. The downlink will not be coded or encrypted.

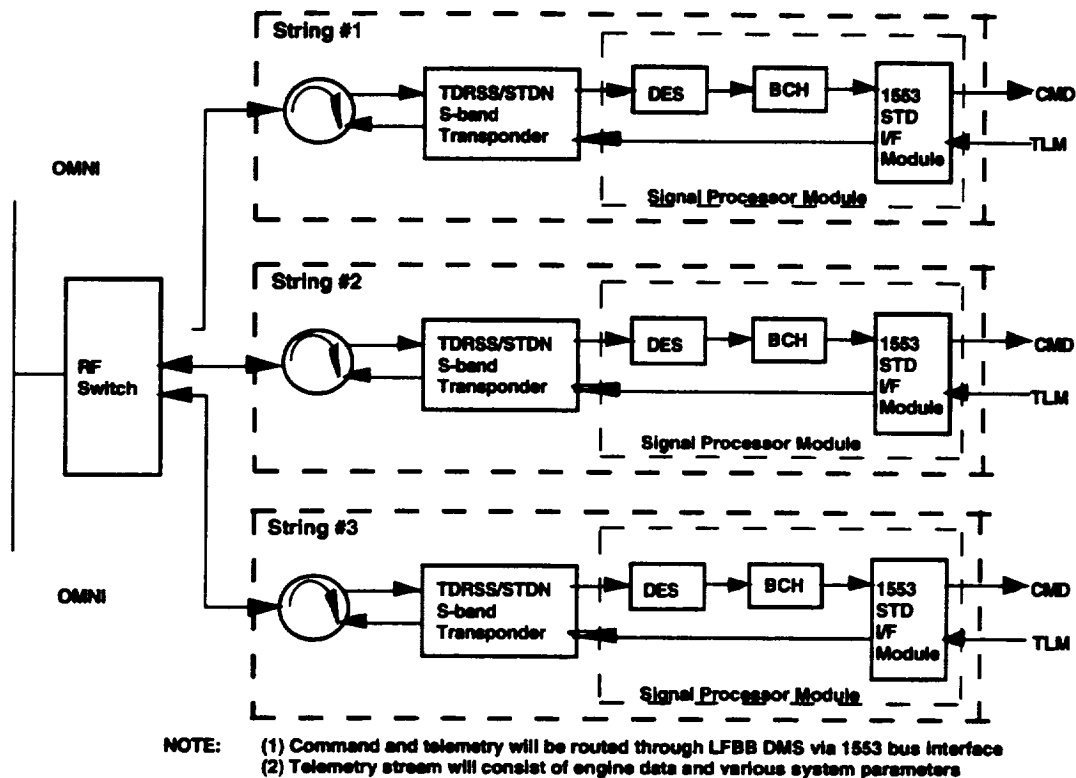


Figure 5.9.4.2-1 LFBB communications subsystem architecture.

5.9.4.3 Major Hardware Components and Assemblies

- S-band Transponder (3)
- Baseband Signal Processor (3)
- RF switch (1)
- Omni antennas (2)

- Note:
- (1) Size/weight/power and cost estimates for the S-band transponder were based on a Cincinnati Electronics model TTC-308/703.
 - (2) All other estimates were based on existing hardware information within the Tracking and Communications Division.

5.9.5 Navalds System

5.9.5.1 System Description

The RF Navalds for LFBB will consist of a differential GPS and a radar altimeter. These subsystems will be part of (and internally located in) the inertial navigation system (INS). Due to the criticality of the functions during automated landing, each subsystem will be triple redundant (fail-op/fail-safe) to the extent feasible. Use of differential GPS and radar altimeters will preclude the need for TACAN and MSBLS systems. Brief separate descriptions of the subsystems follow.

The differential GPS subsystem will consist of redundant ground receiver/transmitter components, onboard GPS receivers and associated antenna/preamp assemblies. The ground components will receive GPS signals, calculate corrections and subsequently broadcast corrections to the onboard receivers. The uplink will be either through the S-band link, or via ground-based pseudolite transmissions which would be received directly by the onboard GPS receivers. Each GPS receiver will have two

opposing, 180° field-of-view antennas and preamp assemblies. The antennas will be skin mounted in optimal locations for full 360° coverage. A preamp assembly will be located as near as possible to each antenna. The preamps require power, which can be obtained either through the GPS receiver or through separate power circuits. GPS will supply data beginning with separation from the Orbiter, but should be powered on during ascent in order to be completely initialized.

The radar altimeter subsystem will consist of onboard receivers/transmitters, each with its own separate receive and transmit antennas. Each antenna will be skin-mounted on the underneath side of the LFBB, so that transmissions will be directed to the ground and subsequently reflected back to the receive antennas. The radar altimeters will operate and supply altitude data for the final 5000 ft of altitude during landing. Since radar altimeters measure height directly above the surface, a terrain map for the landing site will be necessary.

5.9.5.2 Hardware

GPS Antenna/Preamp	(8)
RF Cable Low Loss Flexible (.25 lb/ft)	(8)
RF Combiner	(4)
Radar Altimeter Antenna	(8)
RF Cable Low Loss Flexible (.25 lb/ft)	(8)

5.10 Thermal Control

5.10.1 Introduction

A general thermal analysis was performed in support of the LFBB assessment effort. The purpose of the analysis was to determine the capability of cooling heat generating components by passive means during the LFBB mission.

5.10.2 Assumptions

Component data, shown in table 5.10.2-1, was provided by the Systems Engineering Division at JSC. All components were considered to be thermally isolated, and for transient calculations an additional 20% of the component weight was considered to be support structure. Initial launch temperatures were assumed to be 70°F with no temperature gradients. Maximum temperature responses above 140°F were considered to justify additional means of cooling.

Table 5.10.2-1 LFBB Component Characteristics

Mission Phase>>>> Duration, Hr >>>>	PreInch 2 or 0		Ascent 0.04		Coast 0.09		Landing 0.75		Unit Mass lbm
	Power (watts)	DC %	Power (watts)	DC %	Power (watts)	DC %	Power watts	DC %	
Space Data System									
(4) SDS computer unit	300	1	300	1	300	1	300	1	46
(2) PDMMU	58	1	58	1	58	1	58	1	31
(7) MDMs	455	1	455	1	455	1	455	1	31
GN&C									
• Ascent Systems									
(2)Boostr Control Box	120	1	400	1	120	0.1	0	0	100
(4)Sep Controller	80	1	80	1	560	0.1	0	0	65
(2)Ascent Rate Gyro	50	1	50	1	50	0.1	0	0	22
• Flyback Systems									
(4)Integ Fit Mgt Unit	300	1	300	1	300	1	300	1	30
(4) Air Data System	0	0	0	0	260	1	260	1	20
(2) Reaction Jet Driver	40	1	40	1	490	0.54	40	0.01	30
C&T									
(2) trspder, pwr amp	140	1	140	1	140	1	140	1	11
(2) diplexer, RS swtch									
Aerosurf. Actuation									
(2) inboard elevons	0	0	0	0	735	0.55	735	1	250
(2) outboard elevons	0	0	0	0	439	0.55	439	1	250
(1) canard	0	0	0	0	230	0.55	230	1	250
(1) rudder	0	0	0	0	57	0.55	57	1	125
(2) tip fin	0	0	0	0	114	0.55	114	1	125
(1) nose whl steering	0	0	0	0	0	0	8034	0.022	190
(4) brakes	0	0	0	0	0	0	19420	0.022	190
(2) main gear uplock	0	0	0	0	0	0	16068	0.002	190
(1) nose gear uplock	0	0	0	0	0	0	4017	0.002	125
(16) controllers	400	1	400	1	400	1	400	1	37.5

5.10.3 Analysis

Using the component data, maximum temperature values were calculated for two cases: 1) a nominal mission scenario with a 2-hr prelaunch hold; and 2) a nominal mission scenario without any prelaunch heat generation representing an LFBB design with a purge requirement.

5.10.4 Results and Conclusions

Table 5.10.4-1 shows the results of the thermal analysis. The column titled "Max Temp With 2-Hr Hold" shows the maximum temperature for the first case explained in the analysis paragraph. The data in the column titled "ΔWeight for 2-Hr Hold Solution" is the necessary additional weight to keep a component under 140°F for the first case. "Max Time at Max Power" is the time that the component can stay at its maximum power without exceeding 140°F. This would limit the ground test time, in the absence of additional cooling. Some of the components exceed the 140°F limit quickly but are not a problem because the mission profile, shown in table 5.10.2-1, does not require that component to be used for long durations. The last two columns are similar except that they describe the results of the case that assumes a prelaunch purge.

With the two-hour hold and without a purge capability, three types of components exceed their temperature limits before the end of the mission. The most severe case is that of the two transponders, which would need an additional 40 lb of structure per component to compensate for the heat generated. This would be a severe penalty but would have to be weighed against the impact of introducing an active thermal control system. With the purge capability, the transponders are the only components to violate the 140°F limit. However, the weight associated with a solution is only 1 lb per component. This would mean that a prelaunch purge would make any additional design change to accommodate a passive thermal control system negligible.

Table 5.10.4-1 Thermal Analysis Results

Component	Max Temp w/ 2-Hr hold (°F)	Max Time at Max Power (hrs)	ΔWeight for 2- Hr Hold Solution (lb)	Max Temp w/ Purge (°F)	ΔWeight for Purge Solution (lb)
SDS Computer Unit	137	>3	0	90	0
PDMMU	108	>3	0	81	0
MDM	156	2.5	9	95	0
Booster Control Box	130	.8	0	71	0
Sep controller	80	2.4	0	70	0
Ascent Rate Gyro	104	>3	0	70	0
Integ Flight Mgt Unit	172	2.1	17	100	0
Air Data System	107	1.6	0	107	0
Reaction Jet Driver	95	2.4	0	76	0
Transponder	330	.8	40	146	1
Inboard Elevons Actuation	86.0	>3	0	89	0
Oubrd Elevons Act	79.6	>3	0	81	0
Canard Act	80.0	>3	0	82	0
Rudder Act	75.0	>3	0	76	0
Tip Fin Act	75.0	>3	0	76	0
Nose Wheel Steering Act	78.6	.1	0	70	0
Brakes Act	75.2	.2	0	70	0
Main Gear Uplock Act	70.9	.1	0	70	0
Nose Gear Uplock Act	70.7	.2	0	70	0
Controllers	97.2	>3	0	81	0

5.11 Mass Properties And Center Of Gravity

5.11.1 Mass Property Statement

This section contains the final mass property statements for the LFBB. The first statement included here is that of the baseline vehicle, optimized for replacing the current RSRMs of the Shuttle. As per JSC - 23303 (Design Mass Properties), mass property statements are presented in three distinct levels of detail, Design Mass Summary (level 1), Mass Summary (level 2), and Mass and Design Details (level 3). For simplicity, level 1 is shown in figure 5.11.1-1 below. Level 3 (including component cg locations) is included as Appendix D for completeness.

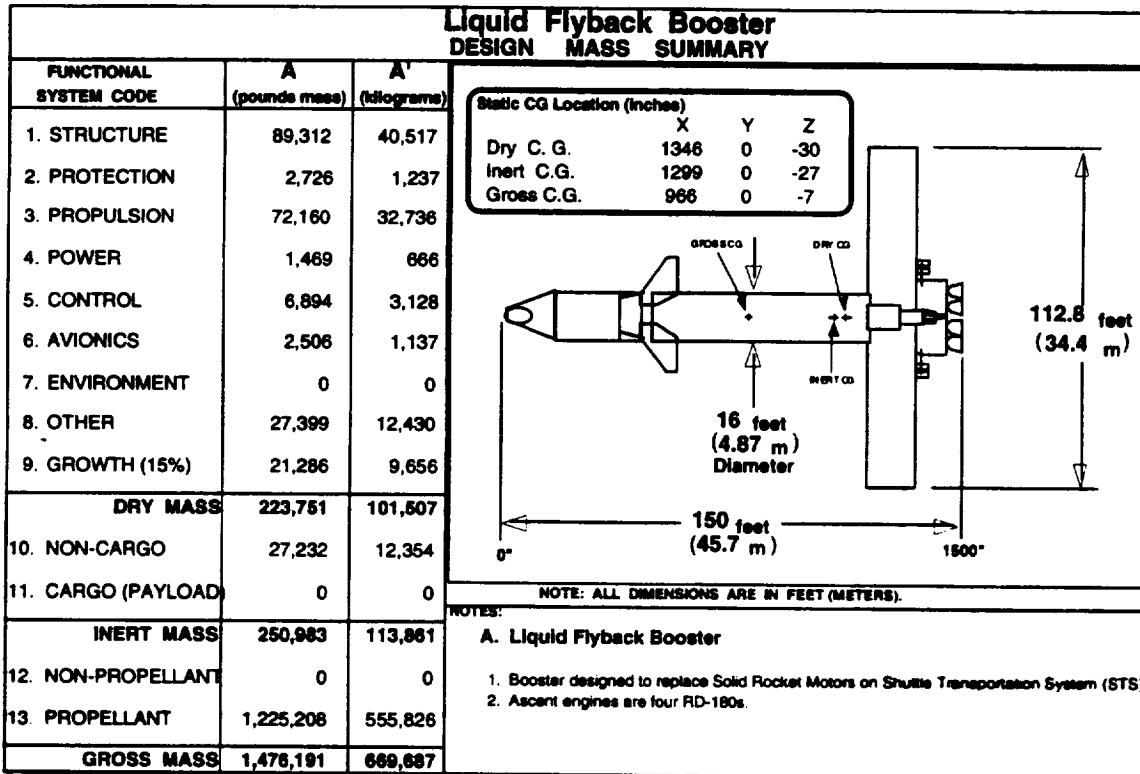


Figure 5.11.1-1 LFBB design mass summary.

5.11.2 Time History of CG (Nominal Mission)

During a nominal Shuttle/LFBB mission, the vehicle cg location moves in both X & Z directions throughout the various flight phases. The Y component of the vehicle cg is very close to zero throughout all phases of the flight. As figure 5.11.2-1 shows, vehicle launch conditions (point 1) produce a vehicle cg that is mid-length and just above the booster centerline. Once the ascent fuel is expended (point 2), the vehicle cg shifts 236 inches to the rear (positive X) and 29 inches up (negative Z). This is the largest shift in the flight profile and occurs while still attached to the ET. Three small shifts (points 2 - 4) aft and down occur as both boosters separate from the ET, maneuver to a lofting point, expend the fairing over the canards and wings, and deploy the wings for the glide portion of the flight. Between points 4 and 5, the remaining RCS is expended and the shroud covering the flyback engine is removed. This has the cg move slightly forward and down. The cg then moves further aft and down (points 5 - 6) as the flyback ABE fuel is consumed. At this point in a nominal mission, the first booster is landed in this condition. The second booster uses the ABE loiter fuel onboard to allow the first booster to clear the runway. The cg shifts another 42 inches aft on the second booster, if all of the loiter fuel (points 6 - 7) is used before landing. Maximum cg shift for the complete mission is 389 inches positive X or 22% of the vehicle length.

#	Mission Phase:	Mass (lbm)	Xcg (in)	% Length	Ycg (in)	Zcg (in)
1	LFBB Gross Mass at Launch	1,476,191	966	53.7%	0	(7)
2	Pre-LFBB Separation	274,848	1,229	68.3%	0	(36)
3	Post-LFBB Separation	274,177	1,230	68.3%	0	(36)
4	Wing Deployment (apogee)	271,790	1,242	69.0%	3	(30)
5	Beginning of Cruise (air-breathing engine Ignition)	270,341	1,240	68.9%	3	(29)
6	End of Cruise (Booster #1 @ landing)	247,411	1,313	72.9%	4	(20)
7	End of Loiter/Final Approach (Booster #2 @ landing)	235,931	1,355	75.3%	4	(21)

Vehicle Conditions during Mission Phases:

- 1 Fully fueled, wings & canards stowed, fairings in place.
- 2 Usable ascent fuel expended.
- 3 50% of separation system mass assumed expended in separation burn.
- 4 Wing/canard fairing expended, wings deployed, 20% of RCS usable expended.
- 5 Remaining usable RCS propellant expended, air-breathing engine (ABE) shroud expended.
- 6 Usable (nominal) ABE fuel expended.
- 7 ABE loiter fuel expended (30 minutes). Only ABE reserve fuel remaining.

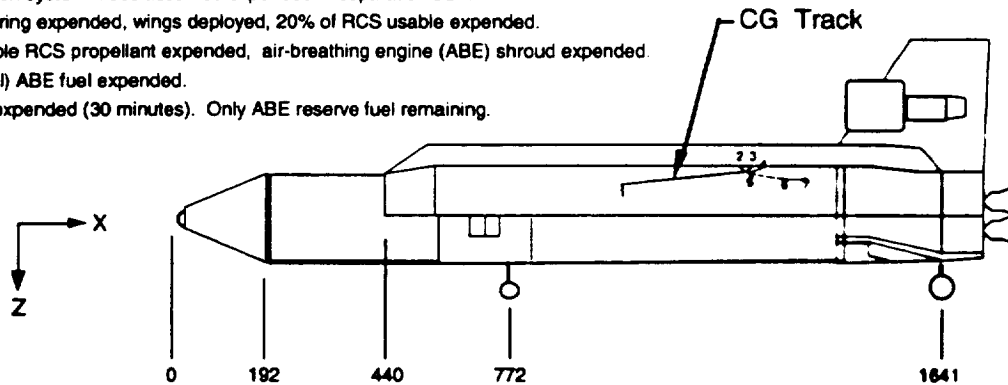


Figure 5.11.2-1 Vehicle weight and cg during mission phases.

References

¹⁴"Optimum Design Procedures for Stiffened Compression Panels"; Space Shuttle Memo B36-196MO-27; Oct 25, 1971.

REPORT DOCUMENTATION PAGE

Form Approved
OMB No. 0704-0188

Public reporting burden for this collection of information is estimated to average 1 hour per response, including the time for reviewing instructions, searching existing data sources, gathering and maintaining the data needed, and completing and reviewing the collection of information. Send comments regarding this burden estimate or any other aspect of this collection of information, including suggestions for reducing this burden, to Washington Headquarters Services, Directorate for Information Operations and Reports, 1215 Jefferson Davis Highway, Suite 1204, Arlington, VA 22202-4302, and to the Office of Management and Budget, Paperwork Reduction Project (0704-0188), Washington, DC 20503.

1. AGENCY USE ONLY (Leave Blank)	2. REPORT DATE <p style="text-align: center;">Sep/94</p>	3. REPORT TYPE AND DATES COVERED <p style="text-align: center;">Technical Memorandum</p>	
4. TITLE AND SUBTITLE Liquid Flyback Booster Pre-Phase: A Study Assessment		5. FUNDING NUMBERS	
6. AUTHOR(S) Wayne L. Peterson, et. al.		8. PERFORMING ORGANIZATION REPORT NUMBERS S-778	
7. PERFORMING ORGANIZATION NAME(S) AND ADDRESS(ES) Systems Engineering Division Lyndon B. Johnson Space Center Houston, Texas 77058		10. SPONSORING/MONITORING AGENCY REPORT NUMBER TM-104801	
9. SPONSORING/MONITORING AGENCY NAME(S) AND ADDRESS(ES) National Aeronautics and Space Administration Washington, D.C. 20546-0001		11. SUPPLEMENTARY NOTES	
12a. DISTRIBUTION/AVAILABILITY STATEMENT unclassified/unlimited Available from the NASA Center for AeroSpace Information 800 Elkridge Landing Road Linthicum Heights, MD 21090, (301) 621-0390		12b. DISTRIBUTION CODE	
Subject category: 15			
13 ABSTRACT (Maximum 200 words) <p>The concept of a flyback booster has been around since early in the Shuttle program. The original two-stage Shuttle concepts used a manned flyback booster. These boosters were eliminated from the program for funding and size reasons. The current Shuttle uses two Redesigned Solid Rocket Motors (RSRMs), which are recovered and refurbished after each flight; this is one of the major cost factors of the program. Replacement options have been studied over the past ten years. The conclusion reached by the most recent study is that the liquid flyback booster (LFBB) is the only competitive option from a life-cycle cost perspective.</p> <p>The purpose of this study was to assess the feasibility and practicality of LFBBs. The study provides an expansion of the recommendations made during the aforementioned study. The primary benefits are the potential for enhanced reusability and a reduction of recurring costs. The potential savings in vehicle turnaround could offset the up-front costs. Development of LFBBs requires a commitment to the Shuttle program for 20 to 30 years. LFBBs also offer enhanced safety and abort capabilities. Currently, any failure of an RSRM can be considered catastrophic, since there are no intact abort capabilities during the burn of the RSRMs. The performance goal of the LFBBs was to lift a fully loaded Orbiter under optimal conditions, so as not to be the limiting factor of the performance capability of the Shuttle. In addition, a final benefit is the availability of growth paths for applications other than Shuttle.</p> <p>Participants included JSC, KSC, and MSFC. If it is determined that a more detailed study is warranted, a new study would be initiated to obtain baseline requirements, which would lead the way for detailed vehicle designs and a reference concept with bottoms-up cost.</p>			
14 SUBJECT TERMS booster rocket engines, space shuttle boosters, launch vehicles, solid propellant rocket engines, recoverable launch vehicles, booster recovery		15. NUMBER OF PAGES 318	
17. SECURITY CLASSIFICATION OF REPORT <p style="text-align: center;">unclassified</p>		16. PRICE CODE	
18. SECURITY CLASSIFICATION OF THIS PAGE <p style="text-align: center;">unclassified</p>		20. LIMITATION OF ABSTRACT UL	
19. SECURITY CLASSIFICATION OF ABSTRACT <p style="text-align: center;">unclassified</p>		21. LIMITATION OF ABSTRACT	